

**ON-PACKAGE ANTENNAS**  
*for*  
**BIOMEDICAL APPLICATIONS**

BY  
**ABDELRAHMAN ELSIR MOHAMED**

A Thesis Presented to the  
DEANSHIP OF GRADUATE STUDIES  
**KING FAHD UNIVERSITY OF PETROLEUM & MINERALS**  
DHAHRAN, SAUDI ARABIA

In Partial Fulfillment of the  
Requirements for the Degree of

**MASTER OF SCIENCE**  
In  
**ELECTRICAL ENGINEERING**

May 2017

KING FAHD UNIVERSITY OF PETROLEUM & MINERALS  
DHAHRAN- 31261, SAUDI ARABIA  
DEANSHIP OF GRADUATE STUDIES

This thesis, written by **ABDELRAHMAN ELSIR ELKHIDIR MOHAMED** under the direction his thesis advisor and approved by his thesis committee, has been presented and accepted by the Dean of Graduate Studies, in partial fulfillment of the requirements for the degree of **MASTER OF SCIENCE IN ELECTRICAL ENGINEERING.**



Dr. Ali Al-Shaikhi  
Department Chairman



Prof. Salam A. Zummo  
Dean of Graduate Studies



6/7/2017  
Date



Prof. Mohammad Sharawi  
(Advisor)



Dr. Sharif Iqbal  
(Member)



Dr. Hussein Attia  
(Member)

© ABDELRAHMAN ELSIR MOHAMED

2017

*Dedication*

This humbled work is dedicated to

My great lovely PARENTS who instilled in me the passion of learning and who were my first teachers in this life and the scarified everything for my sake

My sisters who inspired and supported me forever

My brother, Abdelraheem

## **ACKNOWLEDGMENTS**

I would like to express my sincere and deep gratitude for my great respected Professor, Mohmmad Sharawi, for the intensive knowledge and extreme support that I had while working with him.

Moreover, I would like to acknowledge the valuable comments of Dr. Sharif Iqbal and Dr. Hussein Attia as examiners for this thesis.

Finally, I like to express my profound gratitude for my family: my parents, my brother and my sisters for supporting me throughout the entire process. I also would like to thank all my friends especially Mr. Hussein Abdellatif.

# TABLE OF CONTENTS

ACKNOWLEDGMENTS .....	V
TABLE OF CONTENTS .....	VI
LIST OF TABLES.....	IX
LIST OF FIGURES.....	X
LIST OF ABBREVIATIONS.....	XII
ABSTRACT.....	XIV
ملخص الرسالة .....	XVI
<b>1 CHAPTER 1 INTRODUCTION .....</b>	<b>1</b>
1.1 Wireless Communications.....	1
1.2 Antennas on Package (AoP) .....	1
1.3 Antennas for Biomedical Applications .....	2
1.4 Work Motivation .....	3
1.5 Thesis Contributions .....	4
<b>2 CHAPTER 2 LITERATURE REVIEW.....</b>	<b>5</b>
2.1 Theoretical Background .....	5
2.1.1 On-Package Antennas.....	5
2.1.2 Antennas for Biomedical Applications .....	8
2.2 Literature Review.....	13
2.2.1 Classification According to Fabrication Technology .....	14
2.2.2 Classification According to Operating Frequency.....	33
2.2.3 Classification According to Applications .....	34

2.2.4	Tabulated Summary of previous work in literature .....	35
2.3	Summary.....	42
<b>3</b>	<b>CHAPTER 3 ANTENNA DESIGNS.....</b>	<b>43</b>
3.1	DESIGN I: LTCC Based Patch Antenna .....	43
3.1.1	Geometry .....	43
3.1.2	Design Evolution.....	45
3.1.3	Sensitivity Analysis .....	48
3.1.4	Results and Discussions .....	54
3.1.5	Summary of Design-I .....	59
3.2	DESIGN II: Superstrate Loaded Miniaturized Antenna .....	60
3.2.1	Geometry .....	60
3.2.2	Design Evolution.....	61
3.2.3	Sensitivity Analysis .....	62
3.2.4	Results and Discussions .....	66
3.2.5	Summary of Design-II .....	75
3.3	DESIGN III: Dual-Band Circular Patch Antenna .....	76
3.3.1	Geometry .....	76
3.3.2	Simulation with Skin Model.....	79
3.3.3	Parametric Studies .....	80
3.3.4	Results and Discussions .....	84
3.3.5	Summary of Design-III .....	87
<b>4</b>	<b>CHAPTER 4 CONCLUSION &amp; FUTURE WORK .....</b>	<b>88</b>
4.1	Conclusions .....	88
4.2	Future Work.....	89

<b>REFERENCES.....</b>	<b>90</b>
<b>VITAE.....</b>	<b>100</b>



## LIST OF TABLES

Table 1: ISM bands [5] .....	9
Table 2: Performance Matrix of Proposed Designs in [80] .....	28
Table 3: Tabulated Summary of Design Characteristics in Literature Review .....	36
Table 4: Electrical Properties of Human-Skin at 915 MHz [76] .....	55
Table 5: Summary of Antenna Performance Measurements on Different Spots on Human-Body .....	68
Table 6: Calculated Specific Absorption Rate .....	69
Table 7: Comparison between Measurements and Simulations of Transmission Coefficient S21 .....	72
Table 8: Electric Properties of Human Tissues.....	79

## LIST OF FIGURES

Figure 1: Wireless System Modules .....	5
Figure 2: Different realization technologies [4].....	8
Figure 3: Classification Tree according to Fabrication Technology .....	14
Figure 4: Geometry and dimensions of Implantable antenna [7] .....	16
Figure 5: Geometry of proposed design [17].....	17
Figure 6: Expanded view of LTCC design [56].....	19
Figure 7: Geometry of antenna with air cavity [60] .....	20
Figure 8: Proposed Design geometry. (a) Top view. (b) Back view. (c) Side view [76] .	21
Figure 9: Omnidirectional Compact patch antenna: (a) simulated design, (b) Final fabricated device [77] .....	24
Figure 10: Geometry of proposed design [78].....	25
Figure 11: Geometry of proposed antenna [79].....	27
Figure 12: Proposed design [80].....	28
Figure 13: Geometry of proposed design [82].....	30
Figure 14: Geometry of Textile design [81] .....	31
Figure 15: Geometry of proposed design [73].....	32
Figure 16: Classification Tree According to Operating Frequency.....	33
Figure 17: Classification According to Design Application.....	35
Figure 18: Proposed Antenna Geometry: (a) Top view of patch (superstrate is not shown). (b) Bottom view shows slots on Ground Plane. (c) Side view shows feed location and vias. ....	45
Figure 19: Geometry Evolution of Design-I.....	47
Figure 20: Current distribution in patch: (a) slot-free, (b) with shorting posts, (c) with inserted slots.....	47
Figure 21: Effect of Number of Slots .....	48
Figure 22: Effect of Length of Slots on Patch .....	49
Figure 23: Effect of Horizontal Displacement of Feeding.....	50
Figure 24: Effect of Substrate Thickness.....	51
Figure 25: Effect of Superstrate Thickness.....	52
Figure 26: Effect of Changing Shorting Posts Radius .....	53
Figure 27: Effect of Changing the Gap between GND Mid Slots .....	54
Figure 28: Human-body model used for simulations .....	55
Figure 29: Reflection coefficient of proposed antenna in free-space, on skin model (optimized and non-optimized).....	56
Figure 30: Optimized designs in: (a) Free space (Air). (b) On human-body model.....	57
Figure 31: Far-Field Radiation Pattern of Antenna in Air. (a) Azimuth Plane (XY), (b) Elevation Plane (YZ), (c) Elevation Plane (XZ).....	58
Figure 32: Far-Field Radiation Pattern of Antenna on-Skin. (a) Azimuth Plane (XY), (b) Elevation Plane (YZ), (c) Elevation Plane (XZ).....	59

Figure 33: Proposed Antenna Geometry: (a) Top view of patch (superstrate is not shown). (b) Bottom view shows slots on Ground Plane. (c) Side view shows feed location and vias. ....	62
Figure 34: The parametric sweep of for S11 for several design parameters: (a) Length of Patch slots, (b) Length of L-shaped GND slot, (c) Width of patch slots, (d) Gap between patch slots. All dimensions are in mm. ....	64
Figure 35: The parametric sweep of for S11 for several design parameters: (a) Superstrate thickness, (b) Substrate thickness, (c) Feed location, (d) Simulation and Measurement On-Skin Result: Simulation I (HFSS), Simulation II (CST). All dimensions are in mm. 65	65
Figure 36: (a) Fabricated Prototype of Proposed Antenna. (b) Simulation Model for Transmission Coefficient ( $S_{21}$ ) Measurement. ....	66
Figure 37: Measured reflection coefficient of the proposed antenna on various spots of the human-body. (a) Parts (1 to 8), (b) Parts (9 to 16), (c) human-body spots considered in measurements.....	67
Figure 38: Experimental Setup for Transmission Coefficient Measurement. (a) Vector Network Analyzer. (b) Side View, (c) Front View.....	70
Figure 39: Transmission Coefficient $S_{21}$ at different thicknesses of Lean Beef slices: (a) Simulated. (b) Measured. ....	71
Figure 40: 3D Radiation Pattern (HFSS) .....	73
Figure 41: Far-Field 2D Radiation Pattern of Antenna. (a) Azimuth Plane (XY), (b) Elevation Plane (YZ), (c) Elevation Plane (XZ).....	73
Figure 42: Far-Field 3D Radiation Pattern (CST) .....	74
Figure 43: Far-Field 2D Radiation Patterns: Azimuth plane (Green), Elevation plane (Red). ....	74
Figure 44: Geometry of Proposed Dual-Band Design. (a) Top View, (b) Side View .....	78
Figure 45: Tissues Model for Implanted Applications .....	79
Figure 46: Effect of width of inserted slots .....	80
Figure 47: Effect of Length of Arc-Shaped Slot.....	81
Figure 48: Effect of Location of Shorting Posts .....	82
Figure 49: Effect of Substrate Thickness.....	83
Figure 50: Effect of Superstrate Thickness.....	83
Figure 51: Simulated Reflection Coefficient: (a) at 403.5 MHz, (b) at 2.45 GHz .....	85
Figure 52: Radiation Pattern: (a) at 434 MHz, (b) at 2.45 GHz .....	86

## LIST OF ABBREVIATIONS

<b>RF</b>	:	Radio Frequency
$\epsilon_r$	:	Relative Dielectric Constant (Permittivity)
$\tan \delta$	:	Loss Tangent
$f_r$	:	Resonance Frequency
<b>AoP</b>	:	Antenna on Package
<b>AoC</b>	:	Antenna on Chip
<b>ISM</b>	:	Industrial, Scientific, and Medical Bands
<b>MICS</b>	:	Medical Implanted Communication System
<b>ESA</b>	:	Electrically Small Antenna
<b>LTCC</b>	:	Low Temperature Co-fired Ceramic
<b>LCP</b>	:	Liquid Crystalline Polymer
<b>PCB</b>	:	Printed Circuit Board
<b>SAR</b>	:	Specific Absorption Rate
<b>WLAN</b>	:	Wireless Local Area Network
<b>WPT</b>	:	Wireless Power Transmission
<b>GPS</b>	:	Global Positioning System

<b>HFSS</b>	:	High Frequency Structural Simulator
<b>CST</b>	:	Computer Simulation Technology Studio Suite
<b>SMA</b>	:	Sub-Miniature version A
<b>AMSDL</b>	:	Antennas and Microwave Structure Design Laboratory

## ABSTRACT

Full Name : [Abdelrahman Elsir Elkhidir Mohamed]  
Thesis Title : [On-Package Antennas for Biomedical Applications]  
Major Field : [Electrical Engineering]  
Date of Degree : [May 2017]

Wireless communication systems have proliferated in numerous applications ranging from human daily activities to life critical ones. Therefore, the demand for portable and handheld devices has considerably increased. In the medical field, wireless systems have been utilized for telemetry data collection, diagnosis and treatment. These applications require well designed systems with compact size. However, antennas for biomedical applications have to satisfy certain requirements such as: biocompatibility, miniaturization, safety for patients, and acceptable communication quality. The purpose of this thesis is to investigate on-package antennas for biomedical applications and develop several designs that can constitute feasible solutions.

This work presents several antennas that were designed adopting different approaches. The first design was based on low temperature co-fired ceramic (LTCC) technology for biomedical applications to be used on skin or with closed proximity to skin applications. The antenna has a size of  $25 \times 25 \text{ mm}^2$  and resonates around 915 MHz with a bandwidth of 138 MHz. Several miniaturization techniques were applied and the antenna performance was simulated on a numerical skin model.

The second design is a miniaturized biomedical antenna operating around 915 MHz with a size of  $25 \times 25 \text{ mm}^2$  and a bandwidth of 30 MHz. The proposed antenna was fabricated on

Roger RO3006 substrate and the prototype was tested on several spots of the human body. Moreover, the transmission coefficient of the antenna was measured for different lamb meat slice thicknesses. The obtained results show good agreement between simulation and measurement results.

Finally, the third design consists of a dual-band circular patch antenna for implanted biomedical applications. The antenna has a diameter of 15 mm and a thickness of 1.92 mm. The antenna is a multiband one that operates at the 403 MHz Medical Implanted Communication System (MICS) band, 433.9 MHz and 2.45 GHz ISM bands with a total impedance bandwidth of 280 MHz. The performance assessment of the proposed antenna is carried out inside a numerical human-tissues model.

The proposed antennas covered various ISM bands and all have very compact sizes with adequate bandwidth for wireless biomedical applications

## ملخص الرسالة

الاسم الكامل: عبد الرحمن السر الخضر محمد

عنوان الرسالة: الهوائيات المدمجة وتطبيقاتها في المجالات الطبية

التخصص: الهندسة الكهربائية

تاريخ الدرجة العلمية: مايو 2017

لقد أصبحت أنظمة الاتصال اللاسلكي جزءاً أساسياً في عدد هائل من التطبيقات البشرية، بداية من الاستخدامات اليومية وانتهاء ببعض التطبيقات الهامة والحساسة، ولذلك زادت الحاجة إلى الأجهزة اليدوية المحمولة. أما في المجالات الطبية، فإن الاتصالات اللاسلكية قد تستخدم في جمع المعلومات (عن بعد) عن حالة المرضى، أو خلال عملية الكشف الطبي، أو في العمليات الجراحية. وجميع هذه التطبيقات تستلزم استخدام هوائيات ذات حجم صغير (مصغرة). إن من الضروري بالنسبة للهوائيات المستخدمة في التطبيقات الطبية أن تستوفي بعض الاشتراطات كالتوافق الطبي مع الأجسام، والحجم المحدود، والسلامة بالنسبة للمرضى بالإضافة إلى توفير جودة اتصال مقبولة. إن العرض الرئيسي من هذه الأطروحة هو استكشاف الهوائيات المدمجة والعمل على تقديم تصاميم جديدة لتوفير حلول ممكنة لاستخدام الهوائيات المدمجة في التطبيقات الصحية والطبية.

اعتماداً على نتائج البحث الاستقصائي للتصاميم السابقة، فقد تم تصميم عدة هوائيات باستخدام تقنيات متعددة. أول هذه الهوائيات تم تصميمه باستخدام تقنية LTCC للتطبيقات الطبية. مساحة الهوائي  $25 \times 25$  مم مربع ويعمل عند تردد 915 ميغاهرتز بعرض نطاق قيمته 138 ميغاهرتز. تم استخدام عدة طرق لتصغير مساحة الهوائي (miniaturization) وتم تقييم أداء الهوائي المقترح داخل نموذج محاكاة رقمي.

أما التصميم الثاني فقد كان لهوائي مصغر مخصص للاستخدامات الطبية يعمل عند تردد 915 ميغاهرتز ومساحته  $25 \times 25$  مم مربع بعرض نطاق 30 ميغاهرتز. الهوائي المقترح تم تنفيذه على قاعدة Roger RO3006 والنماذج المصممة تم اختبارها وقياس أدائها على عدة مواضع من الجسم. بالإضافة لذلك، فقد تم قياس معامل الإرسال على قطع من اللحم ذات سُمكٍ متعدد وأظهرت النتائج المعملية توافق جيد مع نماذج المحاكاة والحسابات الرقمية.

أخيراً، تتطرق هذه الأطروحة إلى تصميم مصغر لهوائي ثنائي النطاق للاستخدامات الأجهزة الطبية المزروعة (Implanted). ويعمل هذا الهوائي عند النطاقات ذات التردد 403 ميغاهرتز (MICS) و433.9 ميغاهرتز (ISM)، و2.45 غيغاهرتز (ISM) ويبلغ عرض النطاق الكلي لهذا التصميم 280 ميغاهرتز. الهوائي المقترح له شكل دائري بطول قطر 15 مم وسُمك 1.92 مم. وقد تم اختبار أداء الهوائي داخل نموذج رقمي للأنسجة الحيوية.



# CHAPTER 1

## INTRODUCTION

### 1.1 Wireless Communications

During recent years, wireless communication systems have proliferated in numerous applications ranging from human daily activities to extremely critical applications. Therefore, the demand for portable and handheld devices has considerably increased. In the medical field, wireless systems have been utilized for telemetry data collection, diagnosis and treatment and these applications require well designed systems with a compact size. Although traditional horizontal integration of multichip modules (where the antenna and RF circuits are designed separately then are integrated through matching networks) allows for using latest technology for each system module, this approach lacks the size compactness which is a fundamental issue when designing implantable devices.

### 1.2 Antennas on Package (AoP)

With the advancement in integrated circuit (IC) technology, the design limiting factor is the antenna size, since wireless system electronics can be highly integrated in a very small area. On the other hand, Antenna on Package (AoP) approach offers a feasible solution to integrate the antenna vertically on the top of an IC. This approach can match the

requirements of compact size, high performance and low cost. In literature, there are different technologies to realize the AoP such as low temperature co-fired ceramic (LTCC) and liquid crystal polymer (LCP). In this work, a comprehensive literature review on AoP designs is conducted to be able to come up with a novel design for compact biomedical applications. The concept of antenna on package has been proposed recently [1], and there are a lot of challenges in this area that needs to be studied and addressed properly when considering a practical design.

### **1.3 Antennas for Biomedical Applications**

Biomedical Telemetry allows the physiological signals to be transmitted over distance. Physiological signals are to be detected by implanted sensors, processed inside the implanted device, then the signal is transmitted to the exterior receiver [1].

Traditionally, inductive links (coils) were utilized for biomedical telemetry at low frequencies (range of 30 KHz). However, they have limitations such as low data rate (because the coil circuits are designed to resonate at single frequency and thus, all circuit components are selected accordingly) [2], short link communication, and they are sensitive to any misalignment in coil position. Nowadays, radio frequency links (RF-links), such as antennas, are used to resolve the inductive link limitations [1].

Millions of people rely on biomedical implanted devices, in one way or another, to improve and assist their lives. The applications of implanted biomedical devices have been increased to include pacemakers, blood-glucose monitors, temperature sensors, glaucoma

monitors, cochlear and retinal applications. It seems that, biomedical applications will continue their rapid increase as the technology improves [1].

## **1.4 Work Motivation**

In this work, the design of on-package antennas for biomedical applications is investigated and small designs are provided. The work in this field is motivated by the increase in demand of biocompatible, safe, and efficient antenna designs. Several works have been conducted in literature to design implanted antennas for biomedical purposes, however, LTCC based designs were not investigated deeply for this field. LTCC offers an excellent solution for on-package antenna realization due to its high efficiency and performance, relative low cost, flexibility in design, wide range in dielectric constants, and robustness of fabricated models [3]. Other PCB based antenna solutions that are: small in size, cost efficient and with good performance are also investigated.

In this work miniaturized based patch antennas is designed with a size of  $25 \times 25 \text{ mm}^2$  to operate at 915 MHz ISM band for biomedical applications using LTCC and PCB technologies. A second design of dual band antenna is optimized to work around 402 MHz and 2.45 GHz ISM bands for implanted designs with a diameter of 15 mm. Several miniaturization techniques are applied to reduce antenna size and enhance the radiation characteristics.

## 1.5 Thesis Contributions

There are several contributions accomplished by this work:

A. A comprehensive literature review of antennas on package and their applications, mainly in the biomedical field is conducted.

B. Designed an LTCC and PCB based miniaturized biomedical antennas for biomedical telemetry to resonate around 915 MHz ISM band, fabricated and tested their performance (reflection coefficient, bandwidth, efficiency, specific absorption rate (SAR), and radiation characteristics), if possible. The antennas were designed with a size of  $25 \times 25 \text{ mm}^2$ .

C. Designed a dual band implantable biomedical antenna to operate around 400 MHz MICS band and the 2.45 GHz ISM band. The design was miniaturized and fabricated and its performance matrices were tested. The proposed design was realized on a low-loss PCB substrate and its size was  $15 \times 15 \text{ mm}^2$ .

## CHAPTER 2

### LITERATURE REVIEW

#### 2.1 Theoretical Background

This section provides an overview of fundamentals in the field of on-package antennas; features, integration approaches, and their applications especially biomedical.

##### 2.1.1 On-Package Antennas

Nowadays, most of communication systems consist of four modules as shown in Figure

1. These modules are:

1. Digital baseband module for signal processing.
2. Mixed signal module that provide signal conditioning.
3. Radio frequency (RF) frond end that provide the carrier, filter and switching.
4. Antenna that transmit or receive the signal in RF bands.

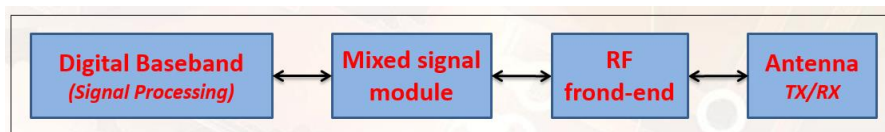


Figure 1: Wireless System Modules

Traditionally, each module is to be designed and optimized individually and then different modules are integrated together within a common board as illustrated in Figure 2(a). This multi-chip module approach enables for best optimization for each module at the expense of size. For instant, a silicon substrate can be used for electronics, while a low-loss substrate

for antenna ...etc. With the developments in handheld and portable devices, the size became a crucial aspect in design. The improvement in integrated circuits, influenced by the huge achievement in transistor industry (size reduction) as well as in analog integration, allowed for vertical integration of circuits of the system. Utilizing antenna miniaturization techniques, a reduced size antenna can be stacked on top of a vertically integrated system to have On-package antenna and On-package system as shown in Figure 2(b). However, in this approach, system interconnection requires low-loss, high frequency bond wires that are costly and have undesired effects of system performance. Several technologies are available to realize on-package systems such as: Low temperature co-fired ceramic (LTCC), liquid crystalline polymer (LCP) as well as traditional printed circuit board (PCB) technology [4].

On the other hand, the advancement in silicon industry in Complementary Metal Oxide Semiconductor (CMOS) allows for on-chip integration of digital components. Moreover, the trend to push for high frequency bands (i.e. millimeters wave) lowers antenna sizes, and thus it became possible and practical to have on-chip integration of antennas as shown in Figure 2(c). That means the antenna is to be realized on the semiconductor substrate where all electronics are integrated. Such approach suffers mainly from the following [4]:

- High losses in the low resistivity semiconductor substrates (i.e. Silicon).
- Electromagnetic interference (EMI) between antenna and circuits.
- Some layout constrains.

- Lack of setups for measurement and performance characterization, due to extremely small size.

Designing antennas using this approach require designers to be familiar with both antenna and electronic design. Co-design approach gains some advantages such as [4]:

- Eliminate the need of 50-ohm matching circuits.
- Eliminate the need for bond wires.
- Offer the designer two degrees of freedom to allow him/her to know the effect of antenna on other electronics response and vice versa.

Furthermore, on-chip antennas open the door of several interesting application such as:

- Tera-Hertz antennas that operates from 300 GHz to 3 THz. It can be used for detection of chemicals, weapons and cancer treatment.
- Electromagnetic collectors; these antennas resonate at optical rang (i.e. Infra-Red IR and visible bands). These collectors show a higher efficiency than Photo Voltaic (PV) cells however, nano-rectifiers are still a hot area for research.
- Implanted antennas where the on-chip antenna is used for energy harvesting as well as communication with outer ones for data telemetry [4].

Note that, the focus of this work is primarily on antenna designs without analyzing the electronic system designs. All proposed designs have ground plan that can provide electromagnetic isolation (EMI) between the antenna and possible integrated electronic circuits for desired applications. Moreover, the feeding mechanesim in proposed designs

is probe feeding for testing antenna performance, however, that can be replaced easily with a pin to feed the antenna through electronic circuit.

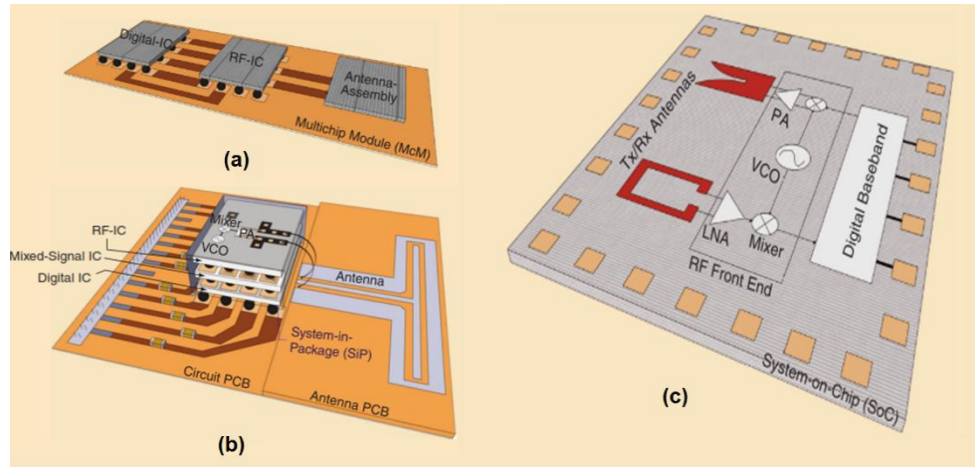


Figure 2: Different realization technologies [4]

## 2.1.2 Antennas for Biomedical Applications

Implantable antennas are key in the design of biomedical devices. The design of a biomedical antenna is required to satisfy several aspects such as biocompatibility, miniaturized size, safety, and accepted quality of communication.

Up to this moment, no specific frequency band has been licensed globally for biomedical applications. However, there are some suggested bands such as the Medical implant communication system (MICS) and industrial, scientific and medical (ISM) bands. MICS covers a bandwidth of 3 MHz from 402.0 MHz to 405.0 MHz and it has been regulated by the European Radio-communication Committee (ERC) and Federal Communication Commission (FCC). On the other hand, ISM bands (shown in Table 1), are suggested in some countries. Several designs utilized MICS band due to its high data rate, better



penetration in human tissues, inexpensive circuitry, and noise is relatively low at this band [1].

Table 1: ISM bands [5]

Frequency range		Center frequency
6 765 kHz	6 795 kHz	<b>6 780 kHz</b>
13 553 kHz	13 567 kHz	<b>13 560 kHz</b>
26 957 kHz	27 283 kHz	<b>27 120 kHz</b>
40.66 MHz	40.7 MHz	<b>40.68 MHz</b>
433.05 MHz	434.79 MHz	<b>433.92 MHz</b>
902 MHz	928 MHz	<b>915 MHz</b>
2 400 MHz	2 500 MHz	<b>2 450 MHz</b>
5 725 MHz	5 875 MHz	<b>5 800 MHz</b>
24 GHz	24.25 GHz	<b>24.125 GHz</b>
61 GHz	61.5 GHz	<b>61.25 GHz</b>
122 GHz	123 GHz	<b>122.5 GHz</b>
244 GHz	246 GHz	<b>245 GHz</b>

#### A. Biocompatibility:

In order to ensure patient safety, designed antennas for biomedical applications are required to satisfy safety conditions in material and shape. Since human tissues are conductive, direct interaction between the metallic layers of implanted antennas and human tissues may cause short-circuiting inside the device, which may lead to injuries. To avoid direct contact with the antenna metallic part, a dielectric superstrate layer such as Teflon ( $\epsilon_r = 2.1$ ), ceramic ( $\epsilon_r = 9.4$ ) and MACOR ( $\epsilon_r = 6.1$ ) can be used to load the antenna. Other designs includes dielectric thin layer to coat the antenna such as Zirconia ( $\epsilon_r = 29$ ), and REEK ( $\epsilon_r = 3.2$ ) however, the thickness of this coating layer need to be optimized and included in the

modeling and simulations to reduce the amount of detuning in the results of the fabricated model.

Moreover, for implanted devices and antennas, sharp edges are to be avoided to prevent possible tissue injuries caused by these sharp edges [1].

### **B. Miniaturization:**

Designing biomedical antennas at very high frequencies is not recommended since the path-loss increases as the square of frequency. Thus, operation bands for biomedical antennas are relatively limited in low RF. Designing patch antennas with classical dimensions of half and quarter wavelengths at low frequencies require large size which makes the antenna not suitable for biomedical implantation. Thus, miniaturization is a necessary step in the design of biomedical antennas. However, since human-tissues have high permittivity, the miniaturization process becomes possible in comparison with the case of free-space [1].

Miniaturization alters the current distribution on an antenna in several ways, two of which are:

1. Increasing the current path between edges of patch (e.g. meandering).
2. Changing the reactance of the antenna (shifts the location of zero crossing of imaginary part of antenna impedance) using shorting posts.

Several miniaturization techniques can be applied for patch antennas as well [1]:

1. Using high dielectric substrate that results in lowering the resonance frequency such as Roger 3210 ( $\epsilon_r = 10.2$ ) or alumina ( $\epsilon_r = 9.4$ ).

2. Increasing the current path by meandering, spiraling, or slotting.
3. Inserting shorting posts to change the reactance of the antenna as well as to increase the effective length of the patch since the ground can be seen as an extension of it.
4. Stacking patches to keep the same length of current path on smaller size.

The aforementioned miniaturization techniques can be used separately or together to achieve the desired miniaturization.

### C. Patient safety:

The transmitted power inside the human-body has to be limited to certain maximum values to avoid biological damage. Globally, the most accepted measure for incident power in human-body is the specific absorption rate (SAR) [6].

IEEE standard (IEEE C95.1 1999) limits the maximum SAR average over 1g to be less than 1.6 W/kg. The ICNRP 2005 and IEEE C95.1 2005 standards set the maximum SAR averaged over 10g to be less than 2 W/kg. So, the limits stated in standards are [6]:

$$SAR_{1g,max} \leq 1.6 \text{ W/kg} \quad (2.1)$$

$$SAR_{10g,max} \leq 2 \text{ W/kg} \quad (2.2)$$

To calculate the electromagnetic energy absorbed by tissues, Eq. (2.3) can be used [1]

$$P_{abs} = \frac{1}{2} \int \sigma |E|^2 dV \quad (2.3)$$

where  $\sigma$  is conductance of tissues, E is intensity of incident electrical field.

#### **D. Power consumption:**

To reduce the power consumption of implanted devices and to extend its lifetime, it is suggested to design implanted devices with two modes of operation “Active mode” and “sleep mode”. The sleep mode is to be set as default and the implanted device continue in this mode unless an activation signal is received from the exterior antenna. If the activation signal is received, the device change its operation mode to “active” and start sending the required information. In this case, to avoid the need of two antennas (activation signal receiver, data transmitter), the implanted antenna can be designed to have dual-band capability. Thus one band can be set for activation signals and other for communication. Moreover, antennas with triple band have been reported in literature [1].

#### **E. Design Strategies and Performance Assessment**

##### **- Tissue Modeling:**

Since most of biomedical antennas are intended to be implanted inside human bodies or will have close interaction with it, modeling the human-tissues is necessary to have realistic results after implementation and correct functionality inside human-bodies.

Human-tissue can be modeled with high accuracy utilizing data produced by magnetic resonance imaging (MRI) and signal processing such as anatomical models. However, this approach requires large amount of time for simulations. Another approach is to use a multilayered model of the body where each layer consists of single material (homogenous) with specific electrical properties (permittivity and conductivity). Layer combinations result in non-homogenous

model that mimics the behavior of real human tissues with some limitations in accuracy. The third approach can be used to save simulation time and obtain elementary results where, human-tissues can be modeled as a single homogenous box with single permittivity and conductivity. However, this approach is not sufficient for optimization and significant mismatching between simulation and measurement result is expected [1].

- Design strategies and testing:

Biomedical antennas can be designed, initially, in free space and then tuned taking into account tissue loading. On the other hand, the antenna can be designed in canonical model of tissues and then optimized in multilayer or anatomic models.

- Fabricated model testing:

Fabricated model (prototype) of implanted antenna cannot be tested in an exact environment where it will operate, inside human-body, thus, to assess the performance of a realized antenna, the antenna can be inserted inside some physical phantom or liquids that have almost similar behavior of human tissues. Several types of phantoms are reported in literature and can be prepared easily in laboratories [1].

## **2.2 Literature Review**

In this section, several works from literature regarding on-package antennas are presented, classified and summarized under several sections. The first subsection classifies the previous work according to fabrication technology. Some examples for each category are

reported in details. The second subsection classifies the previous work according to their operating frequency. Moreover, a classification according to application is provided in third subsection. Finally, a tabulated summary of previous works is given in the fourth subsection.

### 2.2.1 Classification According to Fabrication Technology

In literature, several technologies are utilized to realize on-package antennas. These technologies includes: Printed Circuit Board (PCB), Low Temperature Co-fired Ceramic (LTCC), Liquid Crystalline Polymer (LCP), On-Chip realization on semiconductor substrate, Patterning, Multi-layer organic, and textile realization. A classification tree of previous works according to Fabrication technology is illustrated in Figure 3.

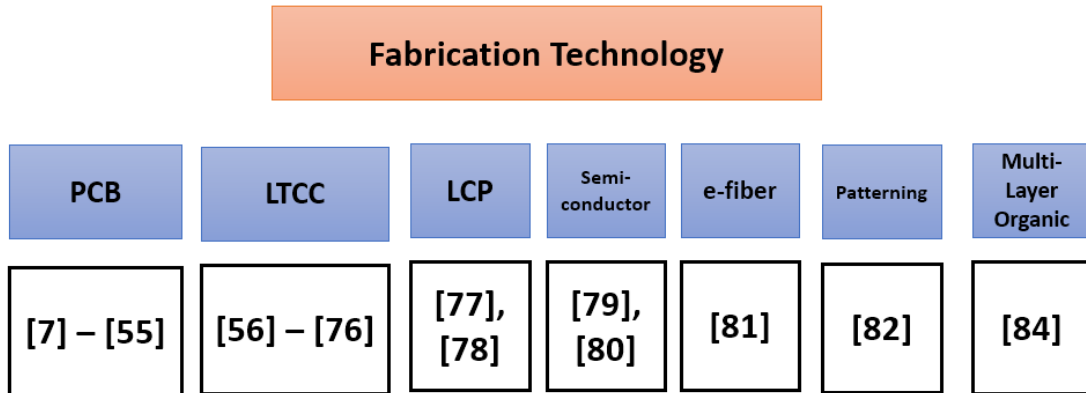


Figure 3: Classification Tree according to Fabrication Technology

#### A. Printed Circuit Board (PCB) Technology

Printed Circuit Board technology of realization is considered to be the most common technology for fabricating modelled design. Large number of works that are reported in literature used PCB machines to fabricate the proposed designs such as in [7]-[55].

For instant, in [7], a hybrid Patch/Slot antenna for biotelemetry devices was presented. The geometry of the proposed antenna is illustrated in Figure 4. This implanted antenna was designed to operate at medical implant communication service (MICS) band (402 – 405 MHz) that has minimal EM pollution. The antenna was realized on two layers of Rogers 3010, each with  $\epsilon_r = 10.2$ ,  $h = 25 \text{ mils}$  and  $\tan \delta = 0.003$ . The dimensions of the proposed antenna are  $10 \times 16 \times 1.27 \text{ mm}^3$ . To lower the antenna's resonance frequency ( $f_r$ ), a meander slot line was embedded into ground plane. In fact, the bottom ground plane was shorted thru a via to a section of the patch that is not connected to feed line. By this approach, the current paths were extended in both ground plane and radiating element leading to lowering  $f_r$  and size reduction. At simulation stage, the skin tissue was modeled in HFSS to have  $\epsilon_r = 40$  &  $\sigma = 0.69 \text{ S/m}$  at 403 MHz with 3 mm thickness.

Simulations shows that changing the dimensions of the surrounding skin has effects on peak gain but not on  $f_r$ . Measurements on fabricated antenna show that it has a 22% impedance bandwidth (372 – 468 MHz) and the peak gain was about -30.5 dBi at 402 MHz.

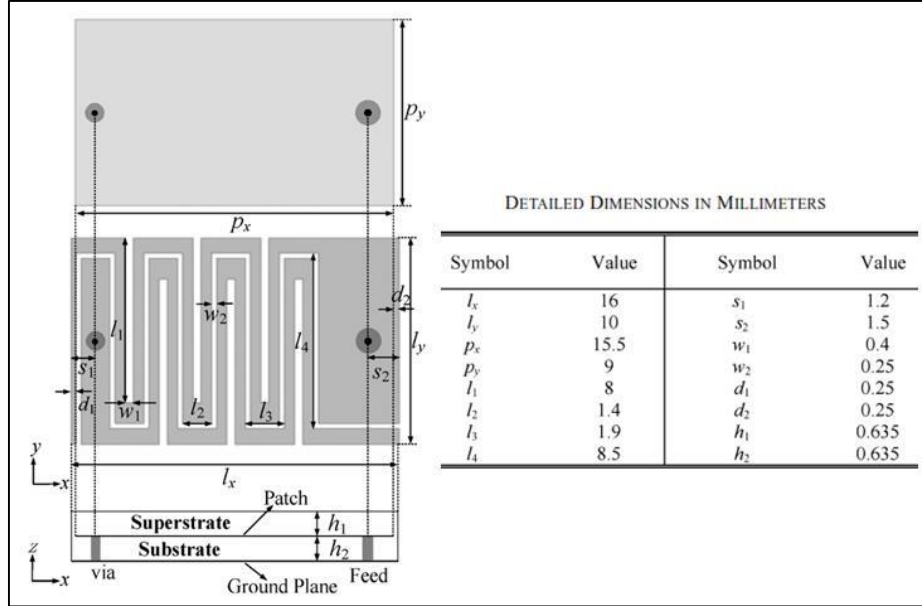


Figure 4: Geometry and dimensions of Implantable antenna [7]

Furthermore, [17] presented a design of a rectenna that can be used for wireless power transfer in the far field. The rectenna consisted of an inverted-F antenna integrated with a rectifier circuit. As the proposed design is for biomedical applications, it is needed to match requirements such as compact size, sufficient efficiency, acceptable bandwidth and user safety. The antenna is designed to operate around 2.45 GHz. The design consisted of two layers of Roger 3010, to serve as substrate and superstrate, with  $\epsilon_r = 10.2$  and  $\tan \delta = 0.0022$  and thickness of 25 mils, as shown in Figure 5. The design occupied a volume of  $4 \times 8 \times 1.28 \text{ mm}^3$ . The design has a folded ground plane along with antenna shorting post to reduce the antenna size. The superstrate is used to cancel the surface waves thus, enhance the radiation pattern.

The antenna performance inside human body was assessed in two environments: one-layer skin phantom in HFSS and voxel human body model in CST. The one-layer model has electrical properties of ( $\epsilon_r = 38$ ,  $\sigma = 1.44 \text{ S/m}$ ) at 2.4 GHz. Simulations showed that the



antenna has a -10 dB bandwidth from 2.37 to 2.47 GHz with -19 dBi peak gain. On the other hand, simulations of antenna in a voxel model showed a 4.1% bandwidth. The measure impedance bandwidth was around 4.2% from 2.395 to 2.498 GHz. The received power by the antenna can be calculated using the Friis equations, if antennas gain, impedance mismatch, polarization mismatch and transmitted power is available. Friis equation is given by [17]:

$$P_r = \frac{G_1 G_2 \lambda_0^2}{(4\pi d)^2} [1 - |S_{11}|^2][1 - |S_{22}|^2] e_p \times P_t \quad (2.3)$$

Since the power levels penetrating the human body are limited by FCC rules, the low input power result in low received power ( $P_r$ ). In order to increase the directivity of  $P$ , parasitic elements placed outside the body are utilized. The design of parasitic element was based on the theory of Yagi antenna considering implanted antenna as driven element and parasitic element as a director. Thus, the size of the parasitic patch is increased beyond the implanted antenna size. Parametric studies were conducted to figure out the effect of parasitic element's size and height. The gain can be enhanced up to 9 dB with size of  $43 \times 43 \text{ mm}^2$ . The final design is combined and attached to rectifier as shown in Figure 5(b).

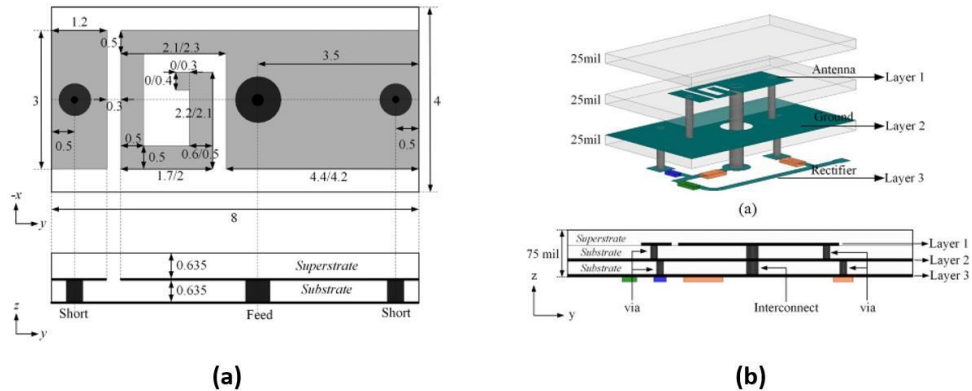


Figure 5: Geometry of proposed design [17]

To sum up, many designs in literature were fabricated using PCB technology. PCB has limitations in fabricating extremely small size designs, and high frequency ones. However, it is still considered a preferred candidate for many designs. The substrate materials that have been utilized in literature in references [7]-[55] includes Roger 3010 ( $\epsilon_r = 10.2$ ), Roger 3210 ( $\epsilon_r = 10.8$ ), FR4 ( $3.5 < \epsilon_r < 4.4$ ), Wover glass ( $\epsilon_r = 3.2$ ), RT Duroid 5870 ( $\epsilon_r = 2.33$ ), RT Duroid 5880 ( $\epsilon_r = 2.2$ ), Ceramics ( $\epsilon_r = 9.7$ ,  $\epsilon_r = 25$ ), Alumina ( $\epsilon_r = 9.7$ ), Plastic ( $\epsilon_r = 4$ ), Silicon ( $\epsilon_r = 11.68$ ), Gallium Arsenate GaAr ( $\epsilon_r = 12.9$ ), and PDMS ( $\epsilon_r = 2.2$ ). Most of the reported works in PCB section consist of single layer however, several works involve multilayers designs.

The number of layers in these designs varies between 2 to 4 layers. The operating frequencies ranges between 400 MHz up to 5.8 GHz and the proposed bandwidths ranges from 5 MHz up to 8.8 GHz. This large variation in bandwidth is influenced by the size and operating frequency of the design. Common antenna structures were patches, monopoles, and dipoles [7]-[55] with modifications. Circular, rectangular, H-shaple and T-shape patches are reported and some designs are loaded with various shapes of slots. Planar inverted-F antennas (PIFA) are design based on monopoles and patches. Moreover, meandered monopole and folded, bowtie dipoles are designed in some works.

### **B. Low Temperature Co-fired Ceramic (LTCC):**

LTCC has been raised as an attractive technology for on-package antenna realization due to several aforementioned factors. In literature, works [56]-[76] discuss in details the design, optimization, fabrication and measuring processes of LTCC designs. For example, in [56], an LTCC based miniaturized multilayer integrated antenna was proposed as shown

in Figure 6 for wireless applications. The antenna was realized on a DuPont 951 substrate with a dielectric constant of 7.8 and loss tangent of 0.0004. The overall thickness of the antenna was around 1.5 mm with a ground size of  $10.3 \times 10.3 \times 1.3 \text{ mm}^3$ . The two top layers were the radiating elements fed in aperture mechanism through a slot line. A shorted conducting plane was inserted between the radiating elements and passive circuits to minimize the electromagnetic interference. The measurements show that as a result of having two radiating elements, the antenna has dual resonance around 5.264 GHz and 5.355 GHz with impedance bandwidths of 40 MHz and 100 MHz respectively. The measured gain was -0.08 dBi for the first resonance and -0.17 dBi for the second. In addition, the paper presented some parametric studies for the effects of package size, ground plane size, antenna height, via connectors and via misalignment on the antenna performance.

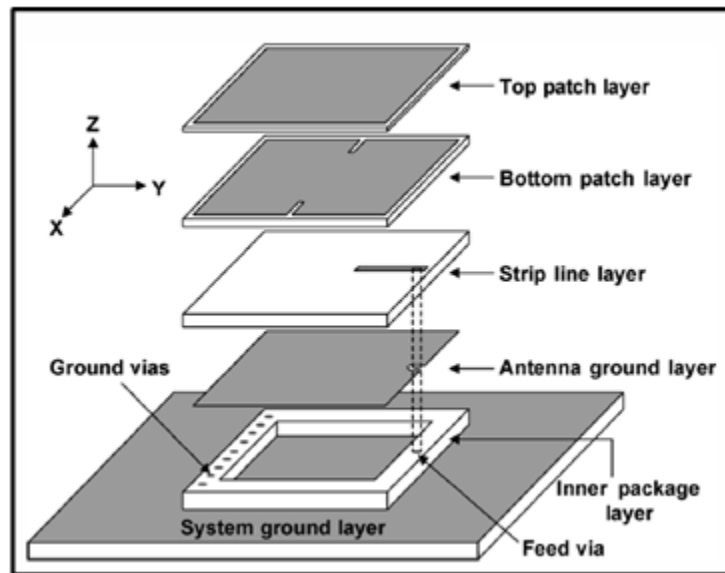


Figure 6: Expanded view of LTCC design [56]

Moreover, in [60], a microstrip antenna with an embedded air cavity on LTCC substrate is proposed. The antenna consists of two layers of substrate separated by a ground plane. There was a patch antenna on the upper substrate fed by aperture feed through a slot in the ground plane as shown in Figure 7 (a). The antenna was designed to resonate around 10 GHz. Beneath the patch there was an air cavity as illustrated in Figure 7(b). The design occupied a space of  $30 \times 30 \times 2.06 \text{ mm}^3$  and was realized on DuPont 951 LTCC substrate with dielectric constant of 7.8 and loss tangent of 0.006 at 3 GHz. The patch has a size of  $10.5 \times 7 \text{ mm}^2$  where the aperture has a size of  $5 \times 0.6 \text{ mm}^2$ . The feed line was terminated with quarter wavelength open circuit and have a length of 1.1 mm. The fabricated antenna showed 10% frequency shift to upper frequency in insertion loss due some distortions in fabricated design. Both simulations and measurements indicates an increase in bandwidth and directivity (gain) for the air cavity design across bulk antenna. For instance, the measured BW was 6.8% and 3.2% for air cavity and bulk antenna, respectively. Also, the measured peak gain around center frequency was 5.4 dBi and 3.2 dBi for air cavity and bulk antenna, respectively.

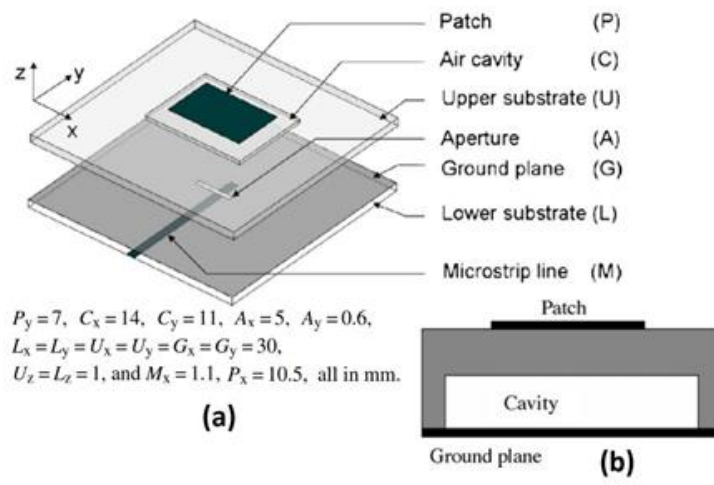


Figure 7: Geometry of antenna with air cavity [60]

Furthermore, in [76], a dual-band printed monopole antenna is designed for biomedical applications. The proposed antenna operates in ZigBee band (868-928 MHz) and (2.4-2.5 GHz). As shown in Figure 8, the antenna structure consisted of meandered monopole on an LTCC substrate with dielectric constant of 7.1 and loss tangent of 0.005. The design was covered with superstrate thus, the geometry had a size of  $17 \times 16.5 \times 0.8 \text{ mm}^3$ . The antenna was intended to operate on the surface of human skin for on/off body communication.

Its performance was simulated at the surface of multilayer skin model. The antenna has metallization thickness of  $0.15 \mu\text{m}$ . Simulations show that the antenna resonates with bandwidths of 80 MHz and 100 MHz around 915 MHz and 2.45 MHz respectively. Simulated far-field patterns indicate that the antenna had peak gains of -16.34 dBi at 915 MHz and -11.58 dBi at 2.45 GHz.

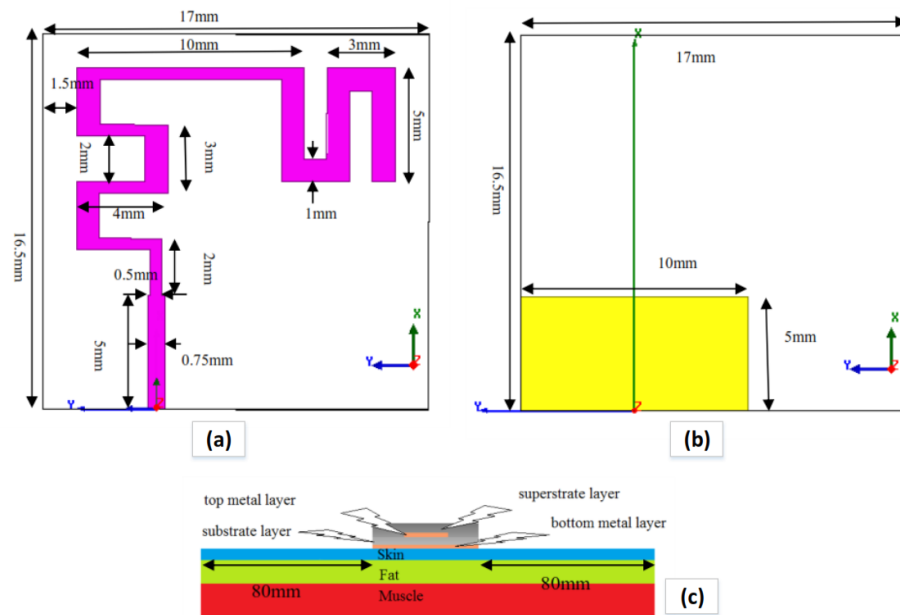


Figure 8: Proposed Design geometry. (a) Top view. (b) Back view. (c) Side view [76]

LTCC technology becomes attractive in fabricating multilayer highly integrated systems due to its flexibility in design, high performance, relative low cost, and variety of substrate and metallization materials. In [56]-[76] various substrate materials were utilized to realize reported designs such as DuPont 943 ( $\epsilon_r = 7.4$ ), DuPont 951 ( $\epsilon_r = 7.8$ ), Ferro A6-M ( $\epsilon_r = 5.9$ ,  $\epsilon_r = 6$ ), Ferro ULF140 ( $\epsilon_r = 14$ ), GL-550 ( $\epsilon_r = 5.7$ ), CBS-10 ( $\epsilon_r = 6$ ), CT 707 ( $\epsilon_r = 6.4$ ), CT 765 ( $\epsilon_r = 64$ ), DP 9699 ( $\epsilon_r = 7.8$ ), and other LTCC materials with dielectric constants of 6, 7.1, 7.7, and 14. Various structures of antennas including monopoles, dipoles, loops, patches, slot Fractals, and Vivaldi were used in the reported designs in [56]-[76]. Monopole designs were reported in rectangular, loop or T-shapes, loaded with stubs, or as PIFA. Moreover, patch antennas were utilized in designs in their rectangular shapes, T- shape, loaded with stacked element, loaded with slots, or loaded with artificial magnetic conductors. The operating frequency for reported LTCC works ranged from 915 MHz ISM band up to 37 GHz millimeter wave band and that illustrates the potential of LTCC technology in fabrication with wide range of operating frequencies. The number of layers in reported designs varies between a single layer to 9 layers.

### **C. Liquid Crystalline Polymer (LCP):**

LCP is a fabrication technology that is utilized in realizing biomedical designs in warped shapes due to the softness of the substrate. The fabricated planar structure could be warped in different shapes according to the desired application. Moreover, LCP constitute a promising approach for antenna design in millimeter waves due to its flexibility, low weight and cost, low moisture, and RF stability characteristics.

For instant, in [77] an omnidirectional patch antenna was reported for endoscopy applications. The design structure and dimensions are shown in Figure 9. The antenna was designed to operate at 433 MHz ISM band since it is less lossy and wireless communication signals require lower power to propagate through human body in this band. The design was fabricated on Liquid Crystalline polymer (LCP) substrate of 4 mils (0.1 mm) thickness and  $\epsilon_r = 2.9$  then it was coated using poly-di-methyl-siloxane (PDMS) layer of 0.5 mm thickness to avoid interaction between inside human body and metallic surface of antenna. The stretched design has dimensions of  $31 \times 18.5 \times 0.6 \text{ mm}^3$ .

The design simulations utilized a numerical human-body model in HFSS as surrounding environment. The HFSS simulations show that the  $62.8 \times 18.5 \text{ mm}^2$  designed antenna resonates at 1.38 GHz. To reduce the resonance frequency, an inductive loading was applied by inserting 39 pairs of notches in the patch. Every notch has dimensions of  $9.15 \times 0.25 \text{ mm}^2$  and gives 0.1 nH inductive loading. The fabricated coated antenna was tested in: air, human hand, and phantom solution and it resonates at 538 MHz, 428 MHz and 430 MHz, respectively. The bare antenna resonates at 540 MHz. Due to the small size of antenna ( $0.07\lambda$ ), the measured gain was -9.6 dBi, however, and its radiation efficiency was 49% in free space and 47.1% in 20g human-body phantom. The deviation in radiation pattern between simulation and measurements was attributed to asymmetrical  $\epsilon_r$  and  $\sigma$  discrepancies in human body. Folding the antenna in cylindrical capsule shape offers: a room for electronic circuits, mechanical support, in addition to electro-magnetic isolation (EMI) between patch and electronics (due to ground plane).

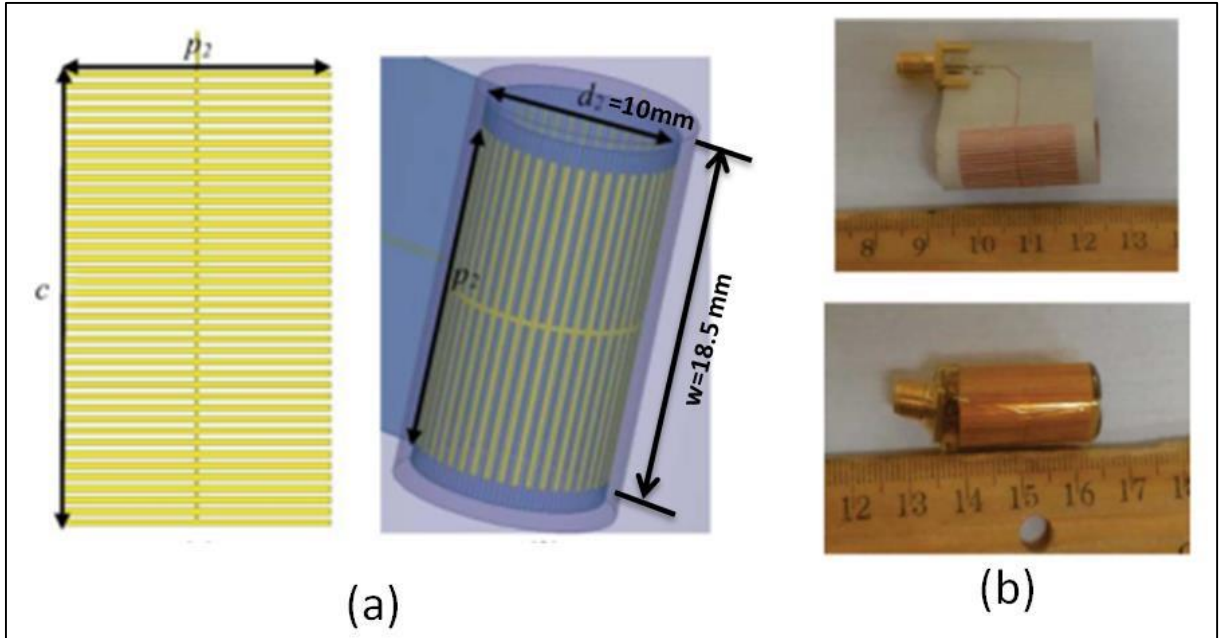


**Figure 9: Omnidirectional Compact patch antenna: (a) simulated design, (b) Final fabricated device [77]**

Furthermore, a design of bowtie antenna for system on package application is reported in [78]. The design is based on LCP substrate with  $\epsilon_r = 2.9$ ,  $\tan \delta = 0.0025$  and thickness of 0.1 mm, as illustrated in Figure 10(a). The bowtie antenna has size of  $4 \times 8.53 \times 0.1 \text{ mm}^3$  and it is fed utilizing a balun to match coplanar waveguide to coplanar strip. The size of ground is optimized for desired radiation characteristics, i.e. gain and matching. The antenna resonates around 24 GHz with a bandwidth of 4.06 GHz. Due to flexibility in LCP substrate, the designed antenna can be bent at different angles, see Figure 10(b). The resonance frequency shifts 1.4 GHz range for bend angles below  $20^\circ - 90^\circ$  with maintaining same directivity. However, for bend angles  $20^\circ - 90^\circ$ , the resonance frequency is maintained with change in maximum gain direction. The proposed design has an average gain of 3.8 dBi with a peak gain of 4.6 dBi.



Due to some limitations in fabrication, the design is scaled down to 5.8 GHz. The fabricated antenna has a bandwidth of 1.19 GHz with a measured peak gain of 5.1 GHz. Around 650 MHz frequency shift is achieved by two different bents.

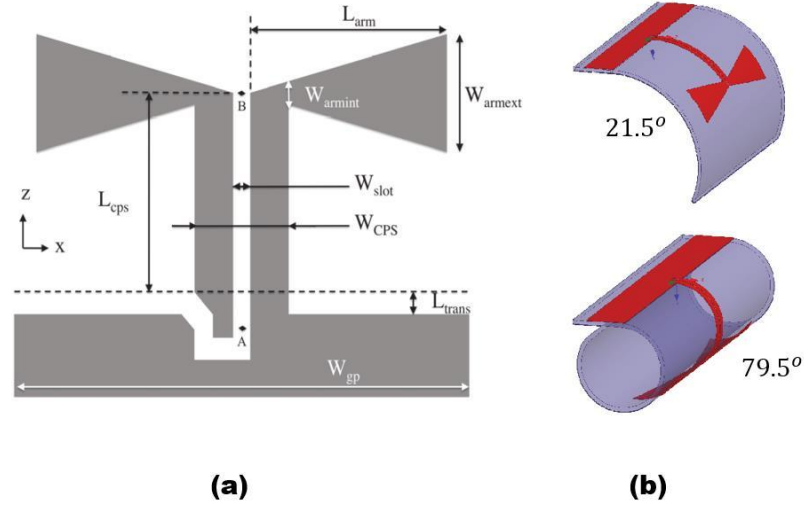


**Figure 10: Geometry of proposed design [78]**

As mentioned in section 2.1.1, on-chip antennas constitute an attractive solution for antenna realization in millimeter wave. In this approach, the antenna is co-designed with circuits and they are fabrication on same substrate of semiconductor material. The common semiconductor materials used to realize on-chip antennas are Silicon (Si) and Gallium Arsenide (GaAs) with dielectric constants of 11.68 and 12.9, respectively. However, the major drawback of semiconductor substrate is their conductivity that leads to high loss in transmitted/received signals [4]. For example, in [79], on-chip dipole based antenna for V-band is reported and antenna structure is shown in Figure 11. The antenna was realized using WIN 0.15  $\mu m$  pseudomorphic high electron mobility transistor (pHEMT) technology on GaAs substrate with dielectric constant of 12.9, loss tangents of 0.005 and volume of  $0.9 \times 1 \times 0.5 \text{ mm}^3$ . The dipole antenna is fed through coplanar strip line with parallel open

stubs to increase the BW and suppress the backside radiation due opposite directions of currents. Inserting the tilted and slotted dipole enhances the directivity and increases the bandwidth due to current multipath. Shorting slotted dipole increases front-to-back radiation from 5dB to 12dB and decreases the cross-polarization to -19dB from -22 dB. Measurement indicates that antenna resonate around 60 GHz with -10dB bandwidth of 24% from 55 to 70 GHz and VSWR of 2. To measure antenna radiation pattern, a three antennas test (A, B and C) is applied to overcome limitations of two antennas test. The spacing distance (r) should satisfy far field condition of:

$$r \geq \frac{2D^2}{\lambda_0} \quad (2.4)$$

Where D is the maximum dimension of antenna and  $\lambda_0$  is free-space wavelength.

The antenna absolute gain was calculated using given formula [79]:

$$G_A^2 = 20 \log_{10} \left( \frac{4\pi r}{\lambda} \right) + 10 \log_{10} \left( \frac{P_t}{P_r} \right)_{BC} + 10 \log_{10} \left( \frac{P_t}{P_r} \right)_{AC} - 10 \log_{10} \left( \frac{P_t}{P_r} \right)_{AB} \quad (2.5)$$

Where, A is antenna under test (AUT) which is the proposed antenna and  $P_t$  and  $P_r$  are transmitted and received powers in dB scale.

The antenna had a measured absolute gain of 3.6 dBi and 12dB front-to-side ratio.

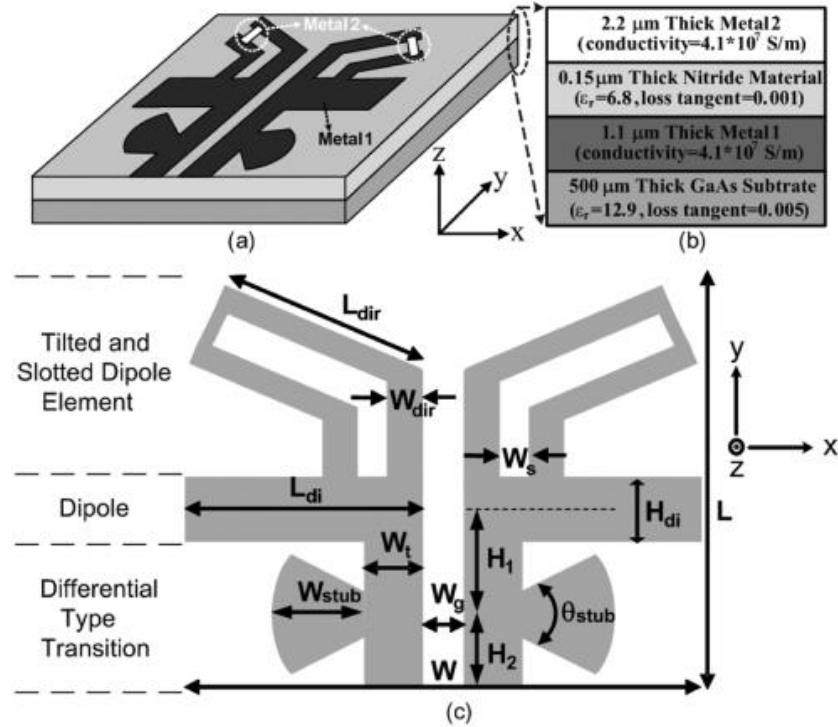


Figure 11: Geometry of proposed antenna [79]

Moreover, in [80], an integrated multi-loop dipoles based on-chip antenna with inductive and resistive loading has been proposed for wireless powering and communication of RFID tags. On-chip antennas constitute low cost and compact size solutions for RFID designs. The proposed design has a size of  $4.5 \text{ mm}^2$  ( $3 \times 1.5$ ) and to be realized on the upper layer of  $0.18 \mu\text{m}$  CMOS. The proposed tag system consists of UWB transmitter antenna that operates on the uplink frequency and used to send information to reader. The receiver antenna operated at ultra high frequency (UHF) band around 5.8 GHz downlink frequency. Each antenna was a dipole antenna loaded with two inductive stubs and resistive stub. The structure of the system design is shown in Figure 12(a) while Figure 12(b) present antennas geometry to decrease imaginary to real ratio. Antenna performance matrix is summarized

in Table 2. The proposed on-Chip antenna (OCA) covers distance of 7.5 cm for power scavenging and 7 cm for UWB data communication.

Table 2: Performance Matrix of Proposed Designs in [80]

	Scavenging antenna	Tx. Antenna
<b>Resonance Frequency</b>	5.8 GHz	UWB (3.5-6.5 GHz)
<b>Bandwidth (BW)</b>	> 50 MHz	> 500 MHz
<b>Radiation Pattern</b>	Omni-directional	Omni-directional
<b>Input Impedance</b>	$10 - j160 \Omega$	$52 - j125 \Omega$
<b>Radiation Gain</b>	-29.5 dBi	

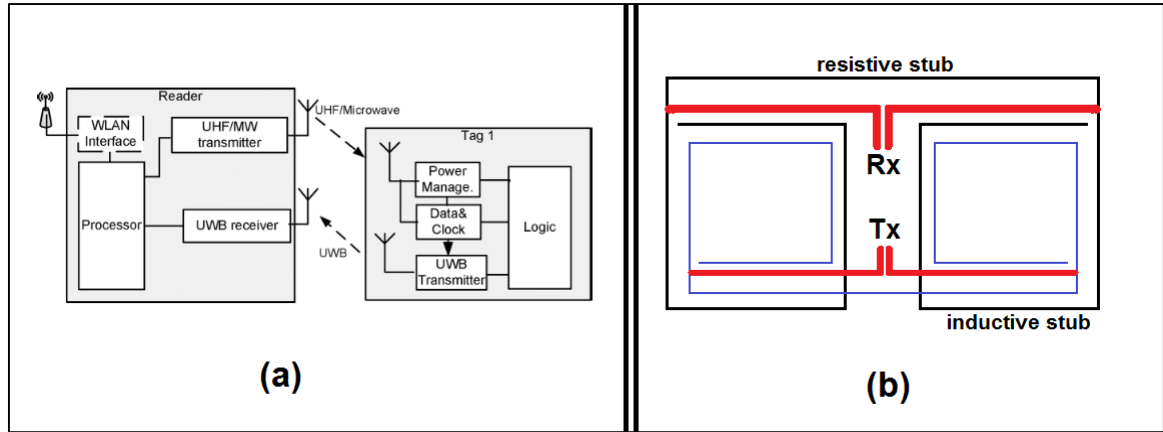


Figure 12: Proposed design [80]

#### D. Other Fabrication technologies:

There are some other fabrication technologies such as: patterning, textile, and multilayer organic. In this subsection, a summary of published design is presented as an example of each technology.

- Patterning:

In [82], a circular patch antenna with polarization reconfigurability is proposed for mobile communications at K-band. K-band includes frequencies from 18 GHz to 27 GHz and it is utilized for satellite and radar applications. To avoid the huge insertion loss in semiconductor switches at high frequencies, radio frequency micro-electro-mechanical system (RF-MEMS) switch is selected for this design. RF-MEMS switches requires a protection from surrounding environment. The switch configures the antenna polarization to be either linear or circular. Circular polarization can be achieved if the antenna radiates fields in orthogonal directions, with 90° phase shift.

The design geometry is illustrated in Figure 13 and it consisted of three layers. Top layer has a disk patch as main radiator on quartz substrate with a size of  $10 \times 7 \text{ mm}^2$ ,  $\epsilon_r = 3.78$  and  $\tan \delta = 0.04$ . This structure is suitable for aperture feeding. The bottom layer has a ring slot as coupling element on a glass substrate with  $\epsilon_r = 4.8$ ,  $\tan \delta = 0.05$ . The ground plane and bottom layer have a size of  $11 \times 10 \text{ mm}^2$ . A stub is added to the ring slot with 90° phase shift from the feed line. RF-MEMS switch is integrated on this stub such that, if the switch is OFF, radiation is linearly polarized and when the switch is ON, radiation is circularly polarized. To integrate the MEMS switch, an air cavity is created by building a silicon rim underneath the top layer.

The fabrication is based on patterning using lift-off process and it is summarized in the reference. The fabricated model has impedance bandwidths of 4.5 GHz (17.4-21.9 GHz) and 5.6 GHz (16.9-22.5 GHz) for linear and circular polarization states,

respectively. Antenna has measured peak gains of 2.63 dBi and 3.9 dBi for linear and circular polarization states, respectively around 21 GHz.

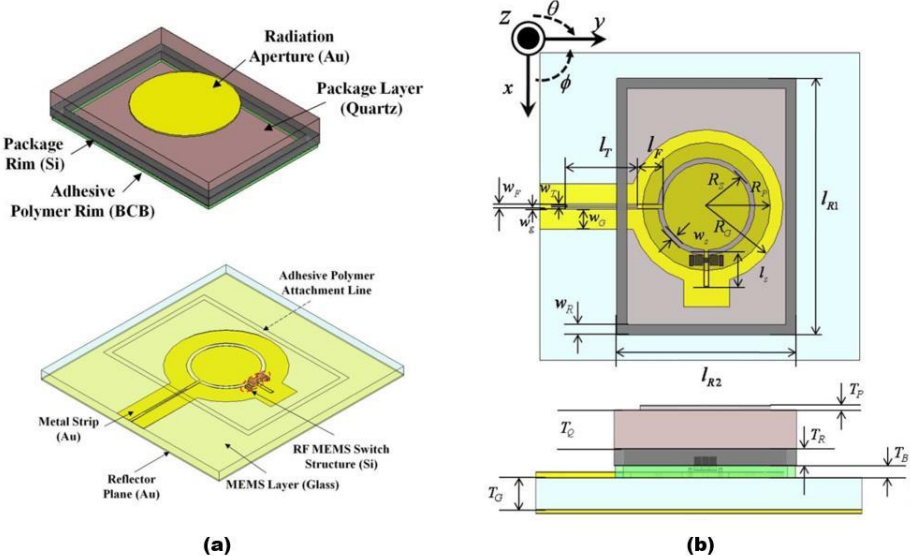


Figure 13: Geometry of proposed design [82]

- E-fiber Textile:

In [81], a textile antenna is proposed for biomedical applications. The design is based on sewing the proposed design on body-worn textiles. The utilized thread in embroidery process is a bundle of e-fiber strands (664 strands per bundle). The e-fiber strand is constructed from thin silver conductors coated with 6-benzobisoxazole, p-phenylene-2 fibers to have  $15 \mu m$  strand. The microstrip structures can be sewn on polydimethylsiloxane (PDMS) substrate to have a full design. This fabrication approach seems to be attractive in biomedical applications since embroidered structures are more robust and have flexibility of bending. E-fiber has 0.07 dB/cm as insertion loss at 1 GHz and 0.15 dB/cm at 2 GHz. Moreover, 332 e-fiber strands have a resistivity of  $0.8 \Omega/m$ .

A multiband patch antenna is designed to operate in three frequency bands, GSM (0.85 GHz), PCS (1.9 GHz) and WLAN (2.45 GHz). The design consists of two elements with inset slots connected with loaded loop, as illustrated in Figure 14. The design is embroidered on PDMS substrate that has  $\epsilon_r = 3$  and  $\tan \delta = 0.01$ . The design has overall impedance bandwidth of 1150 MHz shared by these communication bands. The design has a realized gain of 2 dB. The fabricated antenna maintain same performance even after several washes and drying. Moreover, the design of textile sensor is discussed in the same reference.

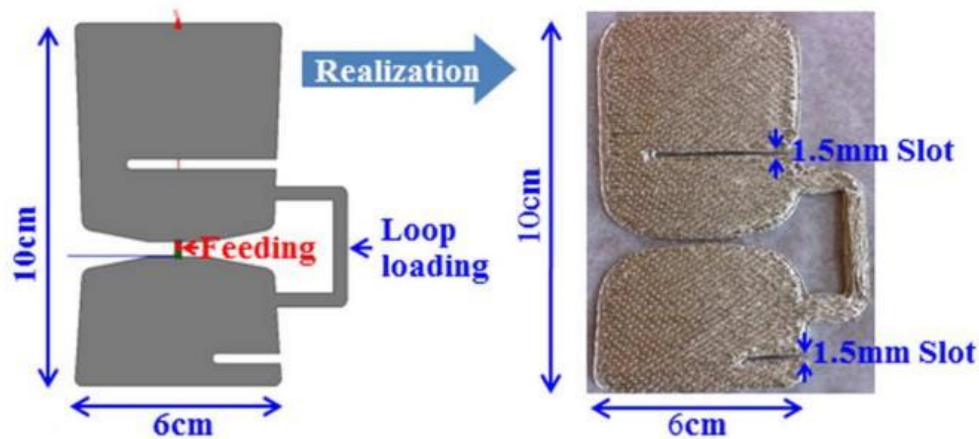


Figure 14: Geometry of Textile design [81]

- Multilayer Organic:

The design of two different models of on-package antennas is discussed in [73] for wireless applications. The first antenna is designed on LTCC substrate with dielectric constant of 7.8 and has a size of  $9.02 \times 9.02 \times 0.75 \text{ mm}^3$ , see Figure 15(a). The ground plane has a size of  $13 \times 13 \text{ mm}^2$ . The proposed antenna is fed thru via that is located to have matched impedance. The design consist of patch antenna with backed cavity obtained by surrounding the patch with several via shorted to

ground. This antenna is proposed to be embedded in RF-blocks. The design has a center frequency of 5.8 GHz with an impedance bandwidth of 69.6 MHz (1.2%). The antenna has broadside radiation pattern with peak gain of 2.7 dBi and 48% radiation efficiency. Obviously, increasing the substrate thickness yields in a higher bandwidth.

The second design consist of a patch antenna on multi-layer organic (MLO) package. The design has FR-4 substrate as main core and it has been coated with organic material with 0.03 mm thickness and 3.7 relative permittivity, as shown in Figure 15(b). The design resonates around 5.8 GHz with 817 MHz (14%) bandwidth and has a peak gain of 3.7 dBi.

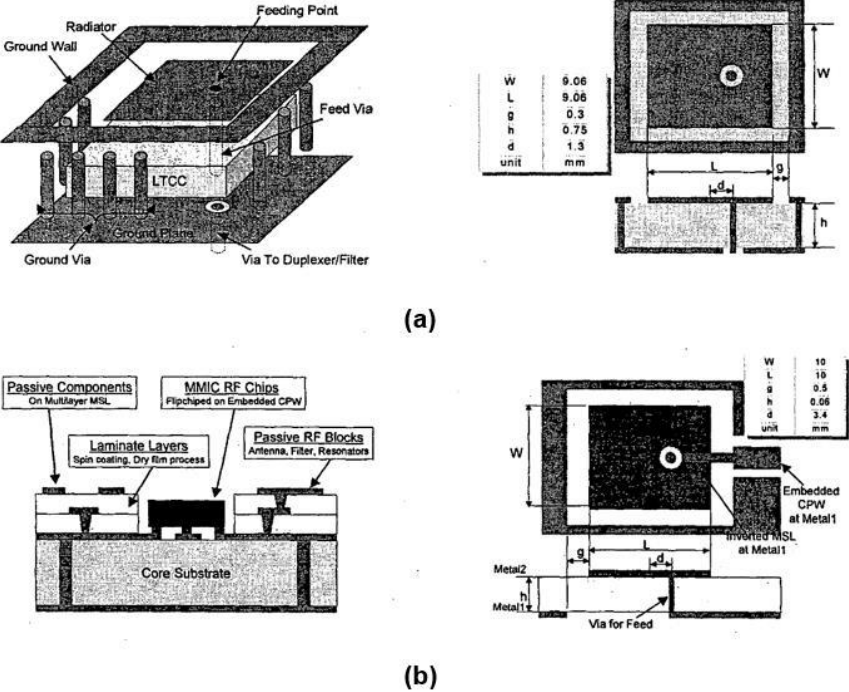


Figure 15: Geometry of proposed design [73]



## 2.2.2 Classification According to Operating Frequency

The proposed designs of on-package antennas in literature can be classified according to their operating frequencies as illustrated in Figure 16. It appears that a lot of on-package designs have been proposed between 1 GHz and 6 GHz. Moreover, the classification tree indicates that few on-package works were proposed to operate at frequencies higher than 10 GHz. Most designs for higher frequency applications utilized on-chip approach in design process rather than on-package approach due to its greater integration capabilities [4]. It is noticed that, in low frequency bands, very few LTCC designs were proposed and thus, this work will focus on investigating the performance of on-package LTCC based antennas for biomedical applications, as well as PCB based ones with new geometries and multi-band operations.

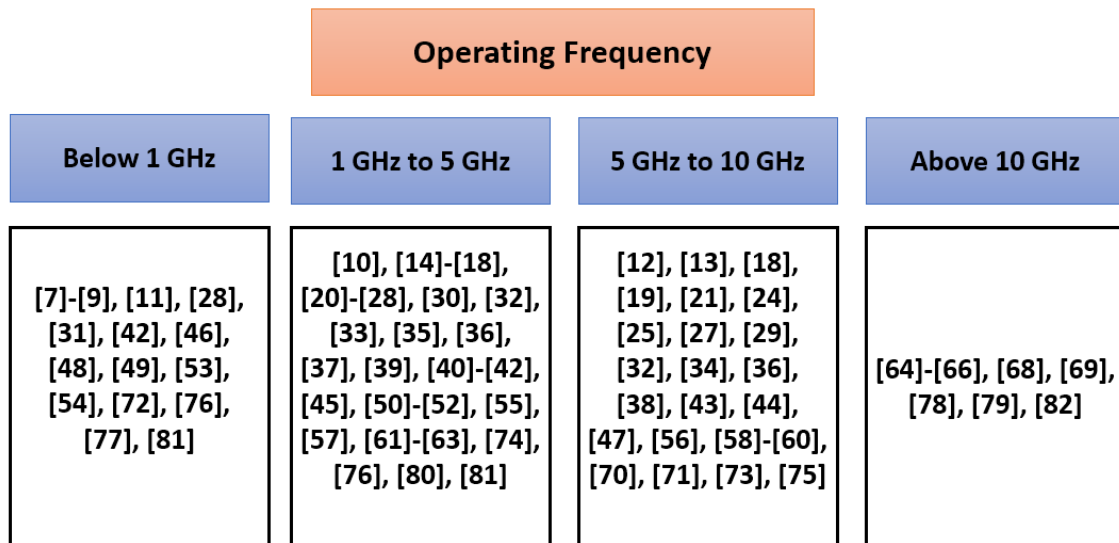


Figure 16: Classification Tree According to Operating Frequency

### 2.2.3 Classification According to Applications

Classification tree of previous designs in literature that are considered in this study is illustrated in Figure 17. The classification is based on stated applications which includes: biomedical purposes, high data rate communications, device integration applications, wireless personal area network (WPAN) and wireless local area network (WLAN) applications, wireless power transfer (WPT) and RF-energy harvesting applications and general purposes wireless communications. Biomedical applications varies between implantable medical telemetry, endoscopy, and monitoring. It is clear that, few works in literature considered LTCC and dual band PCB based antennas for biomedical applications especially around low frequency bands. [71] and [76] reported and LTCC based designs with operating bands around 5.2 GHz and 915 MHz.

Moreover, the classification tree shows that, large effort was spent to integrate antenna within different types of devices such as: handheld and portable devices and phones, sensors, RADARs, GPS, landmine detectors, and USB dongles.

Figure 17 shows that, most of reported designs for short range, high data rate applications utilized LTCC based antenna due to the high performance, low loss capabilities of LTCC designs. Moreover, considerable number of works proposed antenna designs for WPAN and WLAN communication applications, which reflects the need for high quality designs in this field. Furthermore, reported designs of WPT and energy harvesting applications considered radio frequency identification (RFID) and general biomedical purposes. On the other hand, several works did not clarify the exact type of application that they were targeting thus, these work are included under general purposed wireless communication category.

Applications					
Biomedical	High data-rate COMM	Device Integration	WPAN/WLAN	WPT RF-Energy harvesting	General Purposes wireless COMM
[7]-[11], [45], [49]-[55], [71], [76], [77], [81],	[57]-[59], [64], [65], [67], [70],	[15], [16], [18], [19], [29]-[33], [35], [37]-[39], [42], [48], [56], [59], [60], [62], [63], [66], [73], [75], [78], [82]	[13], [14], [21]-[23], [26], [27], [36], [41], [43], [44], [68], [79],	[17], [28], [46], [80],	[12], [20], [24], [25], [34], [40], [47], [61], [69], [72], [74], [83]

Figure 17: Classification According to Design Application

#### 2.2.4 Tabulated Summary of previous work in literature

A detailed summary of previous on-package designs in literature, that are considered under the scope of this work, is provided in Table 3 with detailed features of each.

**Table 3: Tabulated Summary of Design Characteristics in Literature Review**

Ref	Fabrication Technology	# layers	Material	$\epsilon_r$	$\tan \delta$	Size	$f_r$	BW	Gain	Application	Antenna Type
[ 2 ]	LCP	1	Liquid Crystalline Polymer	2.9		31×18.5×0.6	0.433	30	-9.6 dBi	Biomedical Endoscopy	Patch - loaded with slots
[ 3 ]	PCB	1	Rogers 3010/skin phantom	10.2/40	0.003	10×16×1.27	0.403	96	-30.5 dBi	Biomedical-Telemetry	Patch - with slotted ground
[ 4 ]	PCB	1-3	Rogers 3210/mimic skin	10.8/46.72	0.0027	12×12×1.8	0.403			Implantable Medical Telemetry	Patch - circular with slots
[ 6 ]	PCB	1	FR-4	3.48		10×12×1.52	0.44	180		Biomedical	Patch - slotted
[ 7 ]	LTCC	5	DuPont 951	7.8	0.0004	10.3×10.3×1.3	5.2 - 5.355	140	-0.08 / -0.17 dBi	Device Integration	Patch - stacked
[ 8 ]	LTCC	3	Ferro A6-M	5.9	0.0026	12×20×0.58	4.005	2010	2.29 dBi	High Data Rate Communication	Monopole - rectangular
[ 8 ]	LTCC	3	Ferro A6-M	5.9	0.0026	12×20×0.58	3.555	1230	2.08 dBi	High Data Rate Communication	Monopole - rectangular
[ 8 ]	LTCC	3	Ferro A6-M	5.9	0.0026	9×12×0.58	3.8	1640	1.72 dBi	High Data Rate Communication	Monopole - rectangular
[ 9 ]	LTCC	1	DuPont 951	7.8	0.0015	66×50×1	7.5	9000	3.65 dBi	High Data Rate Communication	Slot - volcano smoke
[ 10 ]	PCB	2	Silicon/ skin phantom	11.68/68	0.2677	2.88×1×0.332	2.4-5.2		-29 dBi	Biomedical-Glaucoma Monitoring	Monopole (loaded) + Loop
[ 11 ]	LTCC	1-2	GL-550	5.7	0.0006	35×40×1	7.5	9500	7.5 dB	Wideband Applications	Slot
[ 12 ]	LTCC	2	DuPont 951	7.8	0.006	10.5×7×2.06	10	680	5.4 dBi	System On Package Applications	Patch

Ref	Fabrication Technology	# layers	Material	$\epsilon_r$	$\tan \delta$	Size	$f_r$	BW	Gain	Application	Antenna Type
[ 13 ]	LTCC	1	LTCC	5.9		41×37×0.094	4.7	3966.8	3.8 dBi	Wireless Communication Systems	Monopole-modified rectangular
[ 14 ]	LTCC	1	CBS-10 ceramic	6	0.0014	10×10×2	1.575	100		GPS	Monopole-meander
[ 15 ]	LTCC	2	Ferro ULF140	14	0.001	24.9×24.9×4.6	1.23-1.54	40	2.9 dB/5.5 dB	GPS	Patch - stacked
[ 16 ]	LTCC	9	LTCC	7.7	0.002	12×12×1.2	60		9 dBi	High Speed Wireless Communication	Patch + Rings as reflectors
[ 17 ]	LTCC	4	LTCC	7.7	0.002	1.8×1.8×0.45	25	800	8.7 dBi	High Speed Wireless Communication	Patch - with stacked elements
[ 18 ]	Semi-conductor pHEMT	2	GaAr/ Thick Nitride	12.9/6.8	0.005	0.9×1×0.5	60	15000	3.6 dBi	WLAN	Dipole- loaded with stubs
[ 19 ]	Semi-conductor - CMOS	2	Silicon	11.68		3×1.5×	4.5-5.8	550	-29.5 dBi	RFID Wireless Powering And Communication	Dipole- multi loop
[ 20 ]	LTCC	4	CT707/ CT765	6.4/ 64		24×24×4.8	22.5	1000	9 dBi	Radar Front-End	Fractal Array
[ 21 ]	LTCC	1	LTCC	7.8	0.0015	17×8×0.8	7.1	6700	2.3 dBi	Short-Range High Speed Communication	Monopole-Beveled rectangular
[ 22 ]	LTCC	2	DuPont 943	7.4	0.002	5×5×0.625	60	3000		WLAN	Cavity resonance
[ 23 ]	PCB	1	GML1000 woven-glass/skin phantom	3.2/ 55	0.002/ 0.5	105×60×0.76	0.866	5	1.3/ 1.1 dBi	On-Body UHF RFID Tags	Patch - Coupled
[ 24 ]	PCB	4	FR-4	4.4		100×100×1.6	5.8	150	13.5 dB	Wireless Applications	Patch - with parasitic elements
[ 25 ]	LTCC	3	Ferro A6	6	0.002	26×26×2.496	37	5165.2	19.1 dBi	Communication Systems	Array Patch - with artificial magnetic conductor

Ref	Fabrication Technology	# layers	Material	$\epsilon_r$	$\tan \delta$	Size	$f_r$	BW	Gain	Application	Antenna Type
[ 26 ]	PCB	1	FR-4	4.7		28×9×3	5.25-5.775	400	10 dB	WLAN	Patch - Folded
[ 27 ]	PCB	1	FR-4	0		6×18×1.6	2.4	470	3.2 dBi	WLAN	Monopole-PIFA
[ 28 ]	PCB	1	RT Duroid 5870	2.33		76.3×77.6×0.508	3.57	203		Single Chip RF-Transceiver	Dipole - rhomic
[ 29 ]	PCB	3	Ceramic/Silicon	9.7/11.68		37×15×4	2.4	376.8	-0.2 dBi	On Package Applications	Patch - loaded with semiconductor
[ 30 ]	LTCC	1	Ferro A6S	5.9	0.0007	30×25×1.2	5.14	2960	0 dB	Short-Range High Speed Communication	Monopole - rectangular
[ 30 ]	LTCC	1	Ferro A6-S	5.9	0.0007	50×25×1.2	8.32	3350	2.76 dB/5.1 dB	Short-Range High Speed Communication	Antipodal Vivaldi
[ 31 ]	PCB	3	Roger 3010/Skin model	10.2/38	0.0022	4×8×1.28	2.42	100	-19 dBi	Wireless Power Transfer	Patch - inverted-F
[ 32 ]	LTCC	1	Ferro A6-S/Ferrite	6/6		24×20×3.36	5.2	30	4.8 dBi	Biomedical	Loop - rectangular
[ 33 ]	PCB	2	Rogers RO4004/ Foam	3.3/1.05	0.0012	36×42×31	2.4-5.8	1050	5 dBi/ 8.3 dBi	Fall Detection Radar	Dipole - Bowtie
[ 34 ]	PCB	1	Ceramic (SrNiNbO)	25		21×21×7	5.5	18	2.64 dBi	Portable Devices	Loop - rectangular
[ 35 ]	PCB	1	Ceramic	8		16×14×4	1.84	17	0 dB	Wireless Communication	Monopole - looped
[ 36 ]	PCB	2	FR-4	4.4		10×48×0.8	2.4-5.2	284	2.4 dBi/ 2.9 dBi	WLAN	Monopole - two modified PIFA
[ 37 ]	PCB	1	FR-4	4		50×50×0.8	2.44	1050	0 dB	WLAN	Monopole-PIFA

Ref	Fabrication Technology	# layers	Material	$\epsilon_r$	$\tan \delta$	Size	$f_r$	BW	Gain	Application	Antenna Type
[ 38 ]	PCB	1	FR-4	4.36		100×100×1.6	2.4	1680	7.4 dBi	WLAN	Monopole
[ 39 ]	PCB	1	FR-4	4.4	0.001	100×120×1.6	3.1-10.1	12000	5 dBi/ 8.1 dBi	Wireless Applications	Monopole - circular with slot
[ 40 ]	PCB	1	FR-4	4.4	0.018	28×33×1.6	3-4-5.5-9	8890	7 dBi/ 5.5 dBi	Wireless Applications	Monopole - circular with slots
[ 41 ]	PCB	1	FR-4	4.4		15×15×2.8	2.4-2.5	150	2.2 dBi	WLAN / WiMAX	Monopole - PIFA
[ 42 ]	PCB	1	FR-4	4.4		50×60×1.6	2.4-5.2	900	0.8 dBi/ 0.4 dBi	WLAN / HiperLAN	Monopole - stacked inverted-F
[ 43 ]	PCB	1	FR-4	4.4		66×40×10	0.45	64	2.3 dBi	Power Harvesting	Patch - elevated and slotted
[ 44 ]	LTCC	1	DP 9699/FR-4	7.8/4.4		13×9×4.31	0.9	9	-2.36 dBi	Wireless Communication	Monopole - meander line
[ 45 ]	PCB	2	Alumina	9.7		17×17×2	5.15	64	4.6 dBi	Integrated Chip Devices	Patch - Substrate cavity
[ 46 ]	PCB	1	FR-4	4.6		76×38×2.5	2.09	880	1.49 dBi/ 2.64 dBi	Handheld Devices	Inverted-F with slots
[ 47 ]	PCB	1	FR-4	4.4	0.02	16×17×0.15 7	0.6	340	3.29 dBi	Landmine Detection	Dipole-modified bowtie
[ 48 ]	PCB	1	FR-4	4.5	0.025	40×15×0.8	2.45-3-5.5	1426	2.9 dBi	USB Dongle Devices	Monopole - reconfigurable
[ 49 ]	PCB	1	Plastic	4		10×13×0.8	2.45	269.5	1 dB	Printed Inside Stylus Holder	monopole-inverted-F
[ 50 ]	PCB	1	Rohacell	1		20×23×3	5.5	1050	8 dBi	Wireless Applications	Patch- slotted

Ref	Fabrication Technology	# layers	Material	$\epsilon_r$	$\tan \delta$	Size	$f_r$	BW	Gain	Application	Antenna Type
[ 51 ]	PCB	1	Alumina	9.8		11.5×4×1	1.92	190	1.5 dBi	Mobile Hand Set	monopole-meander
[ 52 ]	PCB	1	FR-4	4.7		13×10.2×0.8	2.45-5.25	1230	1.44 dBi/ 5.24 dBi	WLAN	monopole-open loop
[ 53 ]	LTCC	1	LTCC	7.8		9.06×9.06×0.75	5.8	69.6	2.7 dBi	Embedded RF-Blocks	patch- Cavity backed
[ 53 ]	MOL (Multi-layer organic)	3	Organic material/ FR-4	3.7/ 4	0.03	10×10×0.46	5.8	812	3.7 dBi	Digital Applications	Patch
[ 54 ]	e-fibers Textile	2	Poly-dimrthylsiloxane PDMS	3	0.01	100×60×0.5	0.85-1.9-2.45	1150	2 dB	Biomedical-Body-Worn	Patch - loaded
[ 55 ]	PCB	1	FR-4	3.5		25×5×1	2.45	191.5	1.5 dBi	Cellular Phones RF-PCB	monopole-inverted-F
[ 56 ]	PCB	1	GaAr	12.9		4.1×2.1×0.2	5.8	40.4	-9.9 dBi	MMIC Devices	Patch- H-shape
[ 57 ]	PCB	3	GaAr/ FR-4	12.9		53×48×0.508	2.45	75.95	5 dBi	Embedded In Semiconductors	Patch- H-shape with parasitic element
[ 58 ]	Patterning	3	Quartz/ Glass	3.78/ 4.8	0.04/ 0.05	10×7×3.6	20	10100	2.63 dBi/ 3.9 dBi	Mobile Communications	Patch - circular with aperture feeding
[ 59 ]	LCP	1	LCP	2.9	0.0025	4×8.53×0.1	24	4060	4.6 dBi	System On Package Applications	Dipole- bowtie
[ 60 ]	PCB	1	FR-4	4.4		50×56×1.6	2.164-3.59	1377	2.09 dBi	4th Generation (LTE) Applications	Monopole
[ 61 ]	PCB	2	FR-4/ Foam (air)	4.4	0.02	15×20×2.3	2.45	160	1.68 dBi	WLAN	Monopole-PIFA
[ 62 ]	PCB	1	FR-4	4		15×44×9.6	0.85-2.43	1270	-1.04 / 2.26 dBi	Handheld Devices	monopole-inverted-F



Ref	Fabrication Technology	# layers	Material	$\epsilon_r$	$\tan \delta$	Size	$f_r$	BW	Gain	Application	Antenna Type
[ 63 ]	LTCC	2	LTCC/ LTCC	14/6	0.002/ 0.001	80×80×3	1.27	36	5.69 dBi	Wireless Applications	Patch - stacked
[ 64 ]	LTCC	1	Hereaus CT 2000	9.1	0.002	33×30× 1.016	6	800		AoP Applications	Patch- T-shape slotted
[ 65 ]	PCB	1	FR-4	4		3×11×0.8	5.5	1100	3.5 dBi	WLAN	Monopole- T-shape
[ 66 ]	PCB	2	Teflon	2.65	0.002	21×21×138	5.8	1102	13.35 dBi	WLAN	Patch (stacked) + Helix
[ 67 ]	PCB	1	RT Duroid 5880	2.2	0.0009	62.8×60× 0.271	2.4	40	-5.2 dB	Biomedical- Wireless Endoscopy Capsule	Patch - folded with CSRR loading
[ 68 ]	PCB	2	FR-4	4		35×56×12	0.9	20	0.4 dBi	RF- Energy Harvesting	Monopole- array
[ 69 ]	PCB	4		3.38		29.8×30× 4.572	2.49-5.8	360	2.46 dB/ 2.55 dB	Communication Systems	Patch- slotted
[ 70 ]	PCB	2	air	1		21×12×100	9.8	13800	7 dBi	Broadband Wireless Applications	Monopole - rectangular
[ 71 ]	PCB	2	FR-4	4		18×12×18	0.434	5	0.78 dBi	Wireless Sensor Package	Loop- loaded

## 2.3 Summary

To sum up, system on-chip and on-chip antennas are excellent candidates for extremely miniaturized designs for millimeter waves and they open the door for several new applications. In the meantime, system on package and on-package antennas offer an alternative solution for system miniaturization in low frequencies where all system modules can be integrated vertically.

On the other hand, there are several requirements for antenna design for biomedical applications that need to be satisfied. These requirements include biocompatibility, miniaturized size, patient safety, efficient power consumptions. Operating environments are required to be modeled precisely in simulations to achieve realistic results. Phantoms can be utilized to mimic the environment of human tissue in testing the performance of fabricated model.

Moreover, according to conducted literature review, there are several methods to realize On-Package designs depending on their applications. Biomedical applications constitute a hot area for investigation and research.

## CHAPTER 3

### ANTENNA DESIGNS

#### 3.1 DESIGN I: LTCC Based Patch Antenna

The first proposed design is an electrically small, slotted patch antenna designed and simulated on an LTCC substrate for biomedical applications. The proposed design operates in the ISM band centered at 915 MHz and has a size of  $25 \times 25 \times 1.5 \text{ mm}^3$ . The antenna is loaded with a superstrate to prevent direct interaction between the human-body and the metallic layer and support the design stiffness. Several miniaturization techniques are utilized to lower the resonance frequency.

##### 3.1.1 Geometry

As stated in the requirements of biomedical antennas, small size is mandatory. In order to reduce the antenna size, several miniaturization techniques were applied such as:

- Loading with shorting posts each of radius of 0.5 mm.
- Inserting slots on the patch and ground plane.
- Loading the antenna with a superstrate of thickness of 0.5 mm.

The antenna is designed using DuPont 951 LTCC material with  $\epsilon_r$  of 7.8 and  $\tan\delta$  of 0.001 for substrate and superstrate with heights of 1 mm and 0.5 mm, respectively. As illustrated in Figure 18(a), the proposed antenna consists of a patch of  $19 \times 20 \text{ mm}^2$  loaded with seven horizontal slots, each has a width of 0.8 mm, arranged in two groups. The antenna is fed

coaxially and loaded with two shorting posts in the same axis of the feeding point. Two slots are inserted in the horizontal axis of the feed location to optimize the resonance at the desired frequency. On the other hand, as shown in Figure 18 (b), two L-shaped slots are inserted on the ground plane. Symmetric mirror of each slot was created around the vertical axis to increase the current path and enhance the matching. Figure 18(c) shows a side view of the proposed antenna.

Moreover, five horizontal slots, each with width of 0.3 mm are inserted around the middle of ground plane to increase the current path and consequently, reduce the resonance frequency. The modeling and simulation were carried out numerically using HFSS. Note that, setting the exact position of each slot was achieved by optimization and after carrying out several parametric studies.

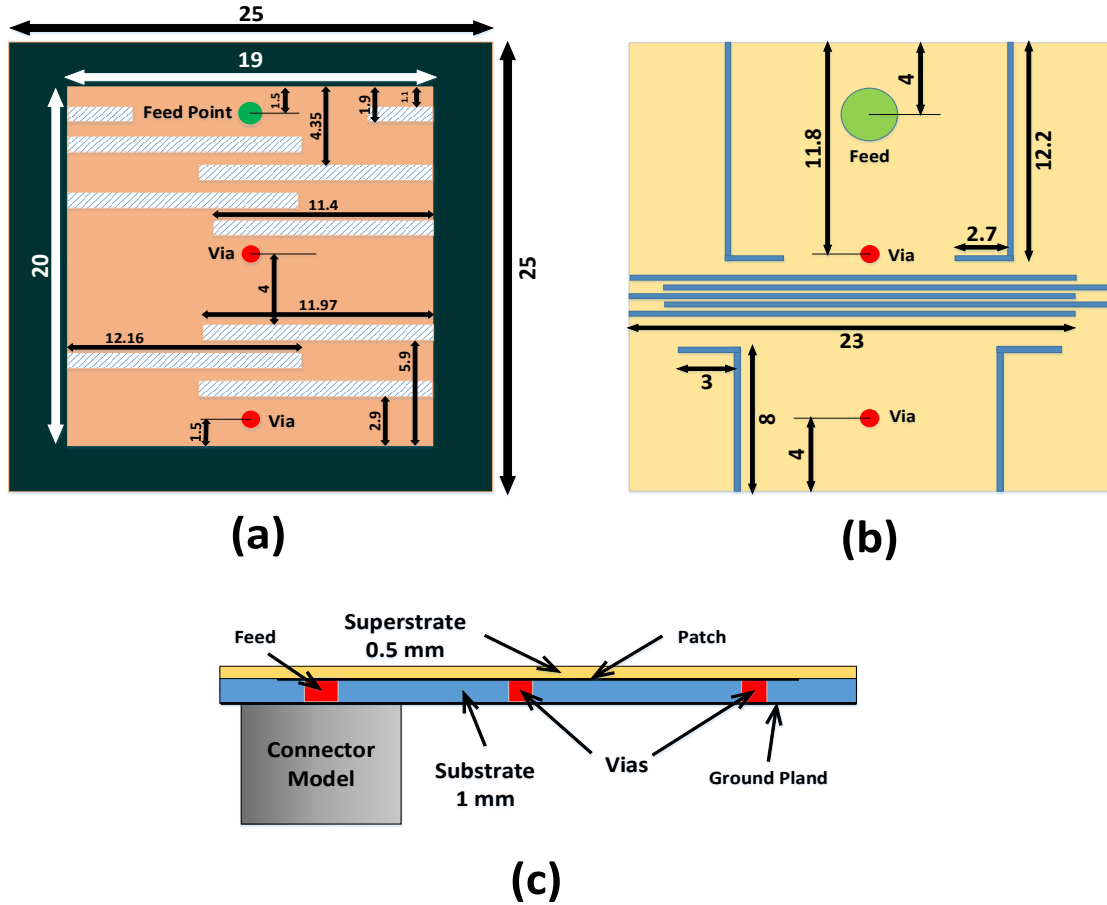


Figure 18: Proposed Antenna Geometry: (a) Top view of patch (superstrate is not shown). (b) Bottom view shows slots on Ground Plane. (c) Side view shows feed location and vias.

### 3.1.2 Design Evolution

To achieve the biocompatibility in the designed antenna, the substrate size was fixed to  $25 \times 25 \text{ mm}^2$ . Without applying any miniaturization technique as shown in Figure 19 (a), the patch antenna resonates around 7.3 GHz as presented in Figure 19 (b). In order to make the antenna resonates at desired frequency band (915 MHz), a shorting post was added in the axis of feeding point. Inserting L-shape slot in ground plan is utilized technique for miniaturization in literature [43], [46], [48]. Therefore, L-shape slot was inserted in ground plan, as shown in Figure 19 (c), however, the antenna resonates at a band higher than the

desired. Thus, the design was modified to have four L-shape slots as an attempt to increase the current path and shift the resonance frequency down, as illustrated in Figure 19 (d). The applied miniaturization techniques in ground plan were not sufficient to set the operating frequency of the proposed design at desired band. Therefore, a pair mirrored slots was inserted on the patch to increase the current path, as presented in Figure 19 (e). It was noticed that, the effect of a single pair was not adequate to set the resonance frequency around 915 MHz, thus, several pairs were added to achieve the miniaturization as shown in Figure 19 (f). Moreover, several optimizations were carried out using HFSS and CST to have robust response and characteristics of proposed design. The design geometry was further modified and the final design is presented in Figure 18.

Figure 20 shows how current distribution affected in a patch antenna by applying miniaturization techniques. Figure 20 (a) illustrates the current distribution in a slot-free patch. Figure 20 (b) shows the altering in current distribution when two shorting posts were added between patch and ground plan. Furthermore, the effect of increasing the current path in a patch by inserting slots is illustrated in Figure 20 (c).

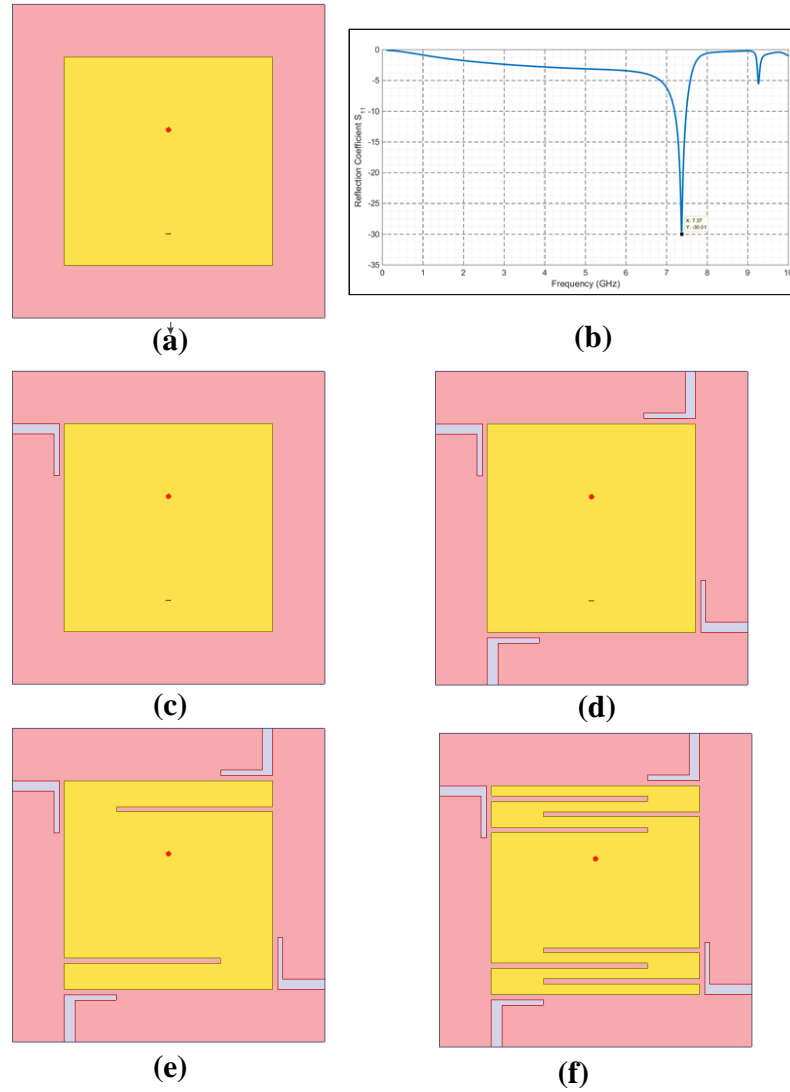


Figure 19: Geometry Evolution of Design-I

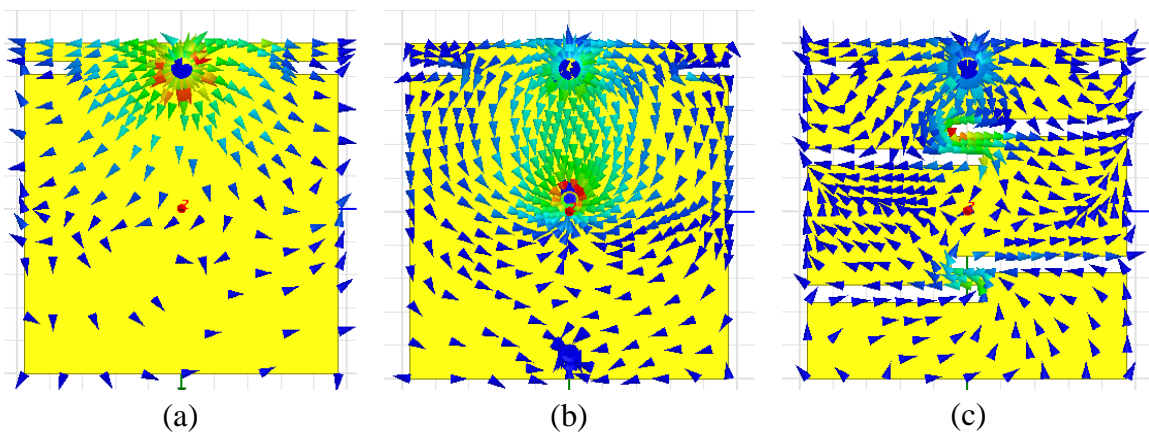


Figure 20: Current distribution in patch: (a) slot-free, (b) with shorting posts, (c) with inserted slots

### 3.1.3 Sensitivity Analysis

Several parametric studies were carried out to investigate the behavior of the proposed design and specify the most effective optimization parameters. The following paragraphs provide various studies with the observed features of each case.

#### A. Number of patch slots:

Increasing the number of inserted slots on the patch increases the current path thus, the resonance frequency of the antenna moves to lower band, as shown in X. The number of inserted slots was determine in the early stage of the design due to geometrical and size limitations.

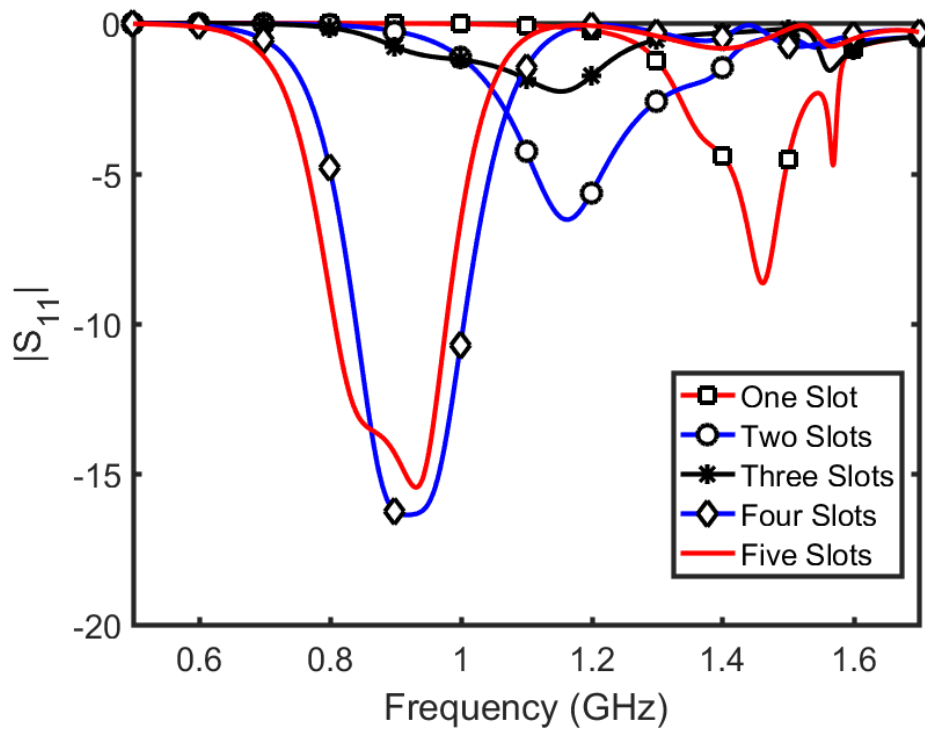


Figure 21: Effect of Number of Slots



### B. Patch slots length:

Figure 22 shows that by increasing the ratio between slot length and patch width, the resonance frequency moves to lower bands. This ratio is used to ease the optimization process and it is the most essential in optimizing the operating frequency of the proposed design. Furthermore, the impedance bandwidth of the antenna gets narrower as the resonance reduces in frequency.

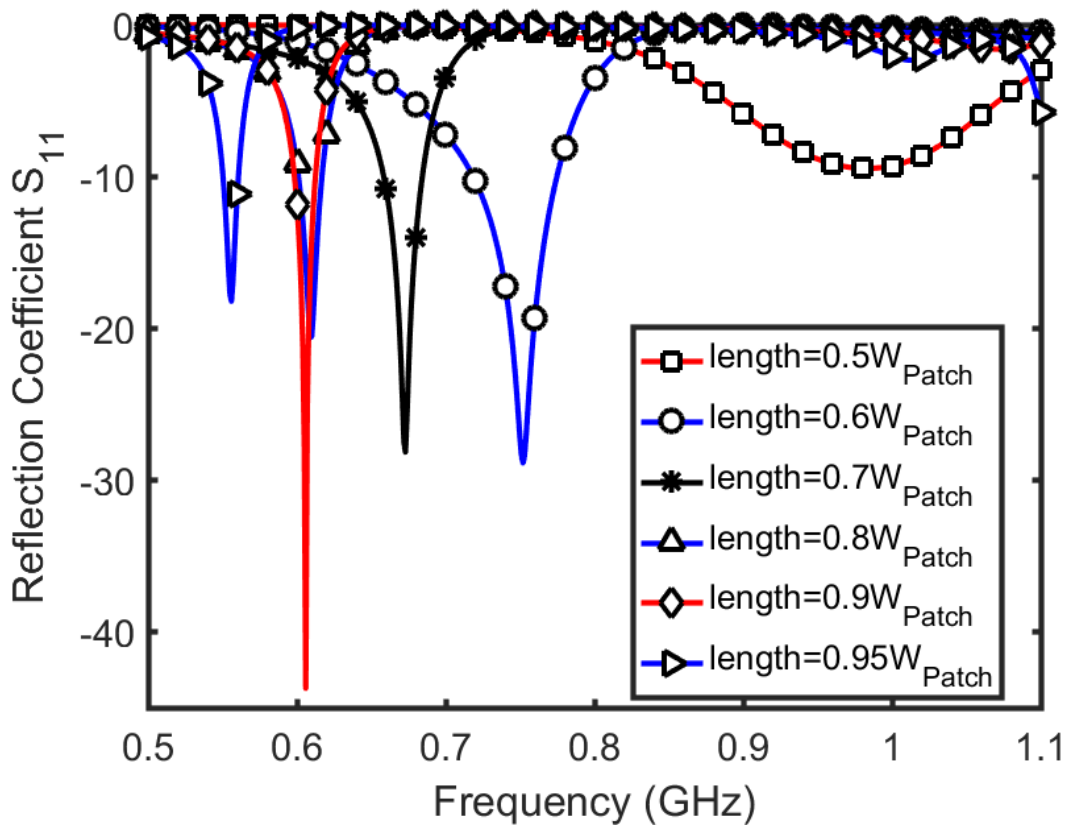


Figure 22: Effect of Length of Slots on Patch

### C. Horizontal Displacement of Feeding:

By changing the position of feeding point horizontally, in parallel to the width of the patch, the resonance frequency is slightly detuned but the impedance matching is affected as shown in Figure 23. This parameter could be used in fine tuning and optimization.

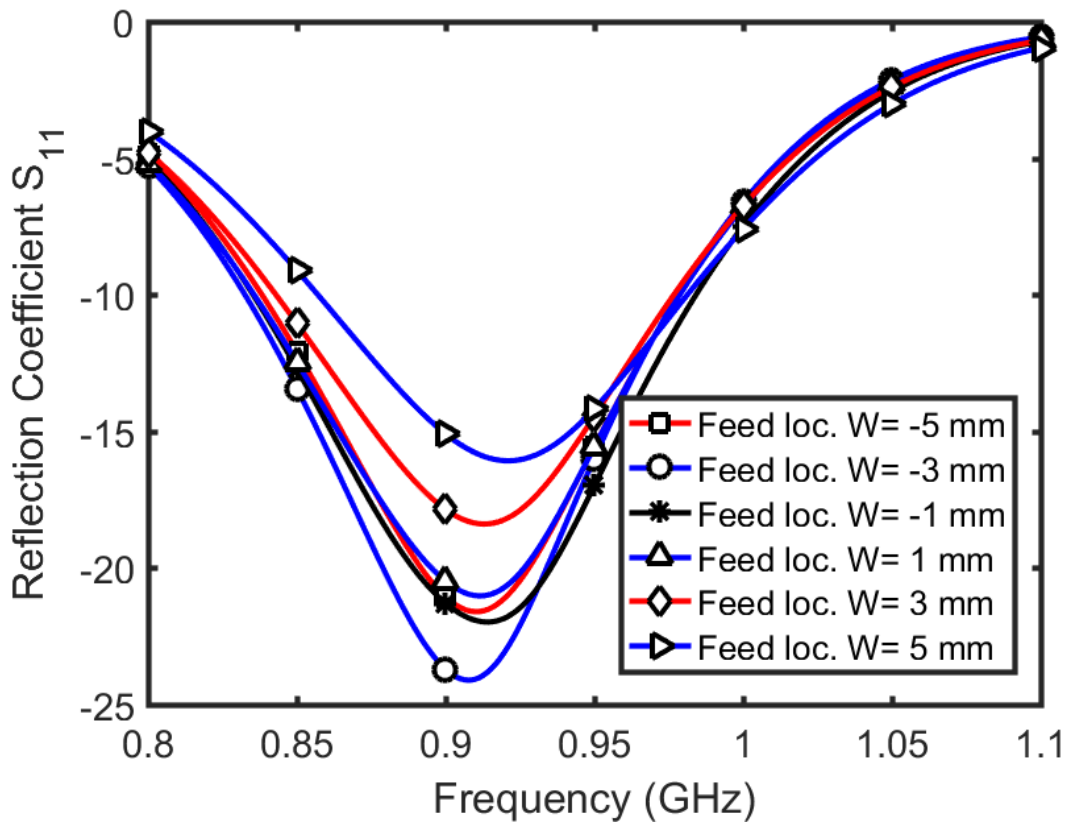


Figure 23: Effect of Horizontal Displacement of Feeding

#### D. Substrate Thickness:

As the substrate thickness increases, the impedance matching decreases and the resonance frequency is slightly shifted downward as illustrated in Figure 24. However, the bandwidth increases as the substrate thickness increases.

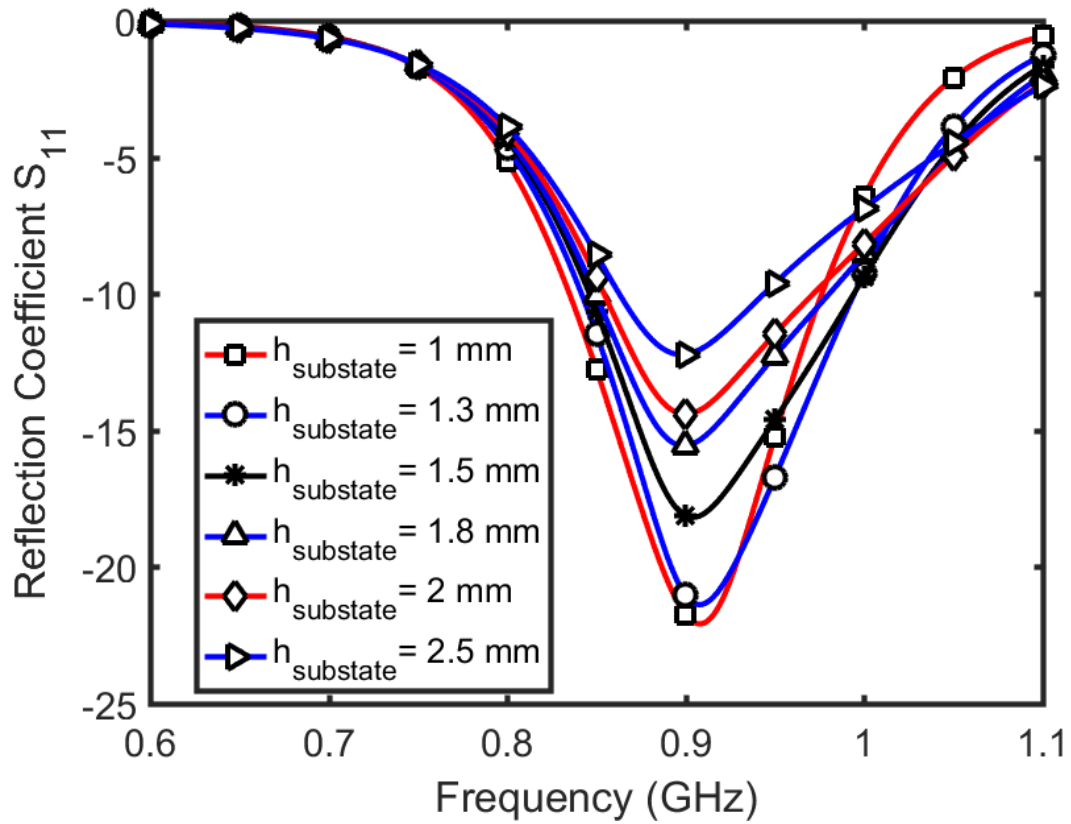


Figure 24: Effect of Substrate Thickness

### E. Superstrate Thickness:

Figure 25 illustrates that increasing the thickness of superstrate shifts the resonance towards higher frequencies. Thus, to achieve better miniaturization, superstrate thickness is required to be minimum.

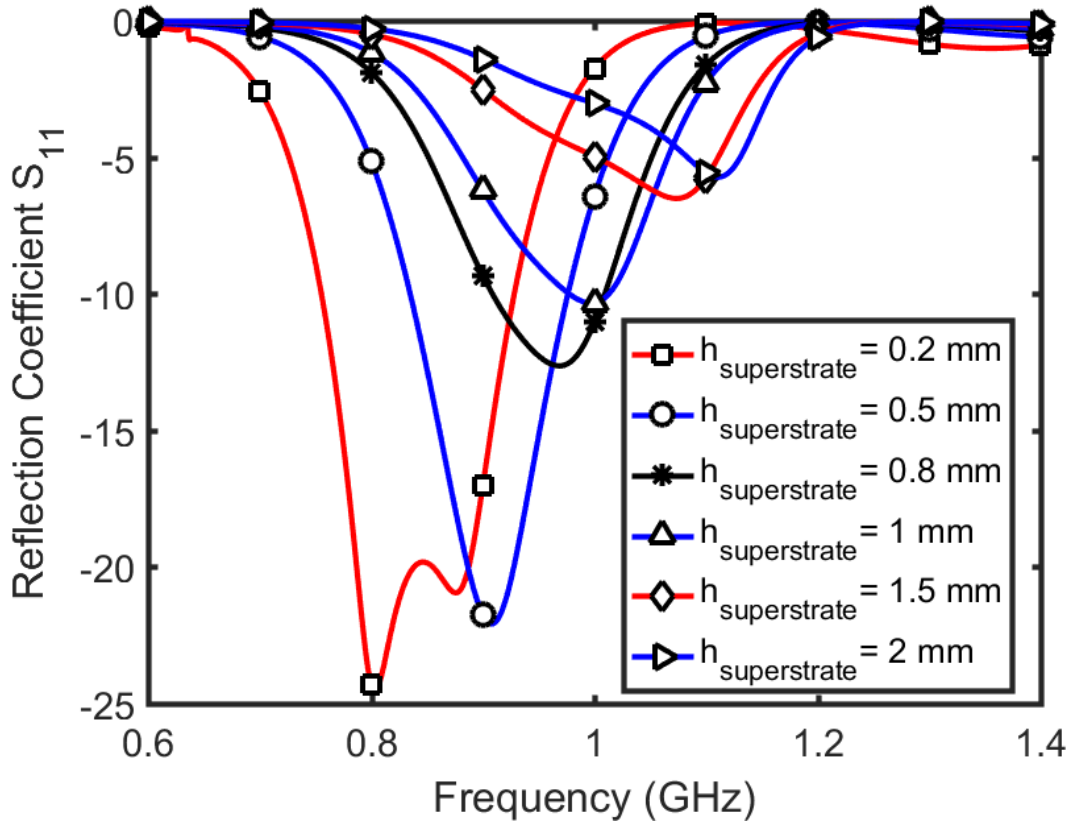


Figure 25: Effect of Superstrate Thickness

### F. Shorting Post Radius:

By increasing the radius of shorting posts, the resonance frequency slightly shifts upward and the matching is considerably improves as shown in Figure 26. Large radius can be used at early stage of design process and other parameters could be utilized to lower the resonance frequency. The freedom in selecting this parameter is restricted by limitations of the fabrication process.

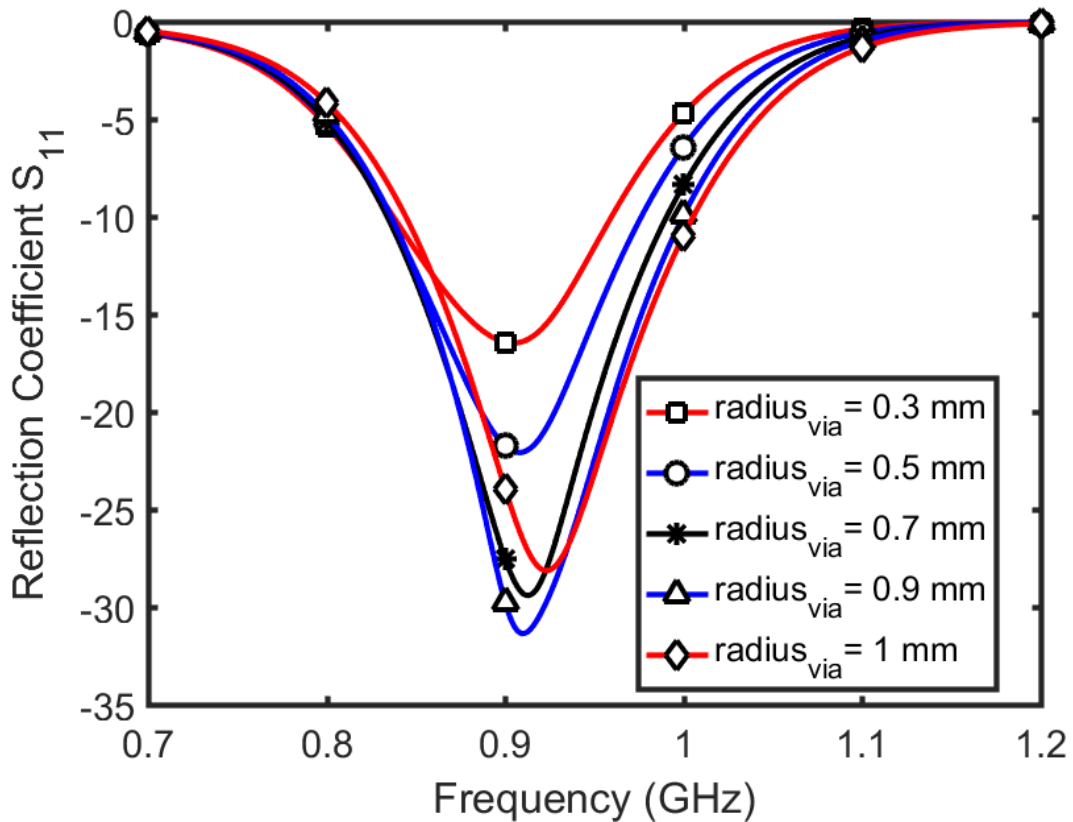


Figure 26: Effect of Changing Shorting Posts Radius

**G. Gap between Ground Middle Slots:**

As presented in Figure 27, by increasing the gap between the slots in the middle of the ground plane, the resonance frequency shifts slightly upward and the matching is degraded as well. However, increasing this gap may participate in easing the fabrication process of given design.

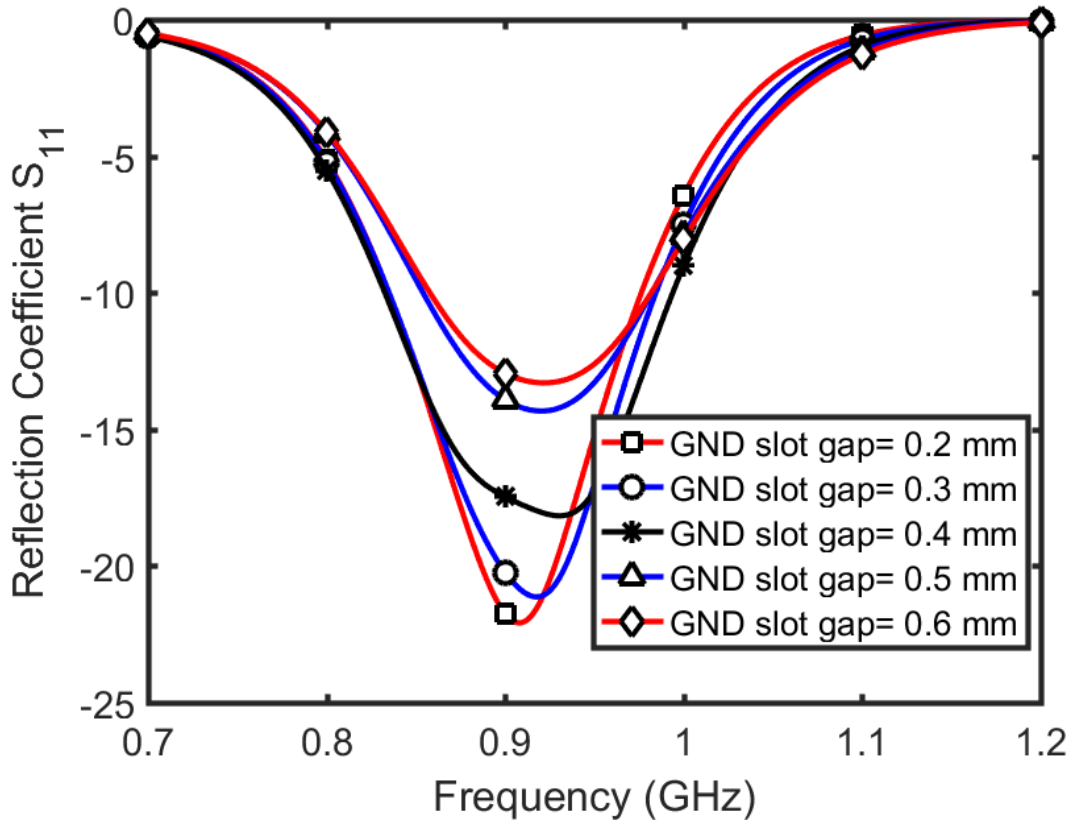


Figure 27: Effect of Changing the Gap between GND Mid Slots

### 3.1.4 Results and Discussions

The slot-free patch of  $20 \times 20 \text{ mm}^2$  resonates originally around 7.37 GHz (in air) as shown in Figure 19 (b) and by applying miniaturization techniques, the resonance is shifted down to 915 MHz. Since the antenna is proposed for biomedical applications, simulations is conducted in free space (air) in addition to skin-loaded antenna case.

#### A. Simulation in Free-Space

The proposed antenna, as shown in Figure 29, is optimized to resonate around 915 MHz in free space. However, a narrow bandwidth of 1.2 MHz in free-space is recorded. This behavior can be analyzed as a result of high quality factor and narrow bandwidth

characteristic of electrically small antennas. Furthermore, loading the antenna with a superstrate with high dielectric constant reduces the bandwidth of operation.

### B. Simulation with Skin Model

Since the proposed antenna is intended to operate while being loaded with human tissues, a numerical model of the skin is required to be included in simulations. The antenna performance on the surface of a human-skin was assessed utilizing a numerical multi-layer skin model that is provided in [76], as illustrated in Figure 28. and do not have constant value.

Table 4 shows the electrical properties of the surface of human-body (dielectric constant and conductivity) at 915 MHz. It is worth mentioning that the electrical properties of human-tissues has dispersive relation with frequency, in other word, electrical properties are a function of frequency and do not have constant value.

Table 4: Electrical Properties of Human-Skin at 915 MHz [76]

Tissue	Dielectric Constant ( $\epsilon_r$ )	Conductivity $\sigma$ (S/m)	Thickness (mm)
Skin	41.19	0.88	2
Fat	11.59	0.092	10
Muscle	55.52	0.902	28

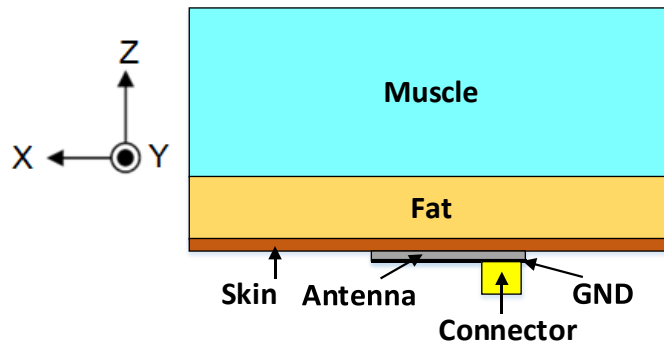


Figure 28: Human-body model used for simulations

Simulation shows that loading the free-space design with skin model yields in resonance around 750 MHz and this is expected with the high permittivity of human tissues. Further optimization on the skin-loaded design is required to resonate at the desired ISM band. Optimization parameters used are the lengths and widths of the antenna slots where the number of inserted slots on the patch was decreased. Thus, the current path decreased and the resonance frequency moved toward higher bands. The feed and via locations are almost fixed. Figure 30 compares between optimized design in free-space in Figure 30(a) and optimized design with skin model in Figure 30(b). The optimized antenna resonates around 915 MHz with an impedance bandwidth of 138 MHz (15%), as presented in Figure 29. The simulated radiation pattern shows that, the proposed antenna has an omnidirectional radiation pattern with a null at the axis of feed point and shorting posts.

The simulations were conducted taking into account the connector effects on fabricated antenna performance. Probe feed SMA connector is modeled and simulated with the proposed design.

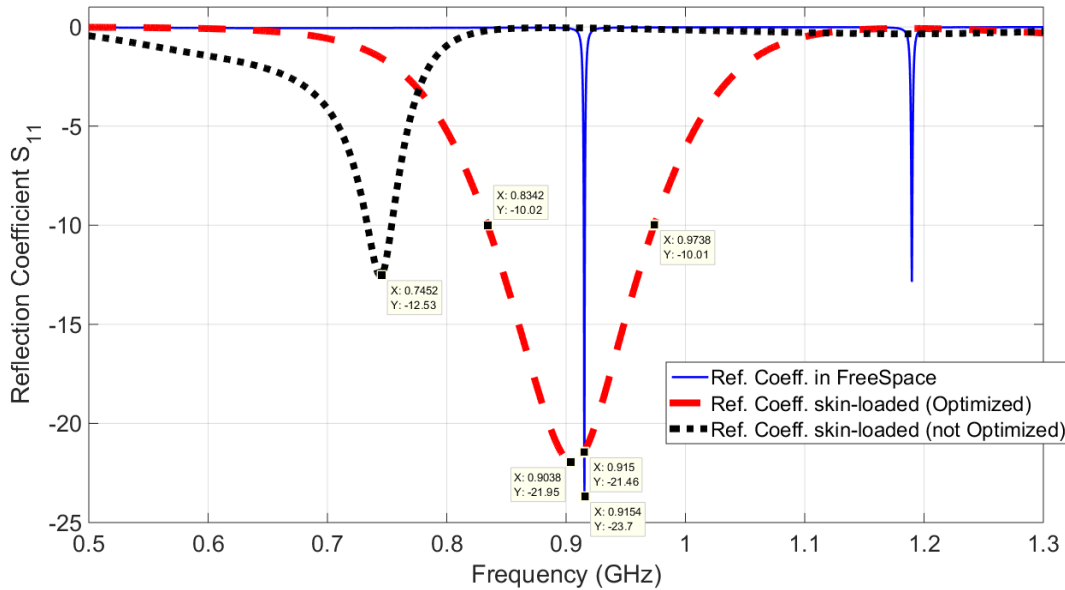


Figure 29: Reflection coefficient of proposed antenna in free-space, on skin model (optimized and non-optimized)



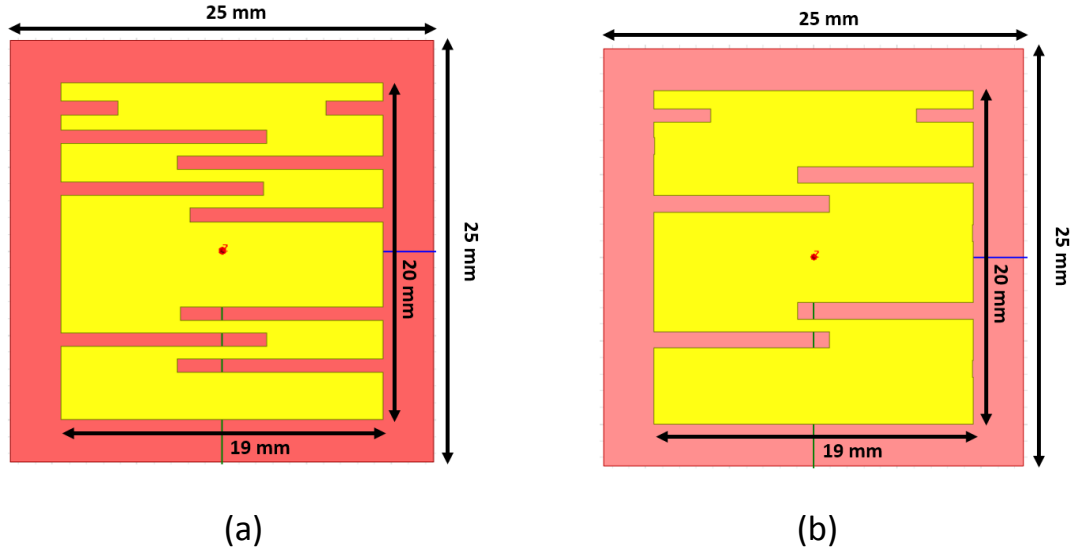
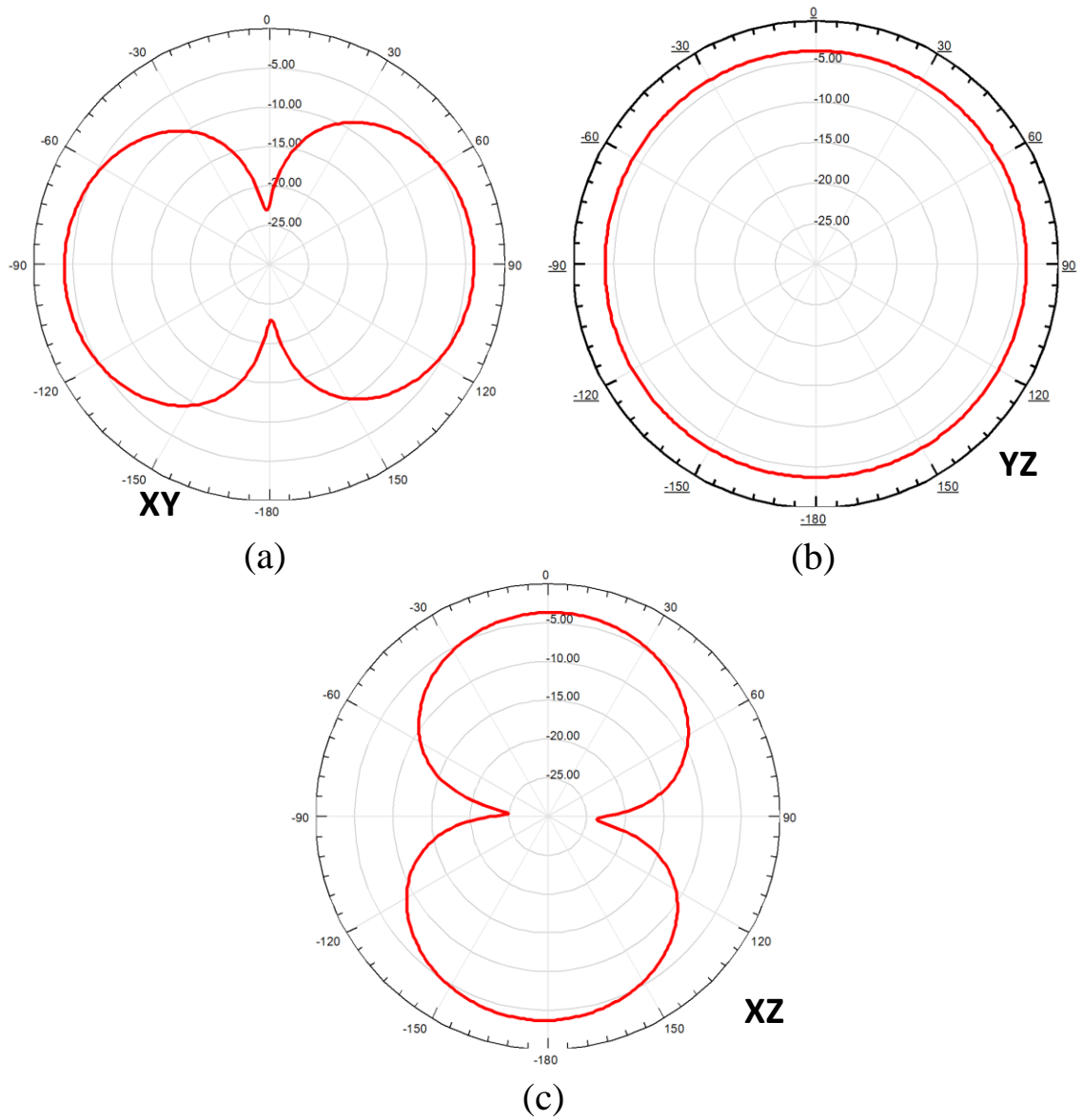


Figure 30: Optimized designs in: (a) Free space (Air). (b) On human-body model

The calculated far field radiation patterns for the proposed antenna indicate that it has omnidirectional radiation pattern as shown in Figure 31 and Figure 32. Emphasizing the fact that the proposed antenna is an electrically small antenna (ESA) can justify its radiation behavior. Figure 31 illustrate the far-field radiation pattern of optimized design in free-space at frequency of 915 MHz. The azimuth plane is presented in Figure 31(a) with the YZ and XZ elevation planes are presented in Figure 31(b) and Figure 31(c), respectively. The calculated realized gain in free space is -3.86 dB at 915 MHz.

The antenna was optimized to operate in very close proximity to human-skin and the radiation patterns were calculated inside numerical skin model. The antenna has a realized gain of -20.8 dB on-skin as shown in Figure 32. The simulation setup used to acquire this radiation pattern is illustrated in Figure 28. The azimuth plane is presented in Figure 32(a) with the YZ and XZ elevation planes are presented in Figure 32(b) and Figure 32(c), respectively. The radiation characteristics shows that antenna has high back radiation, and this is expected due to the fact that this is an electrically small antenna. The radiation

pattern of ESA has similar features to dipole antenna [87]. Moreover, Figure 32 (b) shows that, the proposed antenna is directive inside skin model.



**Figure 31: Far-Field Radiation Pattern of Antenna in Air. (a) Azimuth Plane (XY), (b) Elevation Plane (YZ), (c) Elevation Plane (XZ).**

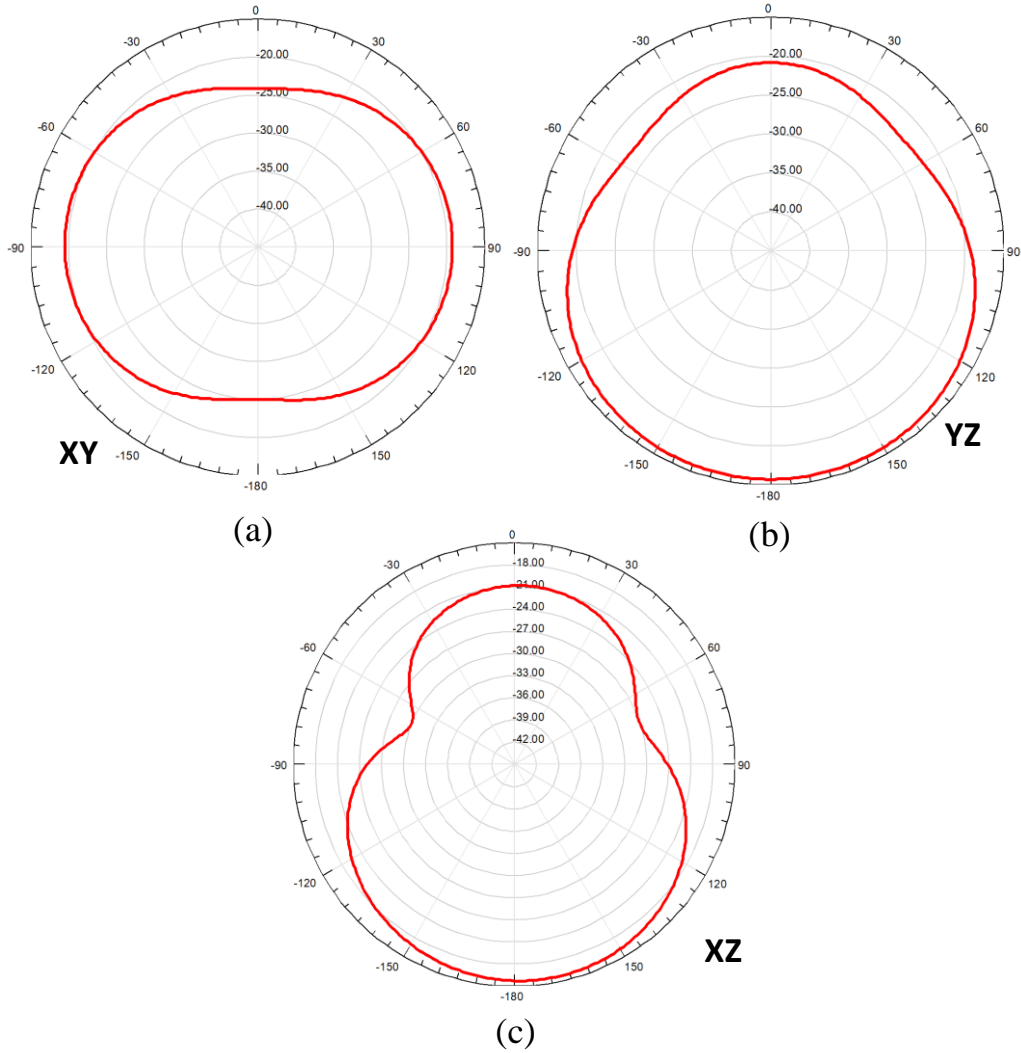


**Figure 32: Far-Field Radiation Pattern of Antenna on-Skin. (a) Azimuth Plane (XY), (b) Elevation Plane (YZ), (c) Elevation Plane (XZ).**

### 3.1.5 Summary of Design-I

The proposed design-I has a large number of optimization parameters that can be used to tune the resonance frequency at a desired value. Sensitivity analysis were carried out to investigate the effect of each parameter on the antenna characteristics and to specify how it can be used to improve the antenna performance. The design occupied  $20 \times 20 \text{ mm}^2$  and had a center frequency of 915 MHz with 139.6 MHz BW when placed on the skin.

## 3.2 DESIGN II: Superstrate Loaded Miniaturized Antenna

The second proposed design is a superstrate loaded miniaturized patch antenna for biomedical applications. The targeted operating frequency is (902-928 MHz) ISM band with a center frequency of 915 MHz. The antenna is designed to operate in close proximity with human-body with a size of 25 x 25 x 1.92 mm<sup>3</sup>. Parametric studies were conducted to specify the dominant parameters and to understand their effect on the antenna performance. Measurements show that the fabricated antenna resonates around 915 MHz with a 30 MHz impedance bandwidth. On-skin measurement results are presented for several spots on the human-body. Furthermore, the transmission coefficient ( $S_{21}$ ) of the fabricated antenna is measured using lean beef slices with various thicknesses and showed good agreement with simulation results.

### 3.2.1 Geometry

The proposed miniaturized patch antenna is fabricated using a two-layer RO3006 substrate with a dielectric constant ( $\epsilon_r$ ) of 6.15 and loss tangents ( $\tan \delta$ ) of 0.002. The antenna has substrate thickness of 1.28 mm while the superstrate thickness is 0.64 mm. The final design had the dimensions of 25 x 25 x 1.92 mm<sup>3</sup> as shown in Figure 33.

Various miniaturization techniques were applied. Mainly, the antenna is loaded with several slots on the patch side and the ground plane to increase the current path, hence, the resonance frequency decreases. In addition, loading the antenna with shorting posts reduced its size even more. First, as shown in Figure 33(a), seven horizontal slots are inserted on the patch. Each slot has a length of 21.85 mm and width of 0.75 mm. Furthermore, two mirrored slots are inserted on both sides of the feeding point with length

of 8 mm and width of 0.75 mm. Moreover, two shorting posts, with 0.5 mm radius, are inserted on the axis of the feeding point. Second, on the ground side, as shown in Figure 33(b), two pairs of L-shaped slots, with thickness of 0.5 mm, are inserted towards the edges. Another four horizontal slots, with thickness of 0.4 mm are inserted around the center of the ground plane. The separation gap between the horizontal slots is kept as 0.4 mm. Third, two shorting posts between the patch and the ground to change the antenna reactance and increase the effective length of the patch, which result in lowering the resonance frequency, are inserted. Since the proposed antenna targets biomedical applications with close proximity to human-body, a numerical multi-layer skin model was utilized for simulations. The skin model has a 20 x 20 cm<sup>2</sup> size and it consists of three layers; skin layer, followed by fat layer and muscle layer as shown in Figure 28. and do not have constant value.

Table 4 presents the thicknesses and electrical properties of each layer in skin model at 915 MHz [101]. The full wave electromagnetic suites CST and HFSS were used to model and optimize the design.

### **3.2.2 Design Evolution**

The proposed design was achieved by adopting Design-I on a Roger RO3006 substrate. Since the dielectric constant of new substrate (Roger  $\epsilon_r=6.15$ ) is lower than LTCC substrate ( $\epsilon_r=7.8$ ), further miniaturization techniques needed to be applied in order to set the resonance frequency at desired band (915 MHz). The dominant optimization parameters were the number and the length of inserted slots on the patch. The optimization process results in having seven slots on the patch instead of four in the previous design. Moreover,

the dimensions of ground slots were modified to optimize the resonance frequency at 915 MHz.

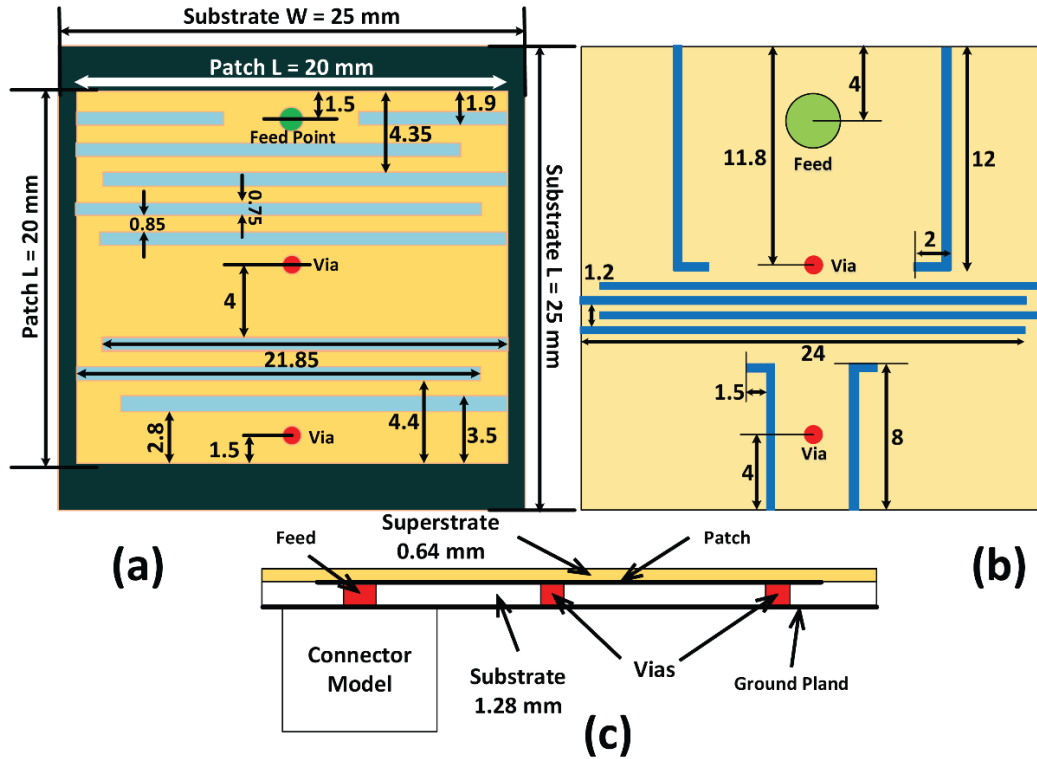


Figure 33: Proposed Antenna Geometry: (a) Top view of patch (superstrate is not shown). (b) Bottom view shows slots on Ground Plane. (c) Side view shows feed location and vias.

### 3.2.3 Sensitivity Analysis

Several parametric studies were conducted to understand the effect of each design parameter on the antenna performance. The study identified the parameters which have considerable effect on the resonance frequency as illustrated in Figure 34 and Figure 35.

The effect of such parameters were:

#### A. Length of the Patch Slot

The length of the patch slot is inversely proportional to the resonance frequency as shown in Figure 34(a). The slot length is defined as a ratio to the patch width and it is

fixed for all patch slots in this study. However, finer tuning is achievable by controlling the length of each patch slot individually. Thus, the longer the slot the lower the achieved resonance.

### **B. Length of L-shaped Ground Slot**

Generally, ground slots are used for enhancing the matching at a certain frequency band rather than shifting the resonance frequency. Figure 34(b) shows that increasing the length of the L-shaped slot near the feeding point slightly decreases the resonance frequency however, it alters the matching as well.

### **C. Width of the Patch Slots**

The width of the patch slots is inversely proportional to the resonance frequency as shown in Figure 34(c). Nearly 200 MHz frequency shift is achievable by tuning the slot thickness between 0.2 mm and 0.8 mm. The tuning process of this parameter is limited by the patch size and inter-element spacing between the slots.

### **D. Inter-element spacing of Patch Slots**

Increasing the inter-element gap between inserted slots on patch decreases the resonance frequency and vice versa. Changing the gap from 0.2 mm to 0.9 mm enables around 50 MHz frequency shifts as presented in Figure 34(d).

### **E. Superstrate Thickness**

Superstrate thickness is directly proportional to the resonance frequency. Standard RO 3006 thick substrates were used. As illustrated in Figure 35(a), increasing the superstrate thickness increases the resonance frequency, however, further tuning would be required for the on patch parameters.

## F. Substrate Thickness

Decreasing the substrate thickness can be used to lower the resonance frequency and miniaturize the antenna as presented in Figure 35(b). Substrate thickness is directly proportional to resonance frequency.

## G. Feeding Point Location

In this study, the location of feed point is swapped with shorting posts locations. As shown in Figure 35(c), feeding the antenna as shown in Figure 33 has the minimum resonance frequency.

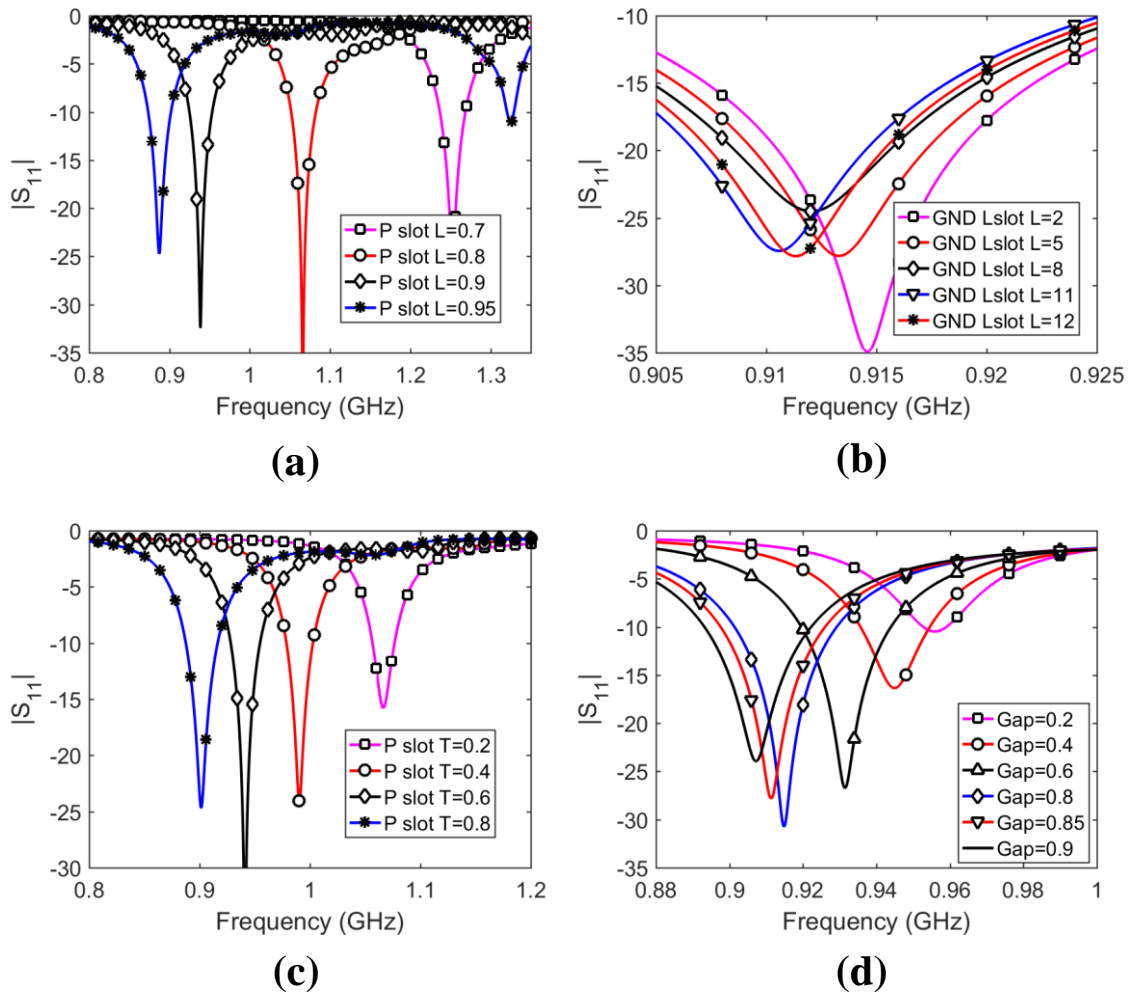
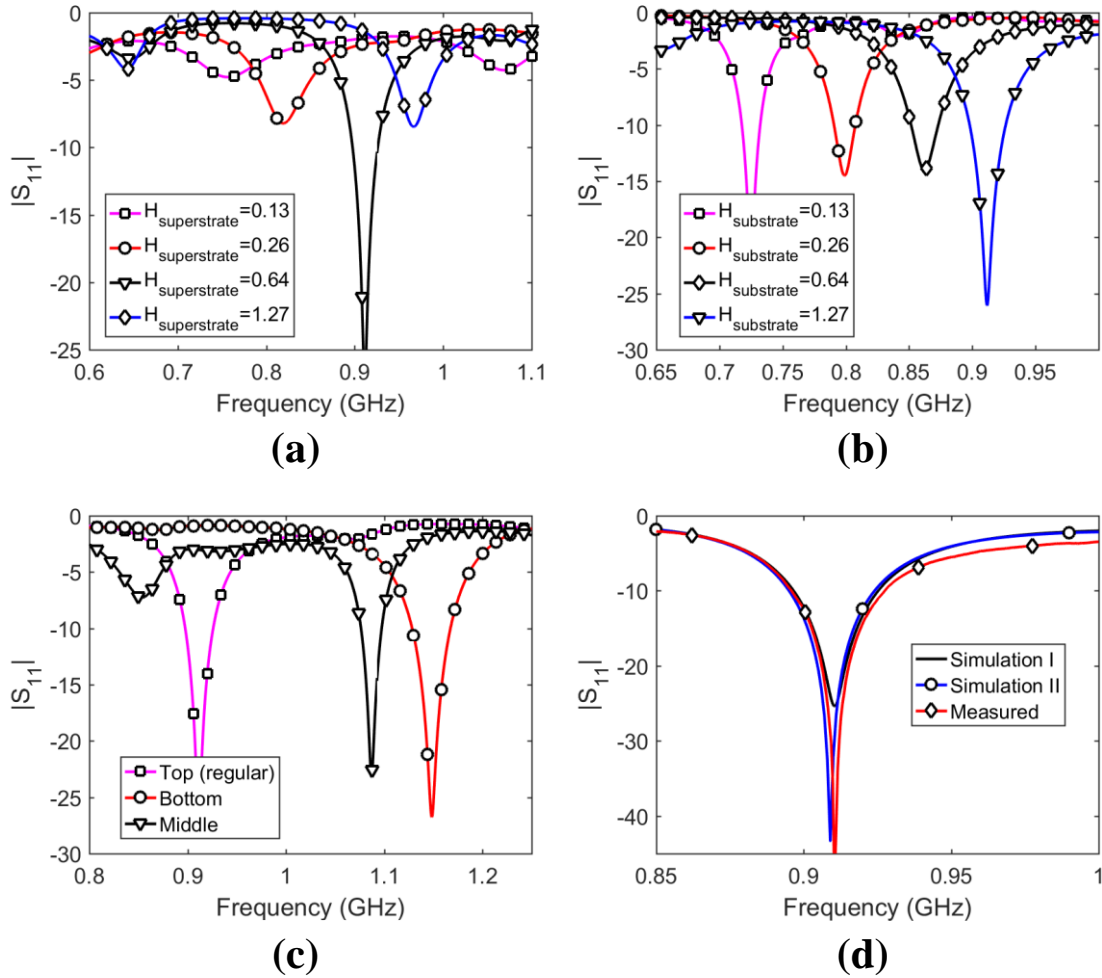


Figure 34: The parametric sweep of for  $S_{11}$  for several design parameters: (a) Length of Patch slots, (b) Length of L-shaped GND slot, (c) Width of patch slots, (d) Gap between patch slots. All dimensions are in mm.





**Figure 35: The parametric sweep of for S11 for several design parameters: (a) Superstrate thickness, (b) Substrate thickness, (c) Feed location, (d) Simulation and Measurement On-Skin Result: Simulation I (HFSS), Simulation II (CST). All dimensions are in mm.**

The proposed antenna is optimized to resonate in the (902-928 MHz) ISM band with 915 MHz as its center frequency. A reflection coefficient of -17.3 dB is obtained around 915 MHz with an impedance bandwidth of 28 MHz as shown in Figure 35(h). Good agreement between HFSS (Sim-1) and CST (Sim-2) results is observed with good agreement with measurements. It should be noted that the SMA connector was modeled and considered part of the antenna models to have closer agreement with the fabricated model, due to the fact that this is an electrically small antenna (ESA).

### 3.2.4 Results and Discussions

The proposed design was fabricated as shown in Figure 36(a) at Printec Labs., UK, and reflection and transmission coefficients measurements were conducted using a vector network analyzer Agilent FieldFox VNA (N9918A) at the Antennas and Microwave Structure Design Laboratory (AMSDL) at KFUPM.

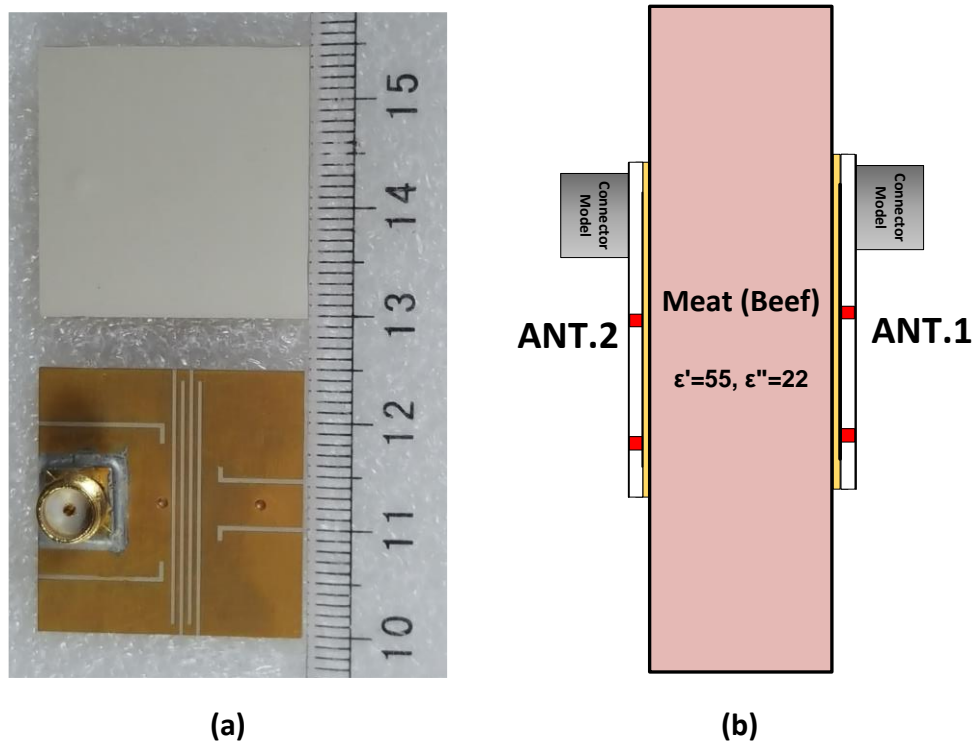


Figure 36: (a) Fabricated Prototype of Proposed Antenna. (b) Simulation Model for Transmission Coefficient ( $S_{21}$ ) Measurement.

#### A. Impedance Bandwidth and Reflection Coefficient

The fabricated antenna was tested (measured) at different spots on a human-body. Figure 37 presents the obtained reflection coefficients with their corresponding body spot. Since human-tissue characteristics vary from one spot to another, the antenna performance changed accordingly. Table 5 summarizes the  $S_{11}$  characteristics at the considered spots. For the majority of the considered body-spots, the resonance

frequency stayed within the targeted ISM band (902-928 MHz) except for the back of the forearm (4) and the sole of foot (13) locations where the resonance frequency were 930.2 MHz and 931.3 MHz, respectively. Regarding the impedance bandwidth, the measured bandwidths varied between 25.4-31.4 MHz showing good agreement with simulation results. The obtained results show that the proposed antenna gives good matching with the human-body with a maximum measured  $S_{11}$  value of -15 dB. This is important when considering this antenna for on-body measurements.

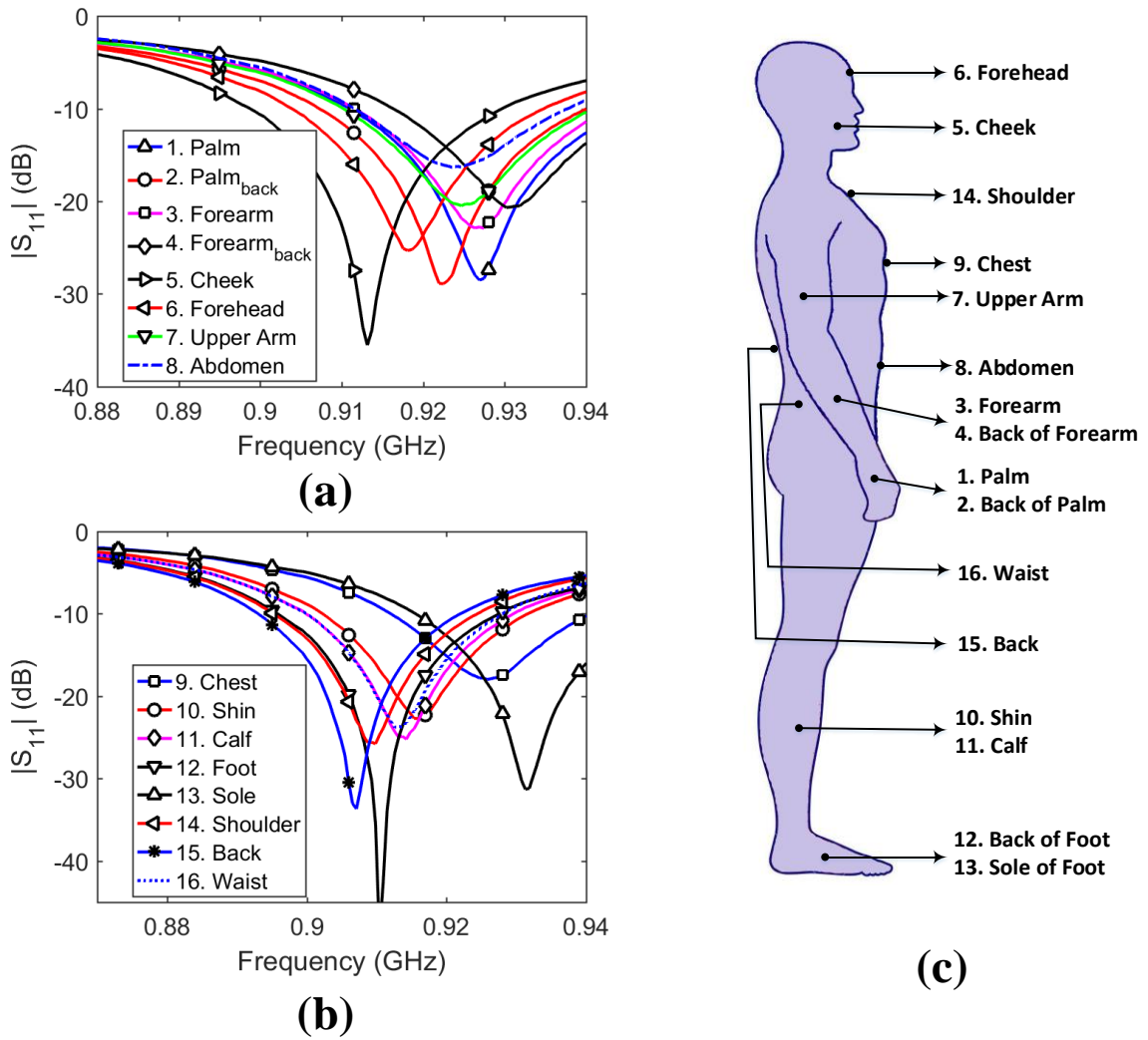


Figure 37: Measured reflection coefficient of the proposed antenna on various spots of the human-body. (a) Parts (1 to 8), (b) Parts (9 to 16), (c) human-body spots considered in measurements.

**Table 5: Summary of Antenna Performance Measurements on Different Spots on Human-Body**

<b>N</b>	<b>Resonance (MHz)</b>	<b>S11min (dB)</b>	<b>BW (MHz)</b>
1	926.9	-28.51	34.1
2	922.5	-28.9	32
3	926.4	-22.87	30.8
4	930.2	-20.67	30.3
5	913.2	-35.53	30.7
6	918.1	-25.31	30.3
7	924.7	-20.48	30.2
8	924.2	-16.23	25.4
9	925.8	-17.96	28
10	915.9	-22.72	28.6
11	914.3	-25.23	28.7
12	910.4	-49.18	31.4
13	931.3	-31.3	34.7
14	909.9	-25.77	28.7
15	907.1	-33.69	28.7
16	912.6	-23.8	27.6

**B. Specific Absorption Rate (SAR)**

In order to assess the safety of the proposed antenna for patients, specific absorption rate (SAR) have to be calculated. According to IEEE C95.1-1999 standard, the incident power to a biomedical antenna shall be limited such that the local maximum absorbed power averaged over a cube of tissues with weight of 1 gram, should not exceed 1.6 W/kg. However, IEEE C95.1-2005 standard release the limits of SAR to become 2 W/kg averaged over a cube of human-tissues with a weight of 10 grams. Equations 3.1 and 3.2 summarize the SAR limits stated by IEEE standards [102]-[103].

$$SAR_{1-g} \leq 1.6 \text{ W/kg} \tag{3.1}$$

$$SAR_{10-g} \leq 2 \text{ W/kg} \quad (3.2)$$

The peak calculated SAR values of the proposed design were 180 W/kg and 40.1 W/kg for SAR<sub>1-g</sub> and SAR<sub>10-g</sub>, respectively. The incident power was assumed to be 0.5W. Thus, to satisfy the SAR<sub>10-g</sub> limit, the maximum incident power should not exceed 24.4 mW. Moreover, to satisfy SAR<sub>1g</sub> boundary, the maximum incident power shall not exceed 4.44 mW by controlling the input signal to the antenna. Table 6 summarizes the simulation results of SAR.

**Table 6: Calculated Specific Absorption Rate**

	<b>SAR<sub>MAX</sub> at 0.5W (W/kg)</b>	<b>Maximum incident Power (mW)</b>	<b>SAR with limited power (W/kg)</b>
SAR 1g average	180.0	4.44	1.56
SAR 10g average	40.1	24.9	1.99

### C. Transmission Coefficient

In order to obtain further performance characteristics of fabricated design, the transmission coefficients  $S_{21}$  were simulated and measured. Simulation and Measurement setups are illustrated in Figure 36(b) and Figure 38(b,c), respectively. Identical prototypes were utilized with lean beef slices with different thicknesses. The experiment is simulated with a single layer meat model ( $\epsilon_r'=55$ ,  $\epsilon_r''=22$ ,  $\tan\delta=0.43$ ) [104]-[105]. Figure 39 and Table 7 illustrate the comparison of the simulated and measured results. Measurement results were acquired at (0 dBm), which is lower than maximum incident power of 4.44W (6.47 dBm). A good agreement between simulation and measurement results is achieved at the frequencies of interest with less than 9% deviation. This deviation is a results of several factors such as using estimated model

for tissues with single layer, while the real tissues consist of several component with different electrical properties. The measurement results show that a transmission coefficient of -18.54 dB is captured across a beef slice of 1 cm thickness. Due to high signal losses in tissues, the ratio of the received signal to the transmitted one is expected to be degraded as the thickness of the beef slice increases. With an 8.5 cm beef slice, the measured transmission coefficient was around -37.84 dB. Such levels are still acceptable when considering in-body microwave transmissions.

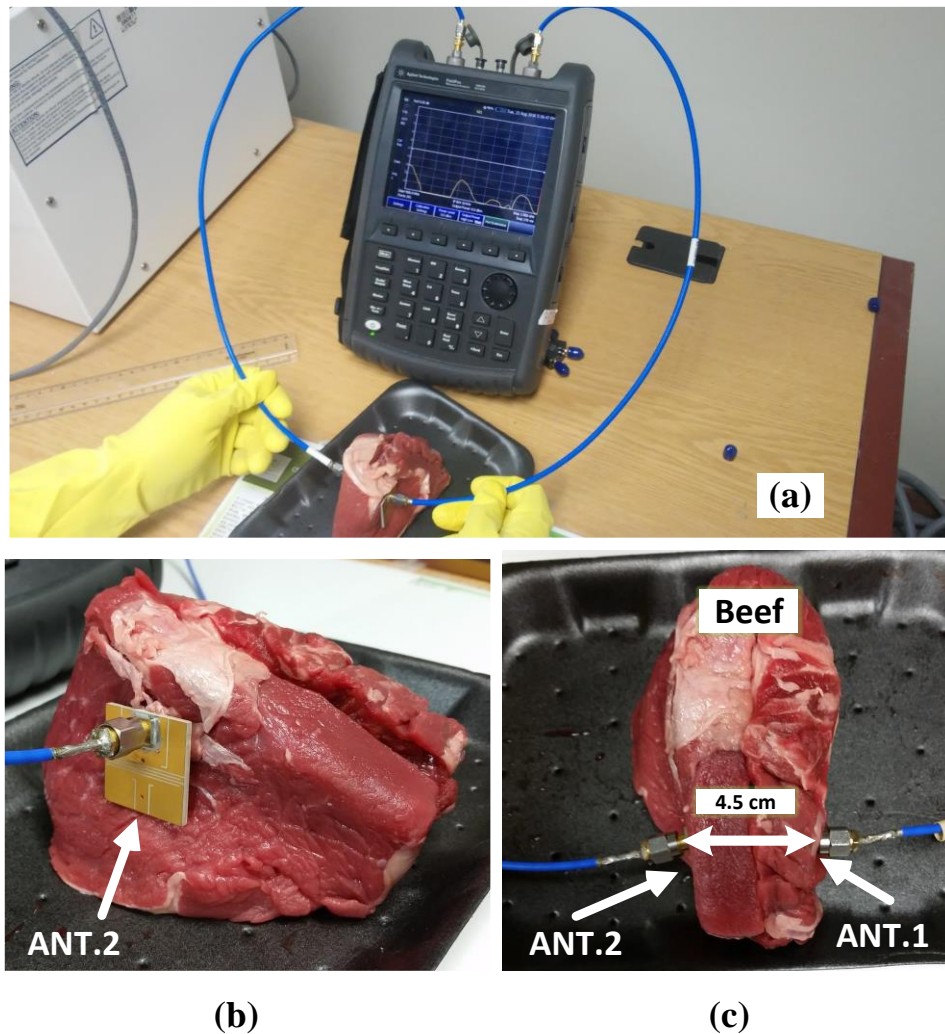
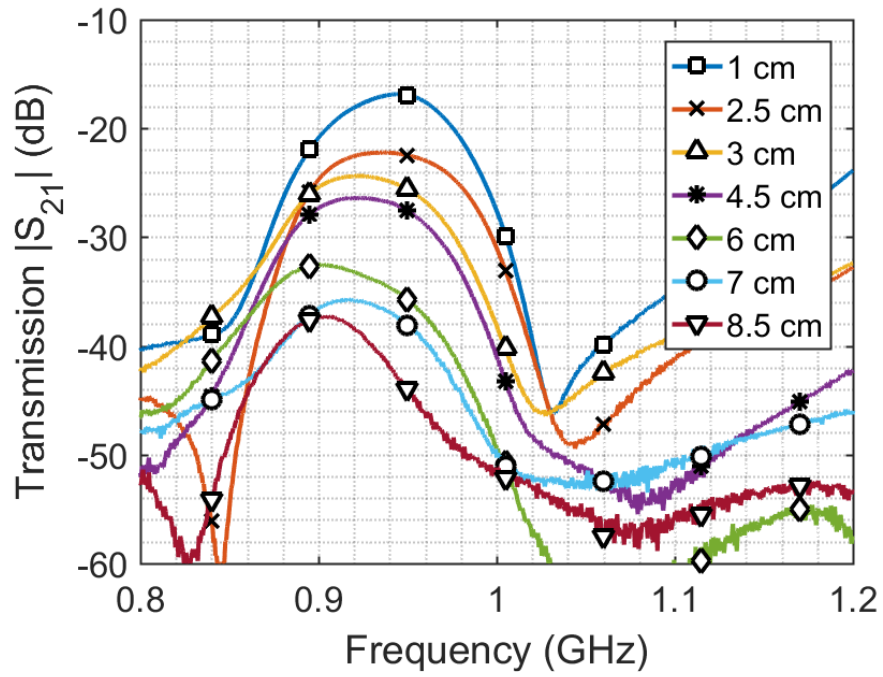
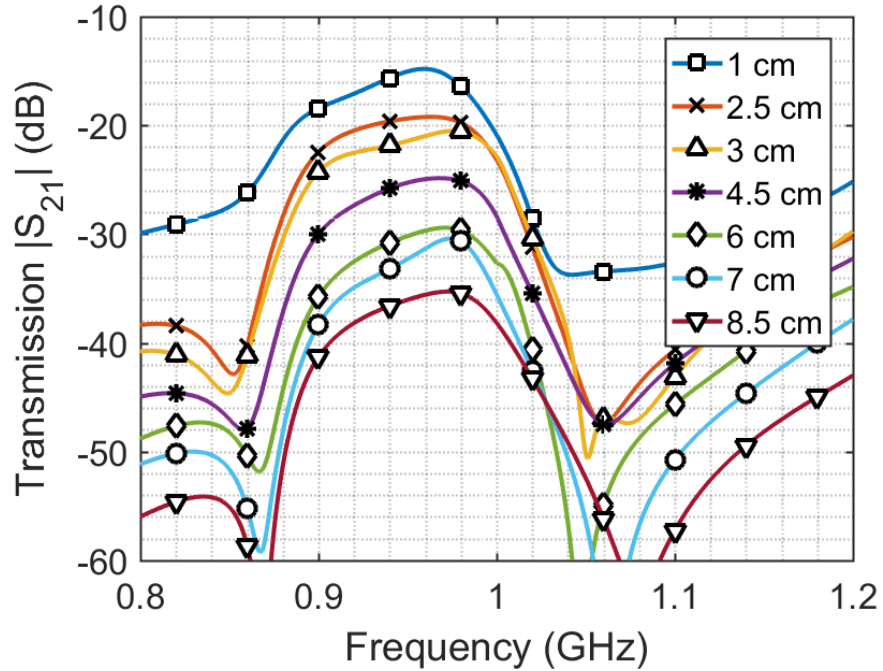


**Figure 38: Experimental Setup for Transmission Coefficient Measurement. (a) Vector Network Analyzer. (b) Side View, (c) Front View.**



(a)



(b)

Figure 39: Transmission Coefficient  $S_{21}$  at different thicknesses of Lean Beef slices: (a) Simulated. (b) Measured.

**Table 7: Comparison between Measurements and Simulations of Transmission Coefficient S21**

<b>Thickness (mm)</b>	<b>Simulated (dB)</b>	<b>Measured (dB)</b>	<b>Difference (dB)</b>	<b>% Difference</b>
1.0	-17.42	-18.54	1.12	6.0
2.5	-20.79	-22.83	2.04	8.9
3.0	-22.74	-24.44	1.70	7.0
4.5	-27.85	-26.44	1.40	5.3
6.0	-33.10	-32.98	0.12	0.4
7.0	-35.49	-35.83	0.34	1.0
8.5	-38.73	-37.84	0.89	2.3

#### **D. Far Field Radiation Pattern**

The far field radiation pattern of proposed design was calculated using two field simulators, HFSS and CST. HFSS shows that, proposed design has a peak realized gain of -15.24 dB around 915 MHz. The calculated radiation pattern has a broadside directivity as shown in Figure 40 and Figure 41. The 3D radiation pattern is illustrated in Figure 40 while the azimuth plane is presented in Figure 41(a) and the YZ and XZ elevation planes are presented in Figure 41(b) and Figure 41(c), respectively.

On The Other hand, CST radiation pattern shows that, the peak realized gain inside skin-model (broadside) is about -20.5 dB and the peak realized gain on backside (air) is around -17 dB as shown in Figure 42 and Figure 43. Figure 42, presents the 3D radiation pattern that has almost omnidirectional shape, which is expected from the theory of electrically small antenna, while Figure 43 illustrates the 2D radiation pattern in with elevation and azimuth planes.



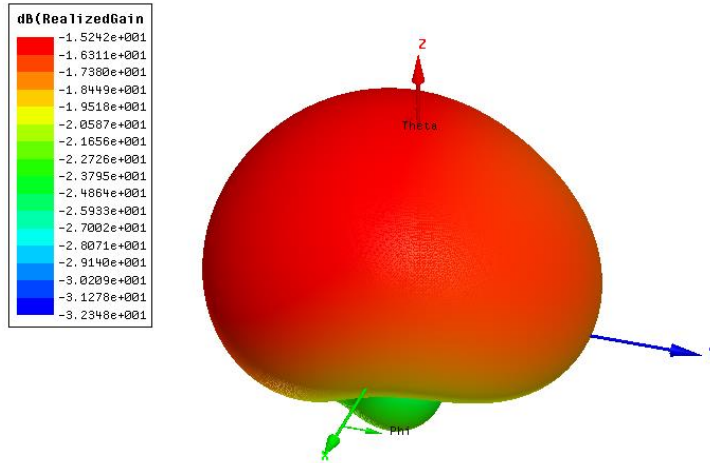


Figure 40: 3D Radiation Pattern (HFSS)

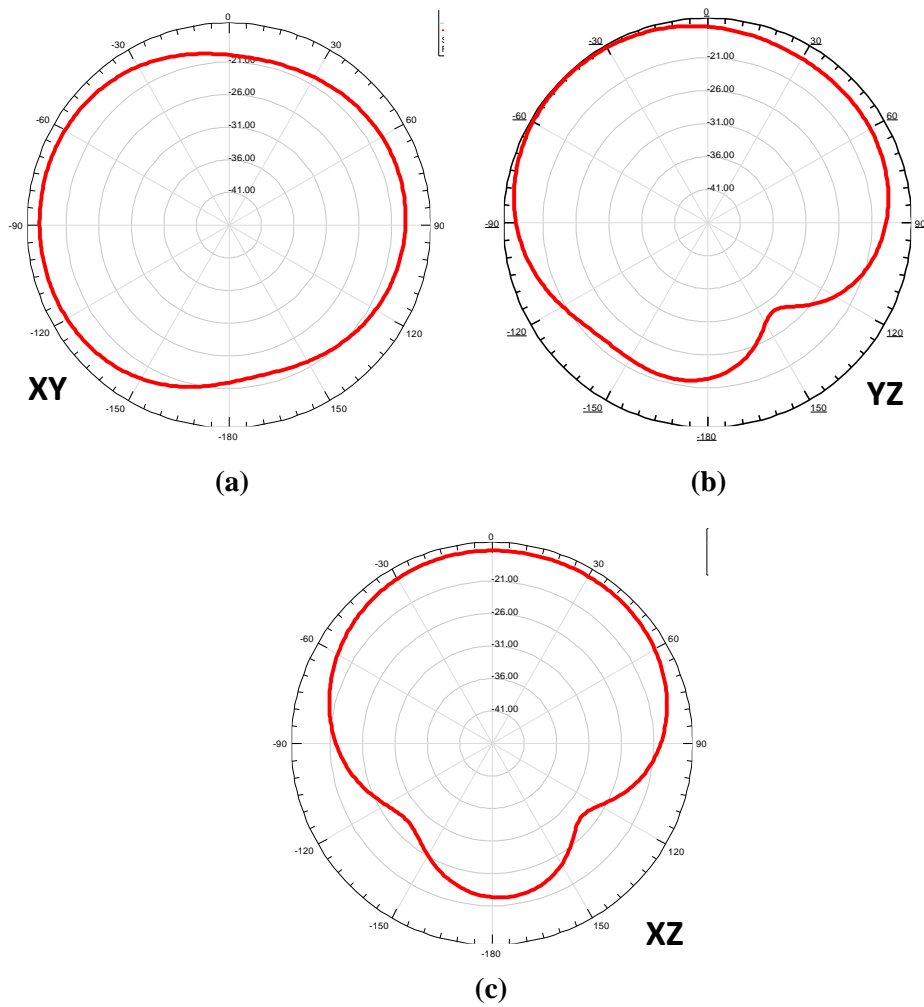


Figure 41: Far-Field 2D Radiation Pattern of Antenna. (a) Azimuth Plane (XY), (b) Elevation Plane (YZ), (c) Elevation Plane (XZ).

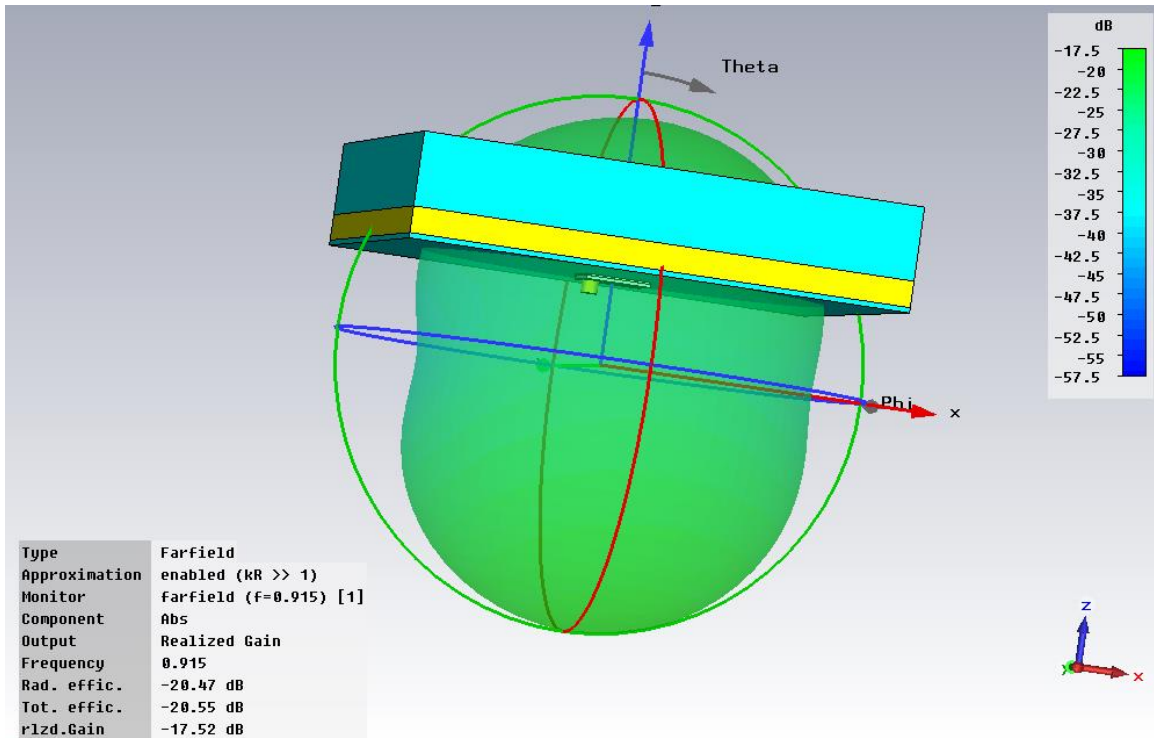


Figure 42: Far-Field 3D Radiation Pattern (CST)

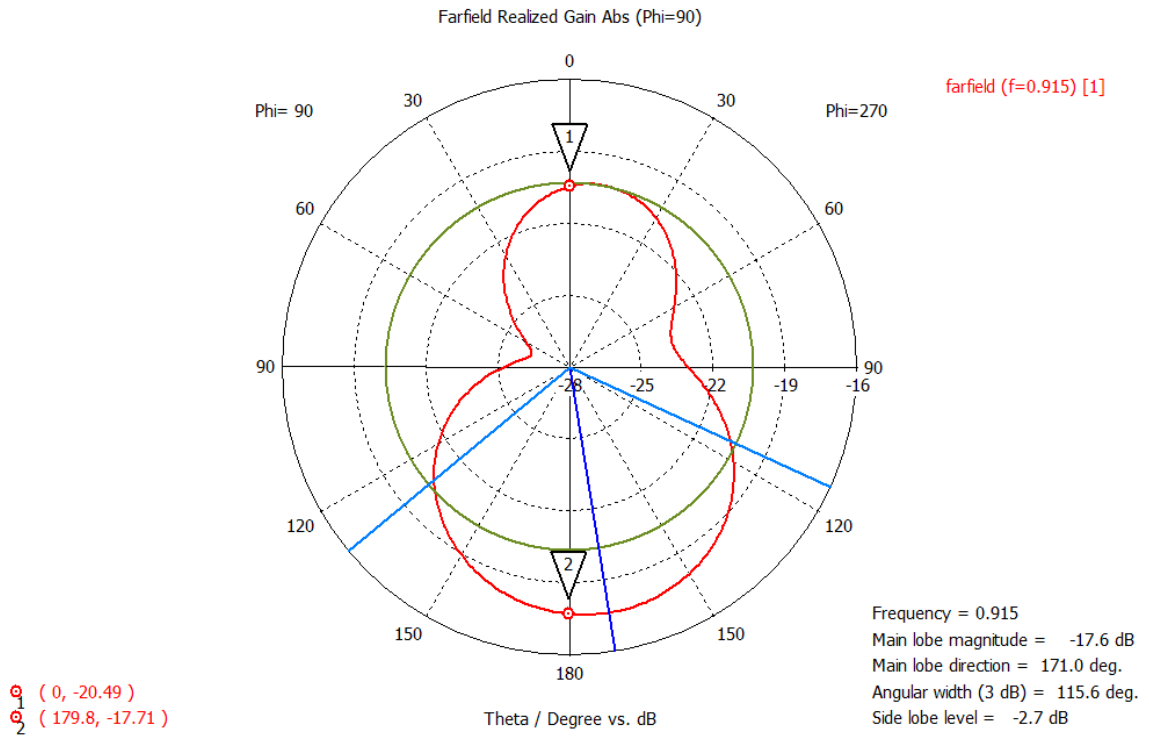


Figure 43: Far-Field 2D Radiation Patterns: Azimuth plane (Green), Elevation plane (Red).

### 3.2.5 Summary of Design-II

The design of a novel miniaturized superstrate loaded patch antenna operating at 915 MHz ISM band is presented. The antenna has a size of  $25 \times 25 \times 1.92 \text{ mm}^3$  which is equivalent to  $0.076\lambda_0 \times 0.076 \lambda_0 \times 0.006 \lambda_0$ . Measurement results show that the fabricated antenna has an impedance bandwidth of almost 30 MHz on various human-body spots. Moreover, a measured transmission coefficient of -18.54 dB is achieved across a 1 cm thick beef slice. Such an antenna can be a suitable candidate for biomedical telemetry applications.

Comparing Design-I and Design-II, LTCC fabrication technology has high integration capabilities in compare with PCB technology, which makes it more suitable for package devices. However, fabrication cost of PCB is much lower than LTCC designs, (about 14% of LTCC cost) thus, PCB technology was utilized in this work instead of LTCC. From the design performance perspective, LTCC design experience wider bandwidth in compare with Roger design, around 4.6 times wider. Both designs have almost identical radiation characteristics although, roger substrate has lower permittivity than LTCC.

### **3.3 DESIGN III: Dual-Band Circular Patch Antenna**

A compact dual-band circular patch antenna is designed for implanted biomedical data telemetry systems. Several miniaturization techniques were applied to have the resonance at the desired frequencies. The antenna has a radius of 7.5 mm, a thickness of 1.92 mm and a total volume of 340 mm<sup>3</sup>.

The antenna covers MedRadio (401-405 MHz), MICS (402-405MHz), and ISM bands (433.2-434.8 MHz, 2.4-2.5 GHz) with a total bandwidth of 285 MHz. The -10dB bandwidth were 368-463 MHz (94 MHz) and 2.392-2.582 GHz (190 MHz). The antenna performance was evaluated inside a human tissue model.

#### **3.3.1 Geometry**

For this proposed design, the antenna type is selected to be a patch antenna due to its compact size, flexibility in design, low cost, and ease of fabrication. The proposed antenna was designed on a circular Roger RO3010 substrate with a dielectric constant of  $\epsilon_r = 10.2$  and loss tangent of  $\tan \delta = 0.0022$ . The design was adapted to have circular shape in order to achieve biocompatibility and avoid sharp edges in implanted devices. The circular patch has a radius of 7.5 mm and a total thickness of 1.92 mm with a total volume of 340 mm<sup>3</sup> as illustrated in Figure 44. The design was modeled and optimized using CST.

The proposed antenna was loaded with a superstrate of the same material with a thickness of 0.64 mm to prevent the direct contact between human tissues and metallic patch. Thus, short-circuit currents through tissues between patch and ground could be avoided and

biocompatibility of proposed design is enhanced also. Superstrates are used to decrease the introduced losses by human-tissues and enhance the radiation characteristics.

The targeted frequency bands are 403.5 MHz MICS band, 433.9 MHz and 2.45 GHz ISM bands. In order to optimize the antenna resonance around these targeted bands, several miniaturization techniques were applied such as meandering, inserting slots, and loading the design with shorting posts.

First, the antenna was designed with meandered slot to increase the current path between the feeding point and the radiator edges and this introduced the lower band resonance. The meandering was achieved by introducing three rings with radii of (1.5 mm, 2.5 mm, and 6.5 mm) and connecting their edges in such a way to obtain a circular meander line. The edge of smallest ring is extended to the patch edge in order to force the current flow in certain directions. The optimal feeding location is found to be between the second and the third (largest) rings as shown in Figure 44(a).

Second, an arc-shaped slot was inserted between the second and third rings on the left side. The inserted slot participates in miniaturization by increasing the current path or altering the current distribution over the patch. The length of this slot plays a critical role in fine optimization of the resonance frequencies. Such slot was introduced at the last stages of design process.

Third, the proposed design was loaded with a shorting post, with a diameter of 0.8 mm, for miniaturization and matching purposes. Loading with shorting post assists the miniaturization process by altering the reactance of the antenna with controlling the location and radius of the shorting post.

Moreover, in this design, from antenna performance perspective, inserting shorting post stabilized and enhanced the matching of the antenna especially at lower resonance bands. The locations of loaded shorting post was optimized to have it just inside the largest ring in the right hand side.

It is worth mentioning that slots on ground plane were avoided since they might not be feasible during the fabrication process, particularly, during soldering process of the SMA connector, due to the compact size of the antenna.

Furthermore, recalling the fact that SMA connectors have serious impact on small antennas' performance, all the provided results in this study were obtained taking into consideration the effect of the SMA connector since the antenna size is extremely compact. Therefore, an SMA model was attached in all simulations.

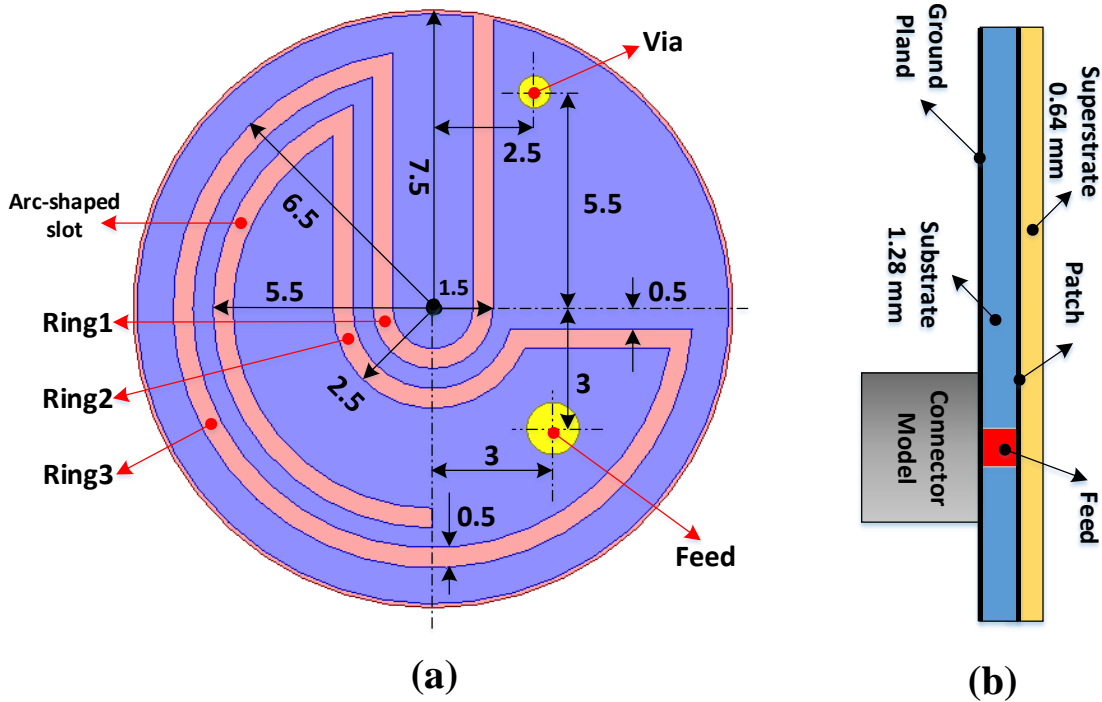


Figure 44: Geometry of Proposed Dual-Band Design. (a) Top View, (b) Side View

### 3.3.2 Simulation with Skin Model

Since the proposed antenna is intended to operate inside human tissues, a numerical model of the skin is required to be included in the simulations. The performance of the proposed implanted antenna was assessed utilizing a numerical single-layer skin model with a size of 100×100 mm. The radiation boundaries are defined in free-space outside this model as illustrated in Figure 45. The antenna was placed at elevation of 10 mm inside the skin model.

It is important to notice that, the electrical characteristics of the skin are dispersive, in other word, electrical properties are function of frequency and do not have constant value, and it is quite complicated to define such properties in numerical simulators. Thus, the optimization process requires a considerable amount of time.

Table 8 shows the electrical properties of the surface of human-body (dielectric constant and conductivity) at dual-band of interest.

Table 8: Electric Properties of Human Tissues

Frequency	Dielectric Constant ( $\epsilon_r$ )	Conductivity $\sigma$ (S/m)	Loss tangent $\tan\delta$
403.5 MHz	46.74	0.69	0.66
2.45 GHz	38.06	1.44	0.226

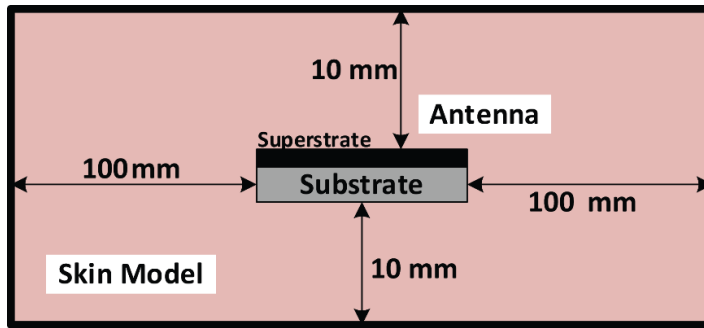


Figure 45: Tissues Model for Implanted Applications

### 3.3.3 Parametric Studies

Several parametric studies were conducted to analyze the effect of each design parameter on the antenna performance. The study identified the dominant parameters on the antenna performance around the resonance frequencies as illustrated in Figure 46 - Figure 50. The effect of such parameters were:

#### A. Width of Inserted Slots

In the proposed design, all slots in the patch have a common width that was used as optimization parameters. The width of the inserted slot in the patch of the proposed design has inverse relation with the resonance frequency at the lower band (403 MHz), as show in Figure 46 (a). Thus, as the width of the slots increase, the resonance shifts down. On the contrary, in the higher operating band (2.45 GHz), as the width of the slot increases, the resonance frequency increases too, as shown in Figure 46(b). This parameter can be utilized during early stages of the design as it yields an opposite effects at the bands of interest.

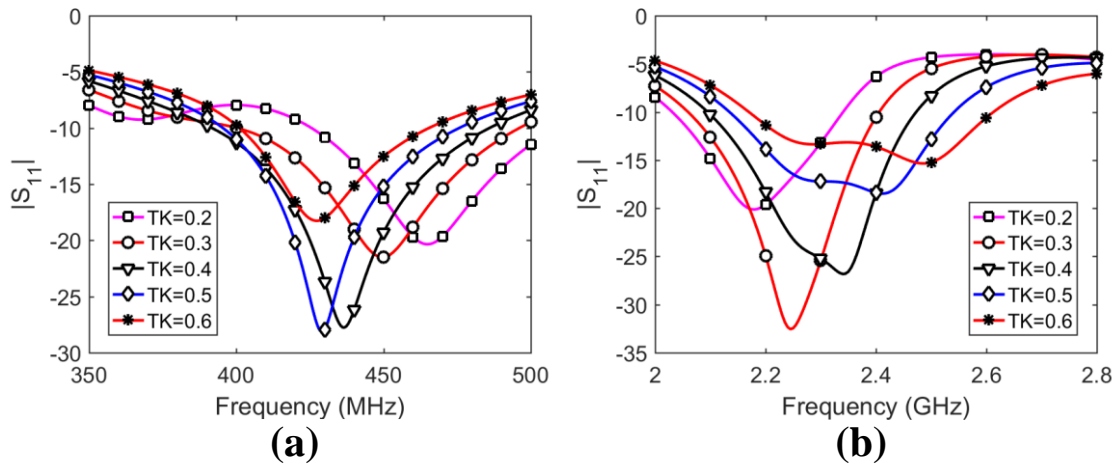


Figure 46: Effect of width of inserted slots



## B. Length of Arc-Shaped Slot

As illustrated in Figure 47, the length of arc-shaped slot on the left hand side has considerable effect on the higher band, while its effect on the lower band is minimum. Considering the upper band, around 2.45 GHz, as the length of the arc slot decrease, the resonance frequency increases. At small lengths of the arc, a second resonance appears, as shown in Figure 47 (b).

On the other hand, the resonance frequency decreases as the length of arc-shaped slot decreases. However, as presented in Figure 47 (a), the effect of this parameter is not significant.

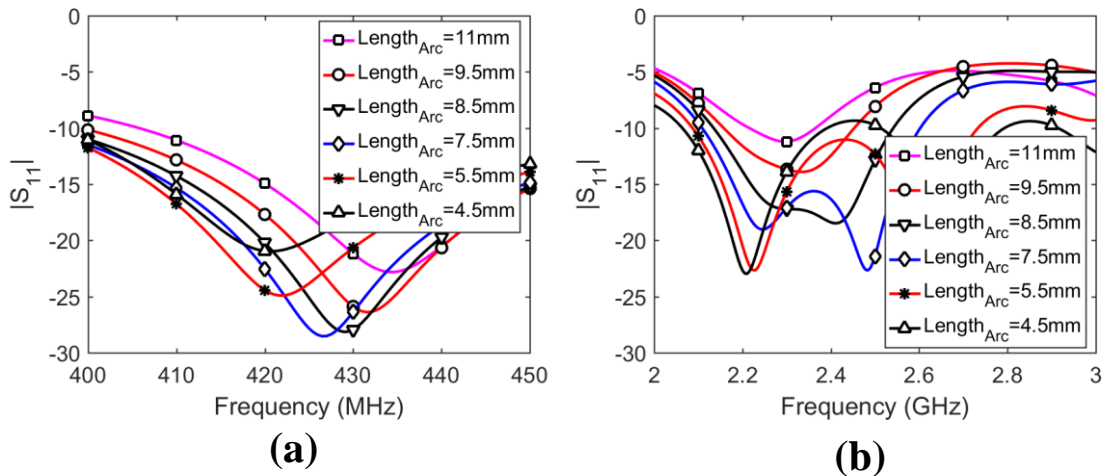


Figure 47: Effect of Length of Arc-Shaped Slot

## C. Location of Shorting Post

Inserting a shorting post in small designs is fundamental approach to achieve miniaturization. The parametric study was conducted by fixing the shorting post 6 mm away on the right side of the center point of the antenna. Then, the location of the shorting post is rotated counter clock wise maintaining the same distance from the center point. According to Figure 48 (a), moving the shoring post away from horizontal axis of the

antenna yields in considerable lowering of the resonance frequency at the lower band (403 MHz). Moreover, higher bands shares similar characteristics but with slighter effect, as presented in Figure 48 (b).

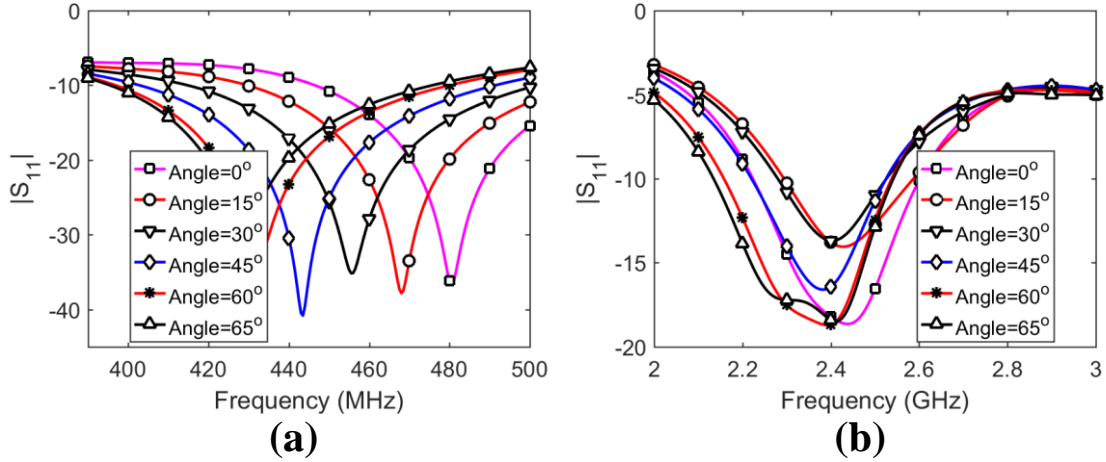


Figure 48: Effect of Location of Shorting Posts

#### D. Effect of Substrate Thickness

This study was based on commercially available thicknesses of Roger RO3010 sheets that are: 0.13 mm, 0.25 mm, 0.64 mm, and 1.27 mm. Regarding the lower band, as the thickness of substrate increases, the resonance frequency increases too, however, the matching is affected dramatically as shown in Figure 49 (a).

On the other side, at the higher band, resonance frequency experience an opposite effect as presented in Figure 49 (b). The resonance frequency increases, as the substrate gets thinner.

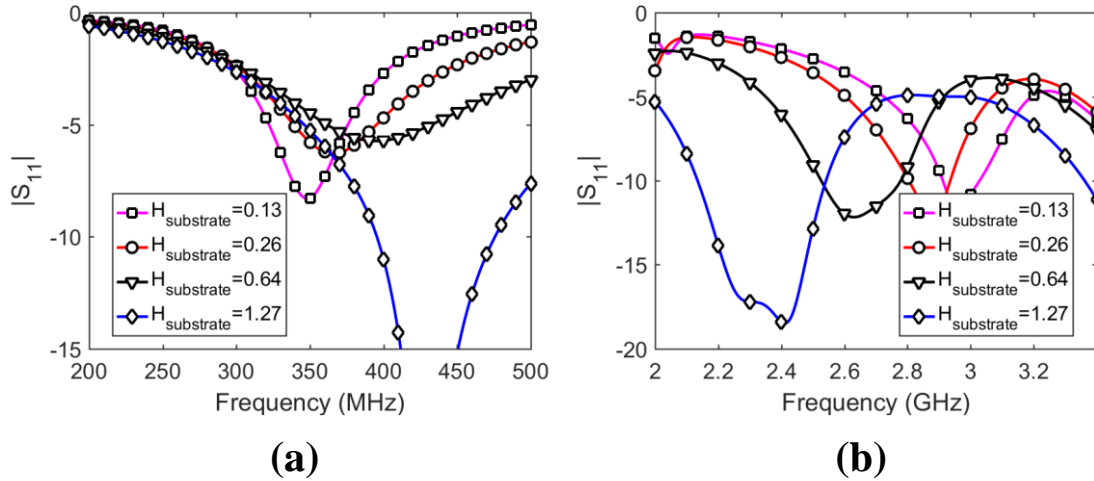


Figure 49: Effect of Substrate Thickness

### E. Effect of superstrate thickness

In line with the previous study, this study was based on commercially available thicknesses of Roger RO3010 sheets. The obtained results show that the resonance frequency is directly related to the thickness of the superstrate. As the superstrate thickness increases, the resonance frequency decreases, regardless whether it is lower or upper band as illustrated in Figure 50 (a), (b).

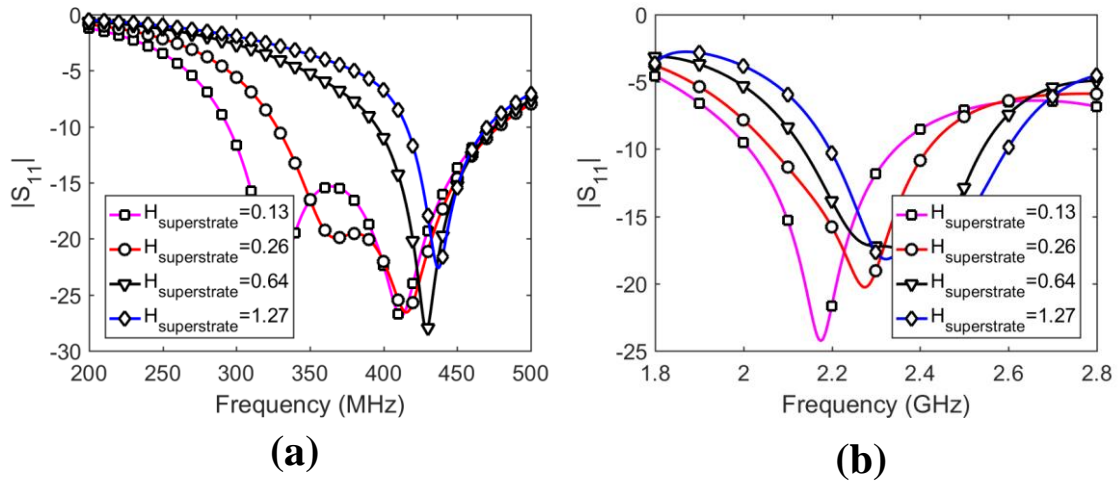
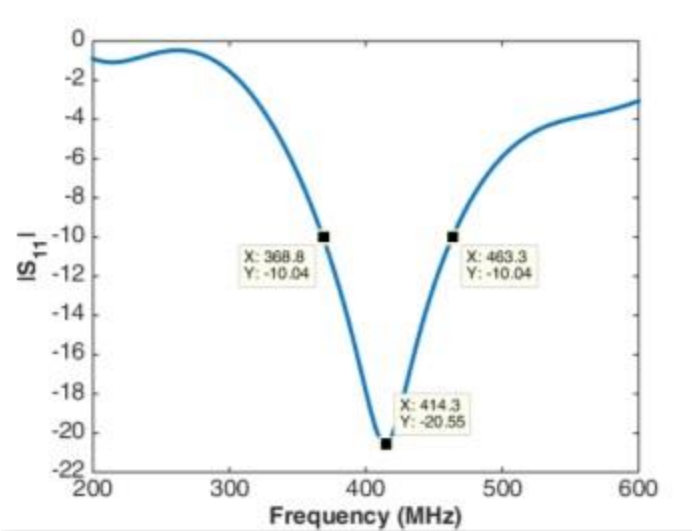


Figure 50: Effect of Superstrate Thickness

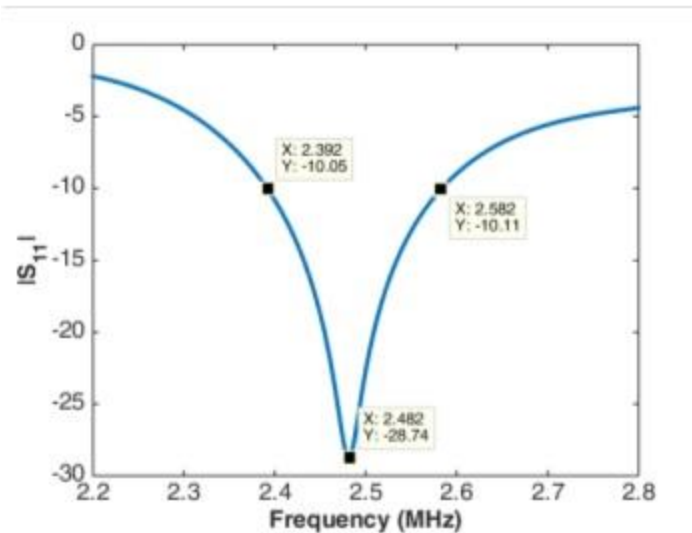
### **3.3.4 Results and Discussions**

#### **A. Impedance Bandwidth and Reflection Coefficient**

The proposed antenna is optimized to resonate in the (402-405 MHz) MICS band, (433-434.8 MHz) ISM band, and (2.4 – 2.5 GHz) ISM band with center frequencies of 403.5 MHz, 433.9 MHz, and 2.45 GHz, respectively. A reflection coefficient of -20.55 dB was obtained around 414 MHz with an impedance bandwidth of 94 MHz (368 - 463 MHz) as shown in Figure 51(a). Moreover, a reflection coefficient of -28.74 dB was obtained around 2.48 GHz with an impedance bandwidth of 190 MHz (2.392 – 2.582 GHz) as shown in Figure 51(b). It should be noted that the SMA connector was modeled and considered part of the antenna models to have closer agreement with the fabricated model, due to the fact that this is an electrically small antenna (ESA).



(a)



(b)

Figure 51: Simulated Reflection Coefficient: (a) at 403.5 MHz, (b) at 2.45 GHz

## B. Far Field Radiation Pattern

The far field radiation pattern of the proposed design was calculated using CST. Obtained results show that, the proposed design has a peak gain of 3.25 dBi around 434 MHz and a peak gain of 3.34 dBi around 2.45 GHz. The calculated radiation pattern has an endfire

directivity as shown in Figure 52(a)-(b). The azimuth and elevation 2D radiation pattern are illustrated beside the 3D patterns in Figure 52 (a)-(b).

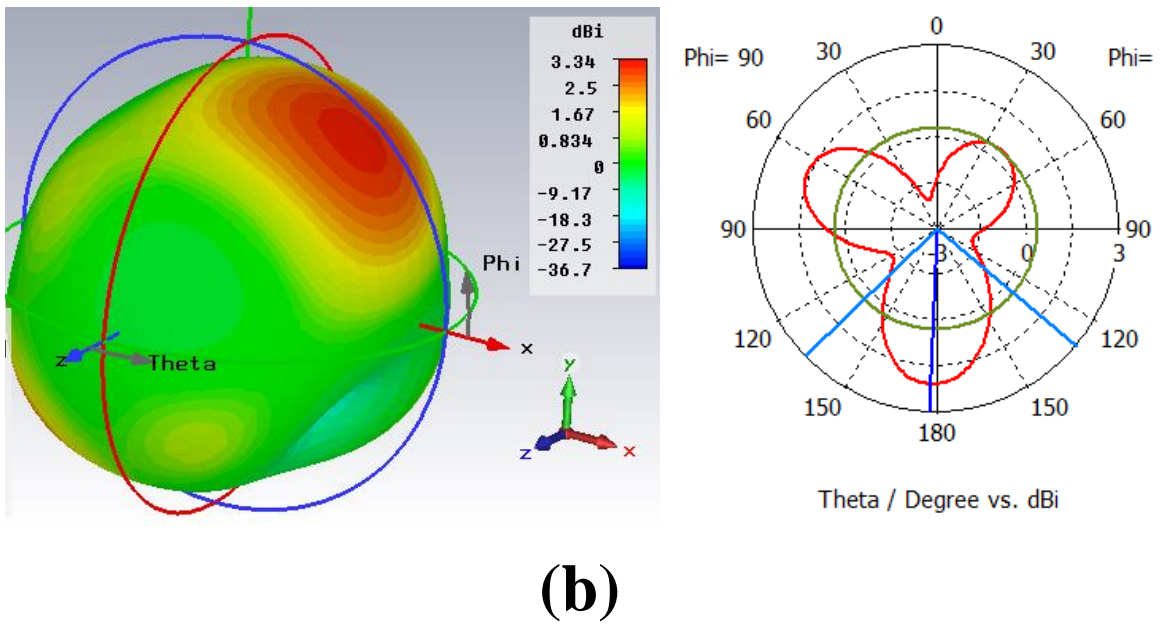
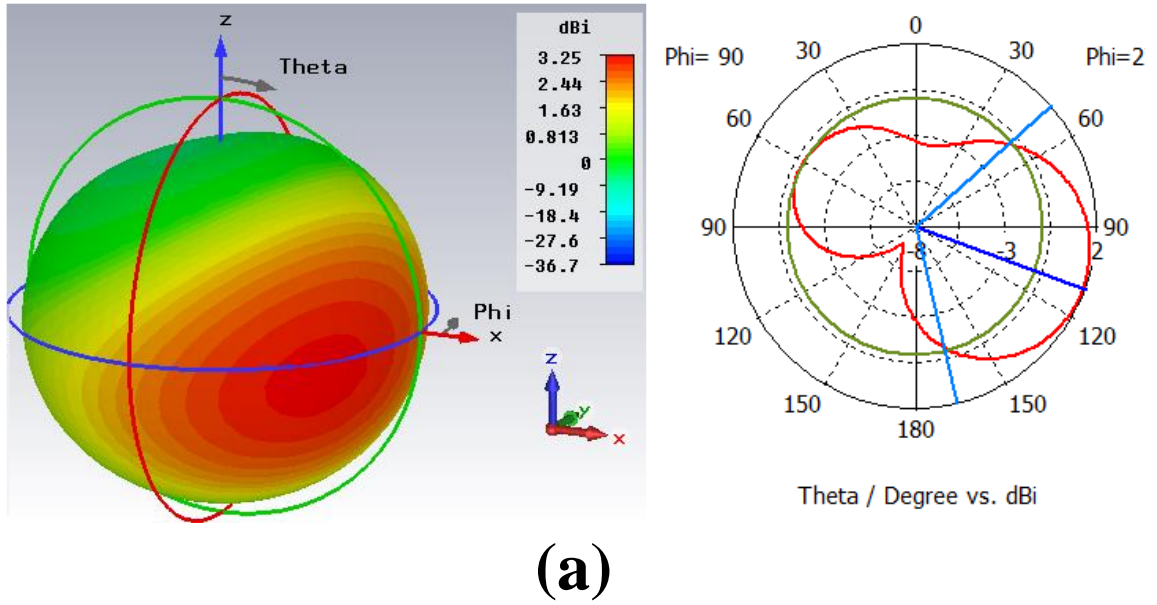


Figure 52: Radiation Pattern: (a) at 434 MHz, (b) at 2.45 GHz

### **3.3.5 Summary of Design-III**

A miniaturized dual-band circular patch antenna was designed for biomedical telemetry applications with a radius of 7.5 mm and a thickness of 1.92 mm. Several miniaturization techniques were applied to assist the resonance at desired frequency bands. The simulated input impedance characteristics and far field radiation patterns were provided, explained, and discussed. The proposed antenna has about 280 MHz impedance bandwidth covering 403.5 MHz MICS band, 433.9 MHz, 2.45 GHz ISM bands. The proposed antenna design is intended for implanted biomedical designs.

## CHAPTER 4

### CONCLUSION & FUTURE WORK

#### 4.1 Conclusions

Wireless communication systems have proliferated in almost every application nowadays. The demand for highly integrated devices for biomedical applications is increasing and this field constitutes a desirable area of research. Fundamentally, antennas for biomedical applications are required to satisfy some design conditions including: biocompatibility, miniaturization, safety for patients, and acceptable communication quality. In this work, we investigated the on-package antennas for biomedical applications and developed several designs that can be considered as feasible solutions.

The first design was based using LTCC technology for biomedical applications for on skin or with closed proximity of skin. The antenna had a size of  $25 \times 25 \text{ mm}^2$  and resonated around 915 MHz with a bandwidth of 138 MHz. Several miniaturization techniques were applied and the antenna performance was simulated using a numerical skin model.

The second model included a design for a miniaturized biomedical antenna operating around 915 MHz with a size of  $25 \times 25 \text{ mm}^2$  and a bandwidth of 30 MHz. The proposed antenna was fabricated on Roger RO3006 substrate and the prototype was tested on several spots on the human body. Moreover, the transmission coefficient of antenna was measured for different thicknesses of lamb slices and the obtained results showed good agreement between simulation and measurement results.



Finally, the third design consisted of a dual-band circular patch antenna for implanted biomedical applications. The antenna had a diameter of 15 mm and a thickness of 1.92 mm. The antenna operated around 403 MHz MICS band, 433.9 MHz and 2.45 GHz ISM bands with a total impedance bandwidth of 280 MHz. The performance assessments of the proposed antenna were carried out inside a numerical tissues model for a human. Results showed good potential suitability in such applications.

## **4.2 Future Work**

1. Fabricate Design-III and test the response of the fabricated prototype to compare with the simulation results.
2. Come up with a complete system to assess the performance of the designed antennas

## References

- [1] A. Kiourti, and K. Nikita. "A review of implantable patch antennas for biomedical telemetry: Challenges and solutions [wireless corner]." *IEEE on Antennas and Propagation Magazine*, Vol. 54, no. 3, pp. 210-228, 2012.
- [2] Z. Tang, B. Smith, J. Schild, and P. Peckham. "Data transmission form an implantable biotelemeter by load-shift keying using circuit configuration modulator." *IEEE Transactions on Biomedical Engineering* 42, no. 5, pp. 524-528, 1995.
- [3] U. Ullah, N. Mahyuddin, Z. Arifin, M. Abdullah, and A. Marzuki. "Antenna in LTCC Technologies: A Review and the Current State of the Art." *IEEE Antennas and Propagation Magazine*, Vol. 57, no. 2, pp. 241-260, 2015.
- [4] H. Cheema, and A. Shamim. "The Last Barrier." *IEEE Microwave Magazine*, Vol 14, no. 1, pp.79-91, 2013.
- [5] Definitions of ISM bands. International Telecommunication Union (ITU). Retrieved from: <http://www.itu.int/net/ITU-R/terrestrial/faq/index.html#g013>
- [6] A. Kiourti, and K. Nikita. "Miniature scalp-implantable antennas for telemetry in the MICS and ISM bands: Design, safety considerations and link budget analysis." *IEEE Transactions on Antennas and Propagation*, Vol. 60, no. 8, pp.3568-3575, 2012.
- [7] C. Liu, Y. Cuo, and S. Xiao. "A Hybrid Patch/Slot Implantable Antenna for Biotelemetry Devices." *IEEE Antennas and Wireless Propagation Letters*, vol, 11, pp. 1646-1649, 2012.
- [8] A. Kiourti, and K. Nikita. "Accelerated Design of Optimized Implantable Antennas for Medical Telemetry." *IEEE Antennas and Wireless Propagation Letters*, vol, 11, pp. 1655-1658, 2012.
- [9] M. Asili, R. Green, S. Seran, and E. Topsakal. "A Small Implantable Antenna for MedRadio and ISM Bands." *IEEE Antennas and Wireless Propagation Letters*, vol, 11, pp. 1683-1685, 2012.
- [10] L. Marnat, M. Ouda, M. Arsalan, K. Salama, and A. Shamim. "On-Chip Implantable Antennas for Wireless Power and Data Transfer in a Glaucoma-Monitoring SoC." *IEEE Antennas and Wireless Propagation Letters*, Vol. 11, pp. 1671-1674, 2012.

- [11] M. Svanda, and M. Polivka. "Matching Technique for an On-Body Low-Profile Coupled-Patches UHF RFID Tag and for Sensor Antennas." *IEEE Transactions on Antennas and Propagation*, Vol. 63, No. 5, pp. 2295-2301, 2015.
- [12] R. Gupta, and G. Kumar. "High-gain multilayered antenna for wireless applications." *Microwave and Optical Technology Letters*, Vol. 50, no. 7, pp.1923-1929, 2008.
- [13] V. Kunda, M. Ali, H. Sheng-Hwang, and T. Sittironnarit. "Study of a dual-band packaged patch antenna on a PC card for 5–6 GHz wireless LAN applications." *Microwave and Optical Technology Letters*, Vol. 37, no. 6, pp. 423-428, 2003.
- [14] K. Wong, C. Lee, B. Chen, K. Huang, and S. Yang. "Wideband printed monopole antenna integrated in a system in package." *Microwave and Optical Technology Letters*, Vol. 48, no.10, pp.2113-2117, 2006.
- [15] A. Yu, F. Yang, and A. Elsherbeni. "A planar rhombic antenna with a broad circular polarization bandwidth for integrated single chip radio transceivers." *Microwave and Optical Technology Letters*, Vol. 51, no.6, pp.1493-1496, 2009.
- [16] Y. Zhang. "Integrated-circuit-pressed ceramic-package antenna." *Microwave and Optical Technology Letters*, Vol.42, no.2, pp.143-147, 2004.
- [17] C. Liu, Y. Guo, H. Sun, and S. Xiao. "Design and safety considerations of an implantable rectenna for far-field wireless power transfer." *IEEE Transactions on Antennas and Propagation*, Vol. 62, no.11, pp. 5798-5806, 2014.
- [18] P. Soh, M. Mercuri, G. Pandey, G. Vandenbosch, and D. Schreurs. "Dual-band planar bowtie monopole for a fall-detection radar and telemetry system." *IEEE Antennas and Wireless Propagation Letters*, Vol.11, pp.1698-1701, 2012.
- [19] H. Tanidokoro, , N. Konishi, Eiichiro Hirose, Y. Shinohara, H. Arai, and N. Goto. "1-wavelength loop type dielectric chip antennas." *IEEE Antennas and Propagation Society International Symposium*, Vol. 4, pp. 1950-1953, 1998.
- [20] H. Matsushima, E. Hirose, Y. Shinohara, H. Arai, and N. Golo. "Electromagnetically coupled dielectric chip antenna." *IEEE Antennas and Propagation Society International Symposium*, Vol. 4, pp. 1954-1957, 1998.
- [21] K. Wong, Y. Chen, S. Su, and Y. Kuo. "Diversity dual-band planar inverted-F antenna for WLAN operation." *Microwave and Optical Technology Letters*, Vol. 38, no. 3, pp. 223-225, 2003.

- [22] C. Su, K. Wong, W. Chen, and Y. Cheng. "A microstrip-coupled printed inverted-F monopole antenna." *Microwave and optical technology letters*, Vol. 43, no. 6, pp. 470-472, 2004.
- [23] M. Suma, P. Bybi, and P. Mohanan. "A wideband printed monopole antenna for 2.4-GHz WLAN applications." *Microwave and optical technology letters*, Vol. 48, no. 5, pp. 871-873, 2006.
- [24] P. Saha, A. Singh, V. Pandey, B. Kanaujia, and M. Khandelwal. "Design and analysis of UWB circular ring two element microstrip patch antenna array with notched band for modern wireless applications." *Microwave and Optical Technology Letters*, Vol. 57, no. 9, pp. 2067-2072, 2015.
- [25] Z. Tang, J. Zhan, and X. Wu. "Compact triple band-notched printed antenna with multislots for UWB applications." *Microwave and Optical Technology Letters*, Vol. 57, no. 9, pp. 2056-2060, 2015.
- [26] S. Su, and K. Wong. "Wideband antenna integrated in a system in package for WLAN/WiMAX operation in a mobile device." *Microwave and Optical Technology Letters*, Vol. 48, no. 10, pp. 2048-2053, 2006.
- [27] Y. Kuo, T. Chiou, and K. Wong. "A novel dual-band printed inverted-F antenna." *Microwave and Optical Technology Letters*, Vol. 31, no. 5, pp. 353-355, 2001.
- [28] H. Contopanagos, P. Broutas, and S. Chatzandroulis. "Embedded multislotted PIFAs for remotely powered passive UHF RFID tags." *Microwave and Optical Technology Letters*, Vol. 54, no. 10, pp. 2379-2383, 2012.
- [29] Y. Zhang, "Integration of microstrip antenna on cavity-down ceramic ball grid array package." *Electronics Letters*, Vol. 38, no. 22, pp. 1307-1308, 2002.
- [30] Y. Kwon, J. Moon, and S. Park. "An internal triple-band planar inverted-F antenna." *IEEE Antennas and Wireless Propagation Letters*, Vol. 2, no. 1, pp. 341-344, 2003.
- [31] R. Badhai and N. Gupta. "Reduced size bow-tie slot monopole antenna for land mine detection." *Microwave and Optical Technology Letters*, Vol. 52, no. 1, pp. 122-125, 2010.
- [32] M. Abou Al-alaa, H. Elsadek, and E. Abdallah. "Compact multiband dual reconfigurable folded planar monopole antenna." *Microwave and Optical Technology Letters*. Vol. 57, no.7, pp. 1557-1565, 2015.

- [33] M. Ali, R. Sadler, and G. Hayes. "A uniquely packaged internal inverted-F antenna for Bluetooth or wireless LAN application." *IEEE Antennas and Wireless Propagation Letters*, Vol.1, no. 1, pp.5-7, 2002.
- [34] G. Yang, M. Ali, and R. Dougal. "A thin wideband microstrip patch antenna with two adjacent slots." *Microwave and optical technology letters*, Vol. 41, no. 4, pp.261-266, 2004.
- [35] W. Choi, S. Kwon, and B. Lee. "Ceramic chip antenna using meander conductor lines." *Electronics Letters*, Vol. 37, no. 15, pp.933-934, 2001.
- [36] Y. Wang, and S. Chung. "A new dual-band antenna for WLAN applications." *IEEE Antennas and Propagation Society International Symposium*, vol. 3, pp. 2611-2614, 2004.
- [37] M. Ali, and G. Hayes. "Small printed integrated inverted-F antenna for Bluetooth application." *Microwave and Optical Technology Letters*, Vol.33, no. 5, pp.347-349, 2002.
- [38] D. Singh, C. Kalialakis, P. Gardner, and P. Hall. "Small H-shaped antennas for MMIC applications." *IEEE Transactions on Antennas and Propagation*, Vol.48, no.7, pp.1134-1141, 2000.
- [39] C. Song, P. Hall, and H. Ghafouri-Shiraz. "Novel RF front end antenna package." *IEE Proceedings Microwaves, Antennas and Propagation*, vol.150, no.4, pp. 290-294, 2003.
- [40] L. Tchoketch-Kebir, and B. Tlili. "Dual frequency broadband planar monopole antenna for LTE applications." *IEEE Antennas and Propagation Conference (LAPC)*, pp. 293-298, 2013.
- [41] C. Ling, C. Lee, C. Tang, and S. Chung. "Analysis and application of an on-package planar inverted-F antenna." *IEEE Transactions on Antennas and Propagation*, Vol. 55, no. 6 pp. 1774-1780, 2007.
- [42] H. Park, K. Chung, and J. Choi. "Design of a planar inverted-F antenna with very wide impedance bandwidth." *IEEE Microwave and Wireless Components Letters*, Vol. 16, no. 3, pp. 113-115, 2006.
- [43] S. Su, K. Wong, and H. Chen. "Broadband low-profile printed T-shaped monopole antenna for 5-GHz WLAN operation." *Microwave and optical technology letters*, Vol.42, no. 3, pp. 243-245, 2004.

- [44] L. Liu, Y. Li, Z. Zhang, and Z. Feng. "Circularly polarized patch-helix hybrid antenna with small ground." *IEEE Antennas and Wireless Propagation Letters*, Vol.13, pp. 361-364, 2014.
- [45] X. Cheng, D. Senior, C. Kim, and Y. Yoon. "A compact omnidirectional self-packaged patch antenna with complementary split-ring resonator loading for wireless endoscope applications." *IEEE Antennas and Wireless Propagation Letters*, Vol. 10, pp. 1532-1535, 2011.
- [46] J. Zhang, K. See, and T. Svimonishvili. "Printed decoupled dual-antenna array on-package for small wirelessly powered battery-less device." *IEEE Antennas and Wireless Propagation Letters*, Vol. 13, pp. 923-926, 2014.
- [47] S. Mazinani, and H. Hassani. "A novel broadband plate-loaded planar monopole antenna." *IEEE Antennas and Wireless Propagation Letters*, Vol. 8, pp. 1123-1126, 2009.
- [48] H. Liu, and Y. Michael. "Electrically Small Loop Antenna standing on compact ground in wireless sensor package." accepted for publication in *IEEE Antennas and Wireless Propagation Letters*, 2015.
- [49] S. Islam, K. Esselle, D. Bull, and P. Pilowsky. "A miniaturized implantable PIFA antenna for indoor wireless telemetry." In *International Conference on Electromagnetics in Advanced Applications (ICEAA)*, pp. 526-530, 2012.
- [50] F. Gozasht, M. Hossain, and A. Mohan. "Miniaturized E-shaped PIFA antenna for wideband implantable biomedical applications." In *International Conference on Electromagnetics in Advanced Applications (ICEAA)*, pp. 832-835, 2013.
- [51] Kumar, S. Akhil, and T. Shanmuganantham. "Implantable CPW fed dual folded dipole antenna for biomedical applications." *International Conference on Computing Communication & Networking Technologies (ICCCNT)*, pp. 1-5, 2012.
- [52] X. Li, M. Jalilvand, W. You, W. Wiesbeck, and T. Zwick. "An implantable stripline-fed slot antenna for biomedical applications." In *IET International Radar Conference 2013*, pp. 1-5, 2013.
- [53] S. Kwak, K. Chang, and Y. Yoon. "Ultra-wide band spiral shaped small antenna for the biomedical telemetry." In *Asia-Pacific Microwave Conference Proceedings APMC*, vol. 1, pp. 4-8, 2005.
- [54] T. Kumagai, K. Saito, M. Takahashi, and K. Ito. "Design of receiving antenna for microwave power transmission to capsular endoscope." In *IEEE MTT-S*

International Microwave Workshop Series on Innovative Wireless Power Transmission: Technologies, Systems, and Applications (IMWS), pp. 145-148, 2011.

- [55] R. Shubair, A. Salah, and A. Abbas. "Novel implantable miniaturized circular microstrip antenna for biomedical telemetry." In IEEE International Symposium Antennas and Propagation & USNC/URSI National Radio Science Meeting, pp. 947-948, 2015.
- [56] S. Wi, Y. Sun, S. Choa, Y. Lee, and J. Yook. "Package-level integrated antennas based on LTCC technology." IEEE Transactions on Antenna and Propagation, vol 54, No 8, Aug. pp. 2190-2197, 2006.
- [57] K. Khoo, Z. Chen, A. Lu, V. Sunappan, and L. Wai. "Miniaturized Multilayer UWB Antennas on LTCC." IEEE Transactions on Antennas and Propagation, Vol. 57, NO. 12, pp. 3988-3992, 2009.
- [58] C. Ying, G. Li, and Y. Zhang. "An LTCC Planar Ultra-wideband Antenna." Microwave and Optical Technology Letters, Vol. 42, NO. 3, pp. 220-222, Aug. 2004.
- [59] A. Abbosh, M. Bialkowski, M. Jacob, and J. Mazierska. "Investigations into an LTCC based ultra wide-band antenna." Microwave Conference Proceedings, Vol. 3, 2005.
- [60] M. Komulainen, J. Mahonen, T. Tick, M. Berg, H. Jantunen, M. Henry, C. Free, and E. Salonen. "Embedded air cavity backed microstrip antenna on an LTCC substrate." Journal of the European Ceramic Society, Vol 27, pp. 2881-2885, 2007.
- [61] Y. Shen, B. Ooi, D. Xu, and J. Ma. "Wide-Band CPW-Fed Multilayered LTCC Antenna.", Microwave and Optical Technology Letters, Vol. 51, No. 3, pp. 648-650, Mar. 2009.
- [62] Y. Chung, J. Sun, S. Wang, S. Huang, and C. Chiang. "Compact Chip Antenna Applications in GPS by LTCC Processing.", Microwave and Optical Technology Letters, VOL. 51, No. 4, pp. 1017-1019, Apr. 2009.
- [63] S. Chen, G. Liu, X. Chen, T. Lin, X. Liu and Z. Duan. "Compact Dual-Band GPS Microstrip Antenna Using Multilayer LTCC Substrate." IEEE Antenna and Propagation Letters, Vol 9, pp. 421-423, 2010.
- [64] T. Seki, K. Nishikawa, Y. Suzuki, I. Toyoda, and K. Tsunekawa. "60GHz Monolithic LTCC Module for Wireless Communication Systems." European Conference on Wireless Technology. Vol. 9, pp. 376-379, Sep, 2006.

- [65] T. Seki, K. Nishikawa, and K. Cho. "Multi-layer parasitic microstrip array antenna on LTCC substrate for millimeter-wave system-on-package." European Microwave Conference, Vol. 33, pp. 1393-1396, 2003.
- [66] F. Ghaffar, M. Khalid, K. Salama, and A. Shamim. "24-GHz LTCC Fractal Antenna Array SoP with Integrated Fresnel Lens." IEEE Antennas and Wireless Propagation Letters, Vol. 10, pp. 705-708, 2011.
- [67] S. Mei, and Z. Ping. "A Chip Antenna in LTCC for UWB Radios." IEEE Transactions on Antennas and Propagation, Vol. 56, No. 4, pp. 1177-1180, Apr. 2008.
- [68] M. Marta, and C. Oikonomopoulos-Zachos. "60 GHz embedded antennas on LTCC substrate." 20th International Conference on Applied Electromagnetics and Communications. 2010.
- [69] W. Yang, H. Wang, W. Che, Y. Huang, and J. Wang. "High-Gain and Low-Loss Millimeter-Wave LTCC Antenna Array Using Artificial Magnetic Conductor Structure." IEEE Transactions on Antennas and Propagation, Vol. 63, no.1, pp.390-395, 2015.
- [70] G. Brzezina, L. Roy, and L. MacEachern, "Planar antennas in LTCC technology with transceiver integration capability for ultra-wideband applications," IEEE Transactions on Microwave Theory and Technology, Vol. 54, no. 6, pp. 2030–2038, 2006.
- [71] A. Shamim, G. Brzezina, M. Arsalan and L. Roy, "5.2 GHz Differential LTCC Antenna and Balun for Biomedical System in Package (SiP) Application," Antenna Technology: Small and Smart Antennas Metamaterials and Applications, 2007. IWAT '07. International Workshop on, pp. 443-446, 2007.
- [72] H. Kim and H. Lee. "Design of a LTCC package Antenna for 900MHz RFID chip application." In IEEE Antennas and Propagation Society International Symposium, 2006.
- [73] K. Lim, A. Obatoyinbo, M. Davis, J. Laskar, and R. Tummala. "Development of planar antennas in multi-layer packages for RF-system-on-a-package applications." IEEE Electrical Performance of Electronic Packaging, pp.101-104, 2001.
- [74] Y. Zhao, Hua Su, X. Shi, and Z. Zhong. "Simulation and design of broadband circular polarization stacked patch antenna in LTCC technology." IEEE Second International Conference on Mechanic Automation and Control Engineering (MACE), pp. 7679-7681, 2011.



- [75] M. Saad, Z. Ambak, R. Alias, S. Shapee, A. Ibrahim, M. Yusoff, and H. Ishak. "6 GHz coplanar waveguide feeding T-shape slot antenna using LTCC technology." IEEE Student Conference on Research and Development (SCOReD). 2010.
- [76] W. Yang, K. Ma, K. Seng Yeo, W. Lim, and Z. Kong. "A compact dual-band meander-line antenna for biomedical applications." IEEE MTT-S International Microwave Workshop Series on RF and Wireless Technologies for Biomedical and Healthcare Applications (IMWS-BIO), pp. 1-3, 2013.
- [77] X. Cheng, J. Wu, R. Blank, D. Senior, & Y. Yoon. "An Omnidirectional Wrappable Compact Patch Antenna for Wireless Endoscope Applications." IEEE Antennas and Wireless Propagation Letters, Vol. 11, 1667-1670, 2012.
- [78] L. Marnat, and A. Shamim. "Liquid Crystal Polymer (LCP) based antenna for flexible system on package (SoP) applications." IEEE International Symposium on Antenna Technology and Applied Electromagnetics (ANTEM), pp. 1-4, 2012.
- [79] I. Chen, H. Chiou, and N. Chen. "V-Band On-Chip Dipole-Based Antenna." IEEE Transactions on Antennas and Propagation, Vol. 57, No. 10, pp 2853-2861, 2009.
- [80] S. Radiom, M. Baghaei-Nejad, K. Aghdam, G. Vandenbosch, L. Zheng, and G. Gielen. "Far-Field On-Chip Antennas Monolithically Integrated in a Wireless-Powered 5.8-GHz Downlink/UWB Uplink RFID Tag in 0.18-Standard CMOS." IEEE Journal of Solid-State Circuits, Vol. 45, no. 9, pp.1746-1758, 2010.
- [81] L. Zhang, Z. Wang, and J. Volakis. "Textile antennas and sensors for body-worn applications." IEEE Antennas and Wireless Propagation Letters, Vol.11, pp.1690-1693, 2012.
- [82] T. Jung, I. Hyeon, C. Baek, and S. Lim. "Circular/linear polarization reconfigurable antenna on simplified RF-MEMS packaging platform in K-band." IEEE Transactions on Antennas and Propagation, Vol.60, no.11, pp.5039-5045, 2012.
- [83] H. Wu, J. Zhang, L. Yan, L. Han, R. Yang, and W. Zhang. "Differential dual-band antenna-in-package with T-shaped slots." IEEE Antennas and Wireless Propagation Letters, Vol.11, pp. 1446-1449, 2012.
- [84] X. Li. Body Matched Antennas for Microwave Medical Applications. KIT Scientific Publishing, 2014 pp. 1-10.
- [85] I. Merunka, O. Fiser, L. Vojackova, J. Vrba, and D. Vrba. "Array of balanced antipodal Vivaldi antennas used for microwave hyperthermia treatment of neck cancer." In International Conference on Radioelektronika, 2014, pp. 1-4.

- [86] M. Hosain, A. Kouzani, M. Samad, and S. Tye. "A Miniature Energy Harvesting Rectenna for Operating a Head-Mountable Deep Brain Stimulation Device." *IEEE Access*, Vol.3, pp. 223-234, 2015.
- [87] J. Volakis, C. Chen, and K. Fujimoto. "Small antennas: miniaturization techniques & application." McGraw Hill Prof., pp. 1-8, 2009.
- [88] D. Ma, and W. Zhang, Radiation pattern of a short dipole nearby human body, *Asia Pacific Microwave Conference*, pp.2184-2187, 2009.
- [89] Y. Wang, L. Li, B. Wang, and L. Wang, A body sensor network platform for in-home health monitoring application, *Proceedings of the 4th International Conference on Ubiquitous Information Technologies & Applications*, pp.1-5, 2009.
- [90] J. Carter, J. Saberlin, T. Shah, and C. Furse, "Inexpensive fabric antenna for off-body wireless sensor communication.", *IEEE Antennas and Propagation Society International Symposium*, pp.1-4, 2010.
- [91] H. Lee, S. Kim, D. Donno, and M. Tentzeris, "A novel "universal" inkjet-printed EBG-backed flexible RFID for rugged on-body and metal mounted applications.", *IEEE MTT-S International Microwave Symposium Digest (MTT)*, pp.1-3, 2012.
- [92] A. Kiourti, and J. Volakis, "Stretchable and flexible E-fiber wire antennas embedded in polymer", *IEEE Antennas and Wireless Propagation Letters*, Vol. 13, pp.1381-1384, 2014.
- [93] A. Baroni, H. Rogier, and P. Nepa, "Wearable active Sierpinski fractal antenna for off-body communication", *IEEE-APS Topical Conference on Antennas and Propagation in Wireless Communications (APWC)*, pp.642-645, 2015.
- [94] D. Xue, B. Garner, and Y. Li, "Electrically-small folded cylindrical helix antenna for Wireless Body Area Networks", *Texas Symposium on Wireless and Microwave Circuits and Systems (WMCS)*, pp.1-4, 2016.
- [95] N. Noda, and H. Iwasaki, "Evaluation related to finger position and rotation of wearable dual band inverted-F finger ring antenna", *International Symposium on Antennas and Propagation (ISAP)*, pp.1-4, 2015.
- [96] A. Garcia-Miquel, S. Curto, N. Vidal, J. Lopez-Villegas, and P. Prakash, "Compact microwave applicator for thermal therapy of breast cancer: Comparative assessment of arrays operating at 434 and 915 MHz.", *European Conference on Antennas and Propagation (EuCAP)*, pp.1-4, 2016.

- [97] D. Rucker, H. Al-Rizzo, M. Wolverson, and H. Khaleel, "A miniaturized dual band bow-tie microstrip antenna for implantable and wearable telemedicine applications.", *Microwave and Optical Technology Letters*, Vol.54, pp.365-369, 2012.
- [98] G. Conway, and W. Scanlon, "Wearable antennas for medical monitoring systems.", *International Workshop on Antenna Technology (iWAT)*, pp.19-21, 2015.
- [99] S. Salman, L. Lee, and J. Volakis, "A wearable wrap-around sensor for monitoring deep tissue electric properties", *IEEE Sensors Journal*, Vol.14, pp.2447-2451, 2014.
- [100] S. Salman, D. Psychoudakis, and J. Volakis, "Determining the relative permittivity of deep embedded biological tissues.", *IEEE Antennas and Wireless Propagation Letters*, Vol. 11, pp.1694-1697, 2012.
- [101] "Dielectric Properties of Body Tissues in the Frequency Range 10 Hz - 100 GHz", Institute for Applied Physics, ITALIAN NATIONAL RESEARCH COUNCIL. Accessed 2016. <http://niremf.ifac.cnr.it/tissprop/htmlclie/htmlclie.php>
- [102] IEEE, "IEEE Standard for Safety Levels With Respect to Human Exposure to Radiofrequency Electromagnetic Fields, 3 kHz to 30 GHz.", *IEEE Std. C95. 1-1999*, 1999.
- [103] IEEE, "IEEE Standard for Safety Levels With Respect to Human Exposure to Radiofrequency Electromagnetic Fields, 3 kHz to 30 GHz", *IEEE Std. C95. 1-2005*, 2005.
- [104] N. Mohsenin, "Electromagnetic radiation properties of foods and agricultural Products", CRC Press, pp.466, 1984.
- [105] N. Basaran-Akgul, and B. A. Rasco. "Effect of marination in gravy on the radio frequency and microwave processing properties of beef.", *Journal of food science and technology* Vol. 52.2, pp. 867-875, 2015.

## Vitae

Name : ABDELRAHMAN ELSIR MOHAMED

Nationality : Sudanese

Date of Birth : 7/23/1990

Email : abdelrahman@kfupm.edu.sa abdoem@gmail.com

Address : KFUPM, Dhahran, Saudi Arabia

Academic Background :

- M. Sc. in Electrical Engineering, May 2017, KFUPM - GPA (3.87 out of 4.0).
- B. Sc. in Electrical Engineering, Jan 2014, KFUPM - GPA (3.86 out of 4.0).

Publications :

- *Journal Paper:* "Implanted Dual-Band Circular Antenna for Biomedical Applications," with Prof. Mohammad Sharawi, *Microwaves and Optical Technology Letters*, Wiley. (Submitted)
- *Journal Paper:* "Superstrate Loaded Miniaturized Patch for Biomedical Telemetry," with Prof. Ali Muqaibel and Prof. Mohammad Sharawi, *Microwaves and Optical Technology Letters*, Wiley, Vol. 59, No. 5, pp. 1212-1218, May 2017.
- *Conference Paper:* "Miniaturized Dual-Wideband Circular Patch Antenna for Biomedical Telemetry," with Prof. Mohammad S. Sharawi, IEEE 11th European Conference on Antennas and (EuCAP 2017), Paris, France, March 2017.

- *Conference Paper:* “LTCC Based Patch Antenna for Biomedical Applications at ISM Band,” with Prof. Mohammad S. Sharawi, IEEE Asia-Pacific Conference on Antennas and Propagation (APCAP 2016), Kaohsiung, Taiwan, July 2016.

Experience :

- Research Assistant at KFUPM: Jan. 2014 to May 2016.
- Summer Trainee at Arabian Consulting and Engineering Center (ACEC): Jun. 2013 to Aug. 2013.
- Grader at KFUPM, Electrical Engineering Department: 2010 to 2014.